

St. John's University

St. John's Scholar

Theses and Dissertations

2021

EFFECT OF INHIBITION OF GLYCOGEN CATABOLISM IN HEPATOCELLULAR CARCINOMA CELLS

Shrikant Barot

Follow this and additional works at: https://scholar.stjohns.edu/theses_dissertations



Part of the [Oncology Commons](#), and the [Pharmacology Commons](#)

EFFECT OF INHIBITION OF GLYCOGEN CATABOLISM IN HEPATOCELLULAR
CARCINOMA CELLS

A dissertation submitted in partial fulfillment
of the requirements for the degree of

DOCTOR OF PHILOSOPHY

to the faculty of the

DEPARTMENT OF PHARMACEUTICAL SCIENCES

of

COLLEGE OF PHARMACY AND HEALTH SCIENCES

at

ST. JOHN'S UNIVERSITY

New York

by

Shrikant Barot

Date Submitted 9/10/2021

Date Approved 10/10/2021

Shrikant Barot

Dr. Vikas Dukhande

© Copyright by Shrikant Barot 2021

All Rights Reserved

ABSTRACT

EFFECT OF INHIBITION OF GLYCOGEN CATABOLISM IN HEPATOCELLULAR
CARCINOMA CELLS

Shrikant Barot

Metabolic reprogramming is one of the important features of cancers, and there has been growing interest in targeting metabolic proteins to treat cancer. Glycogen is a polymer of glucose and serves as its storage unit in cells. Glycogen can provide energy to cells during the situations of high energy demand. A number of tumors are known to contain high levels of glycogen than their normal tissue counterparts. The liver plays an essential role in maintaining glucose homeostasis in the body via storing it into glycogen. The significance of glycogen metabolism in patients suffering from hepatocellular carcinoma (HCC) has not been clearly understood. In this study, we investigated the effects of a metabolic inhibitor targeting glycogen catabolism in HCC cells on the survival, proliferation, mechanism of cell death, metabolic changes, and synergistic effect on multikinase inhibitors. Inhibition of glycogen phosphorylase (GP), a rate-limiting enzyme in glycogen catabolism, was achieved using pharmacological inhibitor CP-91149. GP inhibition caused an increase in glycogen level and changed the expression of proteins involved in various metabolic processes. Mitochondrial metabolism was affected significantly whereas glucose entry and glycolysis were relatively unchanged. Determination of levels of different metabolites showed GP inhibition causes reduction in levels of many intermediates of pentose phosphate pathway (PPP). In addition, increase in ROS levels, cell cycle inhibition, decrease in oxygen consumption rate, and decreased

mitochondrial membrane potential was observed. CP-91149 treatment resulted in the activation of intrinsic apoptotic pathways and cell death in HCC cells and HepG2 3D spheroids. Also, GP inhibition potentiated the effects of multikinase inhibitors sorafenib and regorafenib, which are key drugs in advanced-stage HCC therapy. Our study provides mechanistic insights into cell death by perturbing glycogen metabolism and highlights GP inhibition as a potential HCC pharmacotherapy target.

DEDICATION

To my mother,
Geeta Barot,
for giving unconditional love and strength

ACKNOWLEDGEMENTS

I want to take this opportunity to thank my mother. Nothing would have been possible without your unconditional love and immense support. You have always inspired me to be a better human. You are the beacon of light for me.

I am thankful to Dr. Dukhande for taking me as a mentee in his lab. I am grateful for his knowledgeable instructions and guidance. I am also thankful to him for allowing me to follow my research curiosity and guiding me in the right direction to achieve those goals. He has always been available for help and helped me at every step of my scientific development process. In addition, I am also thankful to him for teaching me to think critically and stay calm when experiments don't work.

A sincerest thank you to Dr. Ochs for generously allowing me to use machines and resources in his lab and be part of my research committee. Weekly journal club with his lab has a significant role in my development as a researcher. I am grateful to him to be part of a process of my nurturing as a researcher.

I am thankful to Dr. Chen for allowing me to rotate in his lab, which gave me first exposure to the exciting research at St. John's University. I am also thankful to him for being part of my research committee and providing me necessary guidance for the advancement of my research. I am grateful to Dr. Reznik for being part of my research committee. Her in-depth knowledge of pharmacology has helped a lot in developing my research project. I want to sincerely thank Dr. Patel for providing insights into various research topics, being part of my research committee, and for emotional help.

I want to sincerely thank Dr. Worpel to be chair of my dissertation committee and sharing his knowledge about respiratory pharmacology.

I am thankful to Dr. Trombetta for sharing knowledge and resources for electron microscopy. I am thankful to Olivia for taking TEM micrographs and explain results and Ali for sharing his valuable knowledge of EM.

I am thankful to Dr. Irwin Kurland and Dr. Yunping Qiu from Albert Einstein College of Medicine for performing and analyzing metabolomics experiments.

I am thankful to Dr. Korlipara and Dr. Gillespie for helping in various administrative process and be available all the time.

I would also like to thank Dr. Billack and Dr. Yoganathan. They were my advisors during first semester and am grateful for their instructions and kindness. I am also thankful to various teachers at St. John's University for sharing their knowledge.

I would like to thank St. John's University and department of pharmaceutical sciences for providing financial support to this project and grant me assistantship through teaching. I want to sincerely thank Ms. Donovan for giving me job in public safety during my first semester.

Thank you to College of Pharmacy and Health Sciences staff Luz Mery Benitez, Susan, Velda, Arlene, Jacqueline, Jessica.

I want to thank my lab mates Ehab, Hari Priya, and Ali for helping with research and making lab a fun environment. I am also thankful to current and previous lab students.

To my friends Igor and Chris- You guys are equally important discovery from me. I am thankful to you guys for providing me different opinion about life. I am also thankful to Arun, Jayshil, Shashank, Snehal, Dharmik, Ashana, Shewta, Dhwani, and Gautam for being their never-ending support.

I am also thankful to graduate students at St. John's University who helped me at different times of my tenure here.

TABLE OF CONTENTS

Introduction	1
1.1 Altered metabolism in cancer cells	3
1.2 Significance of altered metabolism in cancer cells	3
1.3 Targeting metabolism to treat cancer.....	6
1.4 Structure of glycogen and its role in cancer.....	8
1.5 Glycogen metabolism in cells.....	10
1.6 Glycogen phosphorylase (GP) and its structure.....	13
1.7 Hormonal regulation of Glycogen phosphorylase (GP).....	15
1.8 Glycogen in liver and GP as antidiabetic therapy	17
1.9 Glycogen phosphorylase as an alternative approach to treat liver cancer.....	20
1.10 Hypothesis.....	22
1.11 Aims.....	23
Materials and Methods	24
2.1 Reagents.....	24
2.2 Cell culture and transfection	24
2.3 Cell viability determination	25
2.4 Cell proliferation assay	25
2.5 FITC-Annexin V/PI assay.....	26
2.6 HO-PI staining.....	26
2.7 Subcellular fractionation	26
2.8 Western blotting.....	27
2.9 Mitochondrial membrane potential (MMP) assay	27
2.10 Measurement of the total reactive oxygen species (ROS) levels.....	27
2.11 Cell cycle analysis.....	28
2.12 Immunofluorescence microscopy	28
2.13 Formation & treatment of 3D multicellular tumor spheroids	29
2.14 Glucose entry	29
2.15 Glycogen determination.....	30
2.17 Glycolysis Stress assay	30
2.18 Mito stress assay	31
2.19 Cell metabolomics.....	31
2.20 Scanning electron microscopy (SEM) sample preparation	32

2.21 Transmission electron microscopy (TEM) sample preparation	32
2.22 Statistical analysis	32
Results	34
3.1.1 Determination of viability and proliferation of hepatocellular carcinoma cells following treatment with CP-91149	34
3.1.2 Determination of cell cycle analysis and reactive oxygen species in HepG2 cells.....	35
3.1.3 Determination of the molecular mechanism of cell death following CP-91149 incubation in HepG2 cells.....	35
3.1.4 Determination of the synergistic effect of CP-91149 with sorafenib and regorafenib	37
3.2.1 Determination of the effect of CP-91149 on glycogen levels and expression of glycogen-metabolic proteins.....	37
3.2.2 Determination of the effect of CP-91149 on proteins involved in energy homeostasis and glucose uptake.....	38
3.2.3 Determination of the effect of CP-91149 on glycolysis in HepG2 cells.....	39
3.2.4 Determination of the effect of CP-91149 on oxygen consumption rate (OCR) and expression of proteins involved in mitochondrial dynamics in HepG2 cells.....	41
3.2.5 Metabolomic analysis of HepG2 cells following CP-91149 treatment.....	42
3.2.6 Effect of CP-91149 on the growth of 3-D spheroids of HepG2 cells	43
Discussion	100
4.1 Molecular mechanism of CP-91149 induced cell death in HepG2 cells and impact on chemotherapeutic agents	100
4.2 Effect of CP-91149 induced inhibition of glycogen catabolism on overall metabolism of HepG2 cells.....	104
4.3 Conclusion	106
4.4 Future directions	107
References	120

LIST OF TABLES

Table 1: Inhibitors of glycogen phosphorylase.....	18
Table 2: Appendix- A Summary of pathway analysis	108
Table 3: Appendix- B Table for data of individual metabolite analyzed by metabolomics analysis	109

LIST OF FIGURES

Figure 1: Schematic representation of the differences between oxidative phosphorylation, anaerobic glycolysis, and aerobic glycolysis	4
Figure 2: Glycolytic pathway and its inhibitors.....	7
<i>Figure 3: Different types of glycogen granules</i>	<i>9</i>
Figure 4: Schematic representation of glycogen synthesis and breakdown in the cytosol	12
Figure 5 Catabolism of glycogen by glycogen phosphorylase.	14
Figure 6: A schematic representation of a monomer subunit of GP	15
Figure 7: Regulation of hepatic glycogen metabolism	16
Figure 8: chemical structure of CP-91149	22
Figure 9: CP-91149 treatment reduces viability of HepG2 cells.	44
<i>Figure 10 : CP-91149 treatment reduces viability of Hep3B cells.....</i>	<i>45</i>
Figure 11: CP-91149 treatment reduces viability of H4IIE cells.....	46
Figure 12: CP-91149 treatment reduces viability of HepG2 cells.	47
Figure 13: CP-91149 treatment reduces proliferation of HepG2 cells.	48
Figure 14: CP-91149 treatment causes cell cycle disturbance in HepG2 cells.....	49
Figure 15: CP-91149 treatment increases reactive oxygen species level in HepG2 cells.....	50
Figure 16: CP-91149 treatment increases reactive oxygen species level in HepG2 cells.....	51
Figure 17: CP-91149 causes cell death in HepG2 cell via apoptosis.....	52
Figure 18: CP-91149 causes cell death in HepG2 cell via apoptosis.	53
Figure 19: CP-91149 treatment reduces mitochondrial membrane (MMP) potential in HepG2 cells.....	54
Figure 20: CP-91149 treatment promotes intrinsic apoptosis by changing mitochondrial and cytosolic localization of cytochrome c and BAX in HepG2 cells.	55
Figure 21: CP-91149 treatment promotes BAX localization from cytosol to mitochondria in HepG2 cells.....	56

Figure 22: CP-91149 treatment induces cytochrome c release from mitochondria to cytosol in HepG2 cells.....	57
Figure 23: CP-91149 treatment activates intrinsic apoptotic cascade in HepG2 cells.....	58
Figure 24: CP-91149 treatment induces apoptosis by increasing cleaved caspase 3 expression in HepG2 cells.....	59
Figure 25: CP-91149 treatment activates intrinsic apoptosis by increasing cleaved caspase 9 expression in HepG2 cells.	60
Figure 26: CP-91149 treatment has not much impact on cleaved caspase 8 activation in HepG2 cells.....	61
Figure 27: CP-91149 treatment potentiates action of multi-kinase inhibitor sorafenib in HepG2 cells.....	62
Figure 28: CP-91149 treatment potentiates action of multi-kinase inhibitor regorafenib in HepG2 cells.....	63
Figure 29: CP-91149 treatment potentiate action of multi-kinase inhibitors sorafenib and regorafenib in HepG2 cells.....	64
Figure 30: CP-91149 treatment increases glycogen level in HepG2 cells.....	65
Figure 31: CP-91149 treatment activates glycogen anabolic pathway in HepG2 cells.....	66
Figure 32: CP-91149 treatment activates glycogen synthase by decreasing its phosphorylation in HepG2 cells.....	67
Figure 33: High dose of CP-91149 treatment reduces glycogen phosphorylase expression in HepG2 cells.....	68
Figure 34: CP-91149 treatment activates AMP-activated protein kinase (AMPK) by increasing its phosphorylation in HepG2 cells.....	69
Figure 35: CP-91149 treatment activates AMPK by increasing its phosphorylation in HepG2 cells.....	70
Figure 36: CP-91149 treatment increases expression of pyruvate dehydrogenase (PDH) but has no impact on its phosphorylation level in HepG2 cells.....	71
Figure 37: CP-91149 treatment has no impact on glucose uptake of HepG2.....	72

Figure 38: CP-91149 treatment has no impact on glucose uptake of HepG2.	73
Figure 39: CP-91149 treatment has no impact on glucose uptake of HepG2.	74
Figure 40: CP-91149 treatment has no impact on glycolysis but reduces glycolytic capacity of HepG2 cells.	75
Figure 41: CP-91149 treatment has no impact on glycolysis of HepG2 cells.	76
Figure 42: CP-91149 treatment has no impact on non-glycolytic acidification of HepG2 cells. ..	77
Figure 43: CP-91149 treatment reduces glycolytic capacity of HepG2 cells.	78
Figure 44: CP-91149 treatment reduces glycolytic reserve of HepG2 cells.	79
Figure 45: CP-91149 treatment reduces oxygen consumption rate (OCR) and mitochondria linked ATP production of HepG2 cells.	80
Figure 46: CP-91149 treatment reduces basal oxygen consumption of HepG2 cells.	81
Figure 47: CP-91149 treatment reduces glycolytic capacity of HepG2 cells.	82
Figure 48: Determination of proton leak in HepG2 cells following 16 hours of incubation with CP-91149 using Seahorse XF Analyzer.	83
Figure 49: Determination of non-mitochondrial oxygen consumption in HepG2 cells following 16 hours of incubation with CP-91149 using Seahorse XF Analyzer.	84
Figure 50: CP-91149 treatment decreased Drp-1 expression in HepG2 cells.	85
Figure 51: CP-91149 treatment decreased Drp1 expression in HepG2 cells.	86
Figure 52: CP-91149 treatment has no impact on Mfn1 expression in HepG2 cells.	87
Figure 53: Transmission electron micrograph of HepG2 cells.	88
Figure 54: CP-91149 treatment alters level of metabolites of various metabolic pathways.	89
Figure 55: CP-91149 treatment reduces 6-phospho-D-gluconate levels in HepG2 cells.	90
Figure 56: CP-91149 treatment reduces D-gluconic acid levels in HepG2 cells.	91
Figure 57: CP-91149 treatment reduces D-Glycerate levels in HepG2 cells.	92
Figure 58: CP-91149 treatment reduces Sedoheptulose 7-phosphate levels in HepG2 cell.	93
Figure 59: CP-91149 treatment reduces D-Erythrose 4-phosphate levels in HepG2 cells.	94

Figure 60: CP-91149 treatment reduces D-Fructose 1,6-bisphosphate levels in HepG2 cells.	95
Figure 61: CP-91149 treatment reduces D-Glucose-6-phosphate levels in HepG2 cells.	96
Figure 62: CP-91149 treatment reduces growth of 3D spheroid of HepG2 cells.	97
Figure 63: CP-91149 treatment reduces growth of 3D spheroid of HepG2 cells.	98
Figure 64: CP-91149 treatment reduces number of live cells in 3D spheroid of HepG2 cells.	99

Introduction

Cancer is one of the most significant public health problems worldwide and the second biggest cause of death in the United States. Around 1.9 million new cancer cases and six hundred thousand cancer-related deaths are estimated to occur in the United States in 2021 (Siegel et al., 2021). Theories like mutation theory, chromosomal imbalance (aneuploidy), mitochondrial dysfunction, environment ssssand matter, stem cell hypothesis have been proposed to explain the origin of cancer (Hanselmann & Welter, 2016; Tan et al., 2006). A growing amount of evidence suggests that cancer arises from a single cell with stem cell characteristics (Hanahan & Weinberg, 2011). This cell can turn tumorigenic with the characteristics like self-sufficiency in growth signals, limitless replicative potential, evasion of programmed cell death, insensitivity to growth-inhibitory signals, sustained angiogenesis, and tissue invasion with metastasis (Hanahan & Weinberg, 2011). There is no guarantee regarding recovery from cancer, but the treatment of prostate cancer, testicular cancer, thyroid cancer, melanoma, breast cancer (early stage) have a greater success rate (Miller et al., 2019). For other types of cancers, currently available treatments don't provide complete protection. A majority of chemotherapeutic agents are nonspecific to cancer cells. These agents kill tumor cells and also rapidly proliferating cells. Unavailability of a promising biomarker for cancer diagnosis and determine metastasis is also a significant hindrance for cancer treatment (Chakraborty & Rahman, 2012). Cancer therapy is leading towards targeting actionable alterations in oncogene-driven cancers and the use of active or passive immunotherapies (Zugazagoitia et al., 2016). Drugs like Gleevec (imatinib), used to treat Chronic Myelogenous Leukemia (CML), is a prominent example of this. Even though the drug is very effective, it lacks curative property. After discontinuation of the treatment,

recurrence of the tumor has been observed. This results in resistance to chemotherapy (Chakraborty & Rahman, 2012).

Liver cancer is one of the leading types of cancer which arises from liver cells. Based on histopathological features, liver cancer can be classified as a heterogeneous group of malignant tumors with an unfavorable prognosis which ranges from fibrolamellar HCC (FLC), pediatric neoplasm hepatoblastoma, hepatocellular carcinoma (HCC), intrahepatic cholangiocarcinoma (iCCA), and mixed hepatocellular cholangiocarcinoma (HCCCCA) (Liu et al., 2015). There will be around forty-two thousand new liver cancer cases and thirty thousand fatalities (7th highest) in 2021 in the US (Siegel et al., 2021). Infection with hepatitis C/B (HCV/B), Non-Alcoholic Fatty Liver disease (NAFLD), or Hereditary Hemochromatosis (HH) are considered as risk factors for liver cancer. The risk of liver cancer increases for patients with male gender, age, race (Asian descent), HBV or HIV co-infection, and heavy alcohol abuse (Hartke et al., 2017). The prognosis of liver cancer depends on many factors, including stage of diseases. Overall, five years survival rate for liver cancer patients is only 18 %. If tumor hasn't spread outside the liver, the five-year survival rate is 33%. If tumor has spread to surrounding tissues or organs, the five-year survival rate is 11%. For patients where tumor has spread to distant tissues, the five-year survival rate is only 2% (Siegel et al., 2020). A study showed that 41.3% of surviving patients had reoccurrence of cancer with poor disease outcomes (Xu et al., 2019). Resistance to effective first-line therapeutic agent sorafenib is becoming very common (Tang et al., 2020). Thus, there is a dire need for novel therapeutics to treat cancer.

1.1 Altered metabolism in cancer cells

Tumor cells undergo various adaptations for survival, proliferation, and to metastasize to distant tissues. Metabolic alteration is one of the crucial adaptations for these cells as it helps cells in conditions like low availability of nutrients, hypoxia, etc. One of the earliest observations about altered tumor metabolism was by Otto Warburg (Warburg, 1956).

Under normal conditions, most differentiated cells metabolize glucose to pyruvate, which is further used by mitochondria to produce energy. Under the hypoxic state, differentiated cells metabolize glucose to pyruvate and further down to lactate to produce energy. This is a less efficient way of generating energy (Liberti & Locasale, 2016). In contrast, most tumor cells produce a large amount of lactate regardless of the availability of oxygen. This phenomenon is known as “aerobic glycolysis” or the “Warburg effect” (Vander Heiden et al., 2009).

1.2 Significance of altered metabolism in cancer cells

Metabolism of glucose to lactate generates net production of only 4 ATP. The complete metabolization of glucose to CO₂ can generate up to 32 net ATPs (Liberti & Locasale, 2016). As described in figure 1, anaerobic glycolysis is an inefficient way of producing ATP. The underlying mechanism for this adaptation is not entirely understood, but many hypotheses are given for it. For instance, rapid glucose utilization can allow cells to take more glucose to divert towards biosynthetic pathways that can allow cells for de novo generation of intermediates for lipid, nucleotide, and protein synthesis via pathways that emanate from glycolysis (Vander Heiden et al., 2009). Diverting glucose to the pentose phosphate pathway (PPP) pathway via Glucose 6-phosphate dehydrogenase (G6PD) is one of the examples of biosynthetic use. Cells can synthesize ribose 5-phosphate (R5P)

via PPP, a building block for nucleic acid synthesis. Moreover, it also provides NADPH to cells which can help them to fight reactive oxygen species (ROS) via regeneration of reduced glutathione (GSH) and for the synthesis of fatty acids, sterols, nucleotides, and non-essential amino acids (Ge et al., 2020).

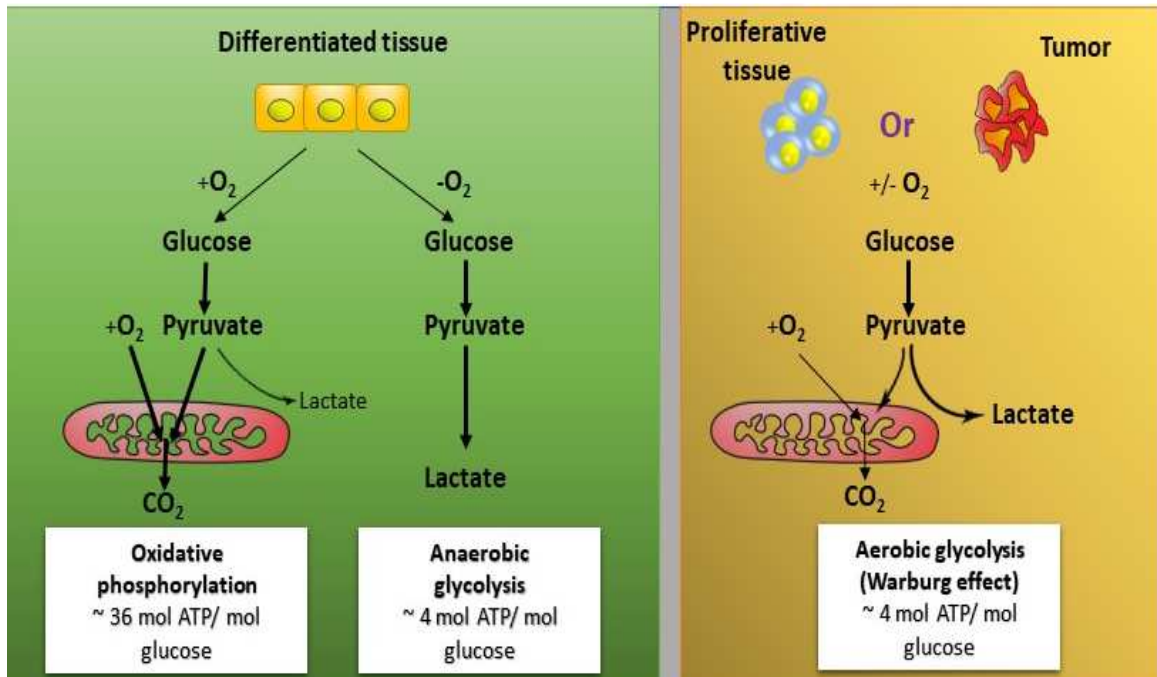


Figure 1: Schematic representation of the differences between oxidative phosphorylation, anaerobic glycolysis, and aerobic glycolysis (Warburg effect).

In tumors, lactate concentration can reach up to 10 - 30 mM (de la Cruz-López et al., 2019). As pKa of lactic acid is 3.8, lactic acid dissociates into lactate and hydrogen ion (H⁺) and alters pH in the tumor micro-environment. Acidic pH inhibits the production of IFN- γ and IL-4 and causes mitochondrial dysfunction of natural killer cells, and inhibits their anti-tumor effect (de la Cruz-López et al., 2019). In addition, lactate can increase VEGF/VEGFR2 signaling pathway expression by macrophages (Song et al., 2018).

Moreover, lactate can also enter into endothelial cells via monocarboxylate transporter (MCT-1) protein, trigger phosphorylation/degradation of I κ B α , and stimulation of NF- κ B/IL-8 (CXCL8) pathway that promotes angiogenesis via cell migration and tube formation (Végran et al., 2011). The rate of glucose utilization is higher through glycolysis and can produce energy 10-100 times faster than oxidative phosphorylation (Mookerjee et al., 2017). Conversion of pyruvate to lactate generates NADH from NAD⁺. This conversion completes aerobic glycolysis in tumors allowing it to continue glycolysis (Liberti & Locasale, 2016).

The liver plays a significant role in various metabolic processes of body. Chronic infection with hepatitis B and C viruses, alcohol intake, obesity, diabetes, and NAFLD can alter metabolism of the liver and are risk factors for HCC (Tenen et al., 2021). Hepatitis B infection has been shown to change lipid metabolism and cause oxidative stress in the liver (Yang et al., 2008). There have been growing numbers of evidence indicating significance of lipid metabolism in development of liver cancer (Ertle et al., 2011). Overall, liver cancer cells show different metabolic patterns for pathways like glycolysis, PPP, tricarboxylic acid cycle (TCA cycle), amino acid metabolism than normal liver cells (Zarrinpar, 2017). Proteins like PI3K/Akt involved in insulin signaling shows higher activity in HCC. Overexpression of proteins like GLUT1, hexokinase 2, pyruvate kinase M2 allows liver cancer to uptake more glucose and show the Warburg phenomenon (Tenen et al., 2021). Thus, targeting metabolism can provide an alternate strategy to treat liver cancer.

1.3 Targeting metabolism to treat cancer

Tumor cells show different metabolic patterns compared to normal cells. They have to manage ATP generation to maintain regular energy demand and nutrient supply to support the synthesis of macromolecules. Tumor cells rewire their metabolic pathways to meet these demands, and these alterations are attractive targets to treat tumors (Vander Heiden, 2011). One of the classic examples is targeting folate metabolism. Thymidylate synthetase (TYMS) catalyzes synthesis of deoxythymidine monophosphate (dTMP), which acts as a precursor in DNA synthesis, from deoxyuridine monophosphate (dUMP). 5',10'-methyltetrahydrofolate (5',10'-MTHF) acts as a precursor in this process and gets oxidized to dihydrofolate (DHF). Dihydrofolate reductase (DHFR) catalyzes the reduction of DHF to 5',6',7',8'-THF, which is then converted to 5',10'-MTHF, a substrate for TYMS. Anticancer antimetabolite methotrexate, due to its very high affinity for DHFR, almost irreversibly inhibits DHFR disrupting purine and pyrimidine synthesis (Hagner & Joerger, 2010). Today, it is used extensively to treat various types of tumors with other chemotherapeutic agents.

3-bromopyruvate (3-BP) is a brominated derivative of pyruvate. It is supposedly known to inhibit tumor cells by disrupting energy metabolism due to depletion in cellular ATP (Davidescu et al., 2015). 3-BP has also been shown to modify covalent association of hexokinase II, triggering its dissociation from mitochondria, leading to the release of apoptosis-inducing factor (AIF) and cell death (Chen et al., 2009). 6-phosphofructo-1-kinase (PFK-1) is a crucial enzyme in glycolysis modulated by many allosteric modulators. Fructose-2,6-bisphosphate (F2,6BP) is a shunt product of glycolysis produced by four different types of bifunctional 6-phosphofructo-2-kinase/fructose-2,6-

bisphosphatases (PFKFB1-4) enzymes. F2,6BP is an allosteric activator of PFK-1 and causes increased glucose uptake and glycolytic flux. Tumor cells are known to increase PFKFB4 expression through hypoxia (Bobarykina et al., 2006). Overexpression of PFKFB4 increases F2,6BP level, and selective inhibition of PFKFB4 markedly reduces F2,6BP level, glucose uptake, ATP in various tumor cell lines (Chesney et al., 2015).

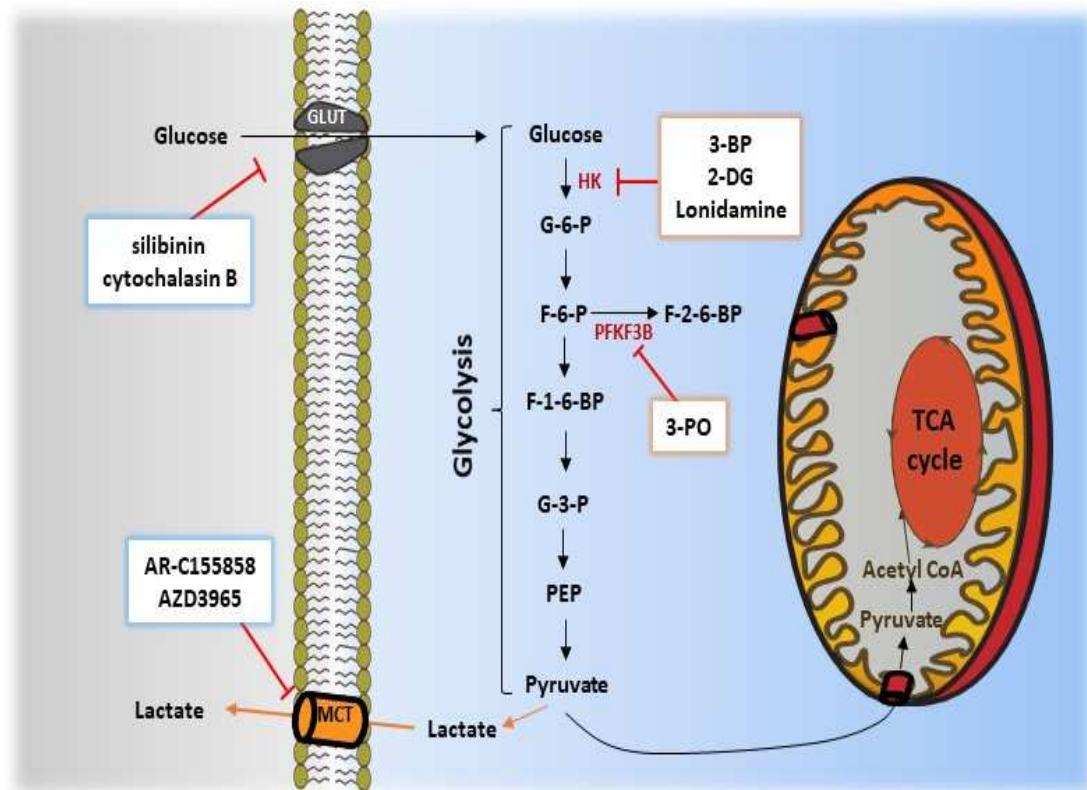


Figure 2: Glycolytic pathway and its inhibitors

Cells uptakes glucose and makes flow of reactions to transform glucose to pyruvate which has two destinies—enter to TCA cycle or convert to lactate. Here, we can see the inhibitors of hexokinase (HK), glucose transporters (GLUT), and monocarboxylate transporter (MCT). G-6-P: glucose-6-phosphate; F-6-P: fructose-6-phosphate; G-3-P: glyceraldehyde-3-phosphate; PEP:

phosphoenolpyruvate; PFK: phosphofructokinase; 2-DG: 2-deoxyglucose; 3-BP: 3-bromopyruvate.

Fatty acids are essential components of all biological membranes and energy metabolism. Exogenously derived fatty acids and endogenously synthesized fatty acids are two sources for fatty acids in the cell (Menendez & Lupu, 2007). Fatty acid translocase/CD36 is a major transporter for fatty acid uptake inside cells. CD36 monoclonal antibody (mAb) therapy has been shown to reduce prostate cancer growth in patient-derived xenografts (PDXs), epithelial to mesenchymal transition, and metastasis in melanomas and breast cancer-derived tumors (Watt et al., 2019). Many therapies targeting metabolism have been shown to cause tumor cell death and can become effective strategies to treat cancer (Farhadi et al., 2020). We have to approach these strategies with caution as targeting central carbon metabolism can cause energy imbalance even in normal cells and be lethal for patients (Feldwisch-Drentrup, 2016). Glycogen is a storage form of glucose and provides energy to cells during nutrient starvation and high energy demand situations (Murray & Rosenbloom, 2018; Pelletier et al., 2012). Under normal physiological conditions, cells are less dependent on glycogen as a primary source of energy, and targeting glycogen metabolism can be a potential target to treat cancer (Zois et al., 2014; Zois & Harris, 2016).

1.4 Structure of glycogen and its role in cancer

Glycogen is a high molecular weight polymer of α -D-glucose. Classical studies show that this macromolecule is composed of linear chains consisting of average 10-14 (1-4)-linked α -D-glucose residues, which are interlinked by (1-, 6)- α -D-glucosidic linkages to form a polymer (Manners, 1991). Based on the size, two types of glycogen structures have been

found by electron microscopy. They are termed as α - and β - granules. Individual glycogen granules are termed as β - granules. They are $\sim 10^6$ - 10^7 in molecular weight, ~ 20 - 30 nm in diameter, and can serve as a rapid energy source. Many β - granules can get organized into broccoli-like fashion to form a larger α - granule. α - granules can be 300 nm in diameter with $>10^8$ molecular weight and serves as a slow source of energy (Prats et al., 2018).

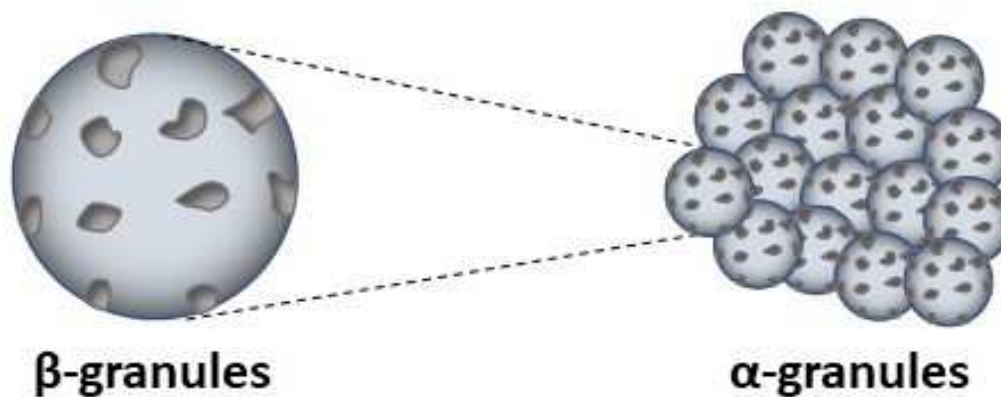


Figure 3: Different types of glycogen granules

Many tumors have a higher amount of glycogen than their tissue of origin (Rousset et al., 1981). These tumors range different types of cancers originating from tissues like breast, kidney, uterus, bladder, ovary, skin, and brain (Rousset et al., 1981). Indeed, clear cell carcinoma is a rare subtype of tumor having a high amount of glycogen and aggressive clinical behavior (Markopoulos et al., 2008). Amount of glycogen, expression of mRNA, and proteins involved in glycogen metabolism changes with the stage of cell growth in many types of cancers. There is a positive correlation between glycogen and cancer cells

in the G1 phase and a negative correlation between glycogen and cancer cells with S and G2-M phases in colorectal cancers. (Rousset et al., 1979; Takahashi et al., 1999).

Growth-factor signaling such as PI3K/Akt/mTOR pathway is known to stabilize proteins like HIF (Hypoxia induce factor) (Z. Zhang et al., 2018). HIF stabilization can support cancer cells by promoting angiogenesis and causing metabolic shift by regulating the expression of key enzymes in glucose metabolism (Eales et al., 2016; Pugh & Ratcliffe, 2003). HIF stabilization is also known to increase glycogen level in cells by increasing the expression of glycogen synthase1 and other crucial proteins involved in glycogen catabolism (Pescador et al., 2010, p. 1). Cancer cells can utilize glycogen to generate energy and support synthetic demand to generate nucleotides via PPP. This can help cells to sustain their growth and promote invasion and metastasis. (Curtis et al., 2019; Favaro et al., 2012)

1.5 Glycogen metabolism in cells

Glycogen is a polymer of glucose having glycogenin as a core protein. The first step in glycogen synthesis in cells is auto-glycosylation of glycogenin. This glycosylated glycogenein acts as a primer for glycogen synthase (GYS), which further elongates the glucose chain (Zois & Harris, 2016). Glucose enters into a cell via various GLUT transporters, gets phosphorylated into glucose-6-phosphate via hexokinase in muscle and glucokinase in the liver. Glucose-6-phosphate can further get converted to glucose-1-phosphate via phosphoglucomutase or enter glycolysis. Glucose-1-phosphate gets primed as UDP glucose, which gets incorporated to the non-reducing end of the existing chain of glycogen via GYS (Bhagavan & Ha, 2011). GYS adds uridine diphospho-glucose (UDP-

glucose) to the existing glucose chain by α -(1-4)- glycosidic bonds. Once the chain reaches sufficient length, glycogen branching enzyme (GBE) transfers a chain of 7 units to the adjacent chain through α -(1-6)- glycosidic bonds. The coordinated function of these two enzymes forms spherical β - glycogen granules. Highly branched structure increase solubility of glycogen molecule and serves as a docking site for many proteins which can bind it through carbohydrate binding modules (CBM) (Roach et al., 2012).

Apart from carbohydrate molecules, glycogen granule also contains proteins involved in its metabolism. As glycogen molecule contains its own metabolism machinery, it is sometimes referred to as organelle type structure or glycosome (Shearer & Graham, 2004). Glycogen degradation occurs through either the cytosolic pathway or the lysosomal pathway. Glycogen phosphorylase (GP) and glycogen debranching enzyme (DBE) are two key proteins involved in glycogen breakdown. GP is a key protein in glycogen catabolism. It cleaves glucose-1-phosphate from the non-reducing end of a linear chain of glycogen molecule using pyridoxal 5' phosphate (PLP) as an essential co-factor. Phosphoglucomutase can further convert glucose-1-phosphate into glucose-6-phosphate. Cells can utilize this glucose-6-phosphate via PPP or glycolysis. GP catalyzes glycogen molecule until four molecules are left from branching point on linear chain (Dombrádi, 1981). At this moment, DBE catabolizes glycogen in two steps. In the first step, DBE transfers last three molecules from branch point to non-reducing end of neighboring chain via glucanotransferase (GT) reaction. In the second step, DBE removes last glucose molecule from the branch point via α -1-6 glucosidase reaction yielding a free glucose molecule (Zhai et al., 2016).

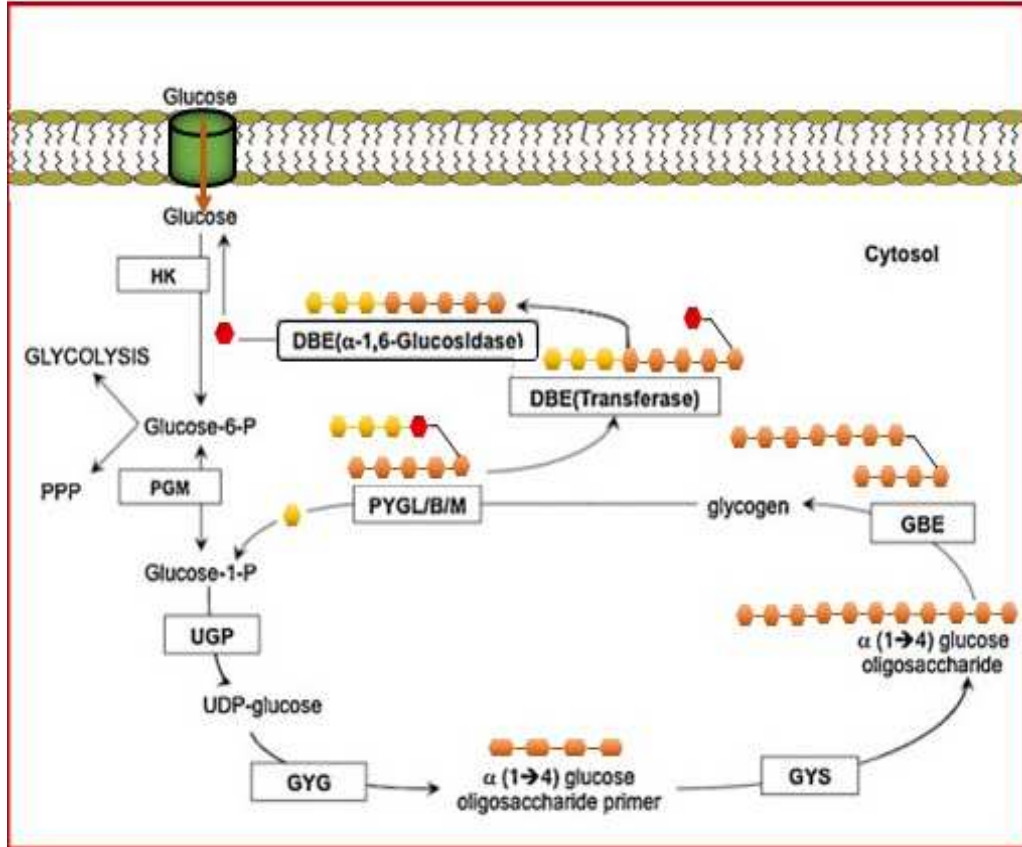


Figure 4: Schematic representation of glycogen synthesis and breakdown in the cytosol

HK: hexokinase; glucose-6/1-p: glucose-6/1-phosphate; PGM: phosphoglucomutase; UGP: UDP-glucose pyrophosphatase; UDP-glucose: uridine diphospho-glucose; GYG: glycogenin; GYS: glycogen synthase; GBE: glycogen branching enzyme; PYGL/B/M: glycogen phosphorylase, liver/brain/muscle; DBE: debranching enzyme; PPP: pentose phosphate pathway.

The precise mechanism involving the lysosomal pathway for glycogen catabolism is not understood. Proteins like starch-binding domain-containing protein (Stbd1) and GABA type A receptor associated protein like 1 (GABARAPL1) are believed to make autophagosomes via interacting with glycogen. This autophagosome further gets

sequestered into lysosome via lysosomal-associated membrane protein 1(LAMP-1), where it gets hydrolyzed by the action of alpha-acid glycosidase (GAA) (Roach et al., 2012; Zois et al., 2014).

1.6 Glycogen phosphorylase (GP) and its structure

As described earlier, glycogen phosphorylase is a key enzyme in glycogen catabolism. There are three known isozymes for this protein in humans, which are liver, muscle, and brain isoforms encoded by genes *PYGL*, *PYGM*, and *PYGB*, respectively. In humans, glycogen phosphorylase is present as a homodimer of monomer units believed to be held together by ionic interaction and stabilized by hydrophobic forces (Dombrádi, 1981). The liver isoform is 846 amino acids in chain length, muscle isoform is 841 amino acids in chain length, and brain isoform is 842 amino acids in chain length (Rath et al., 2000). Glycogen phosphorylase has many regions with biological significance: catalytic site, glycogen storage site, nucleotide site, and regulation site. GP has a serine residue at the 14th position, which can undergo reversible phosphorylation. Phosphorylation converts less active GP_b into more active GP_a conformation. The nucleotide site consists of three subsites: the ribosyl residue, the phosphoryl group, and the purine base-binding loci. Allosteric modulators like AMP and IMP promote relaxed (R) and active form of GP, whereas ATP, ADP, and glucose-6-phosphate promotes tense (T) and less active GP version.

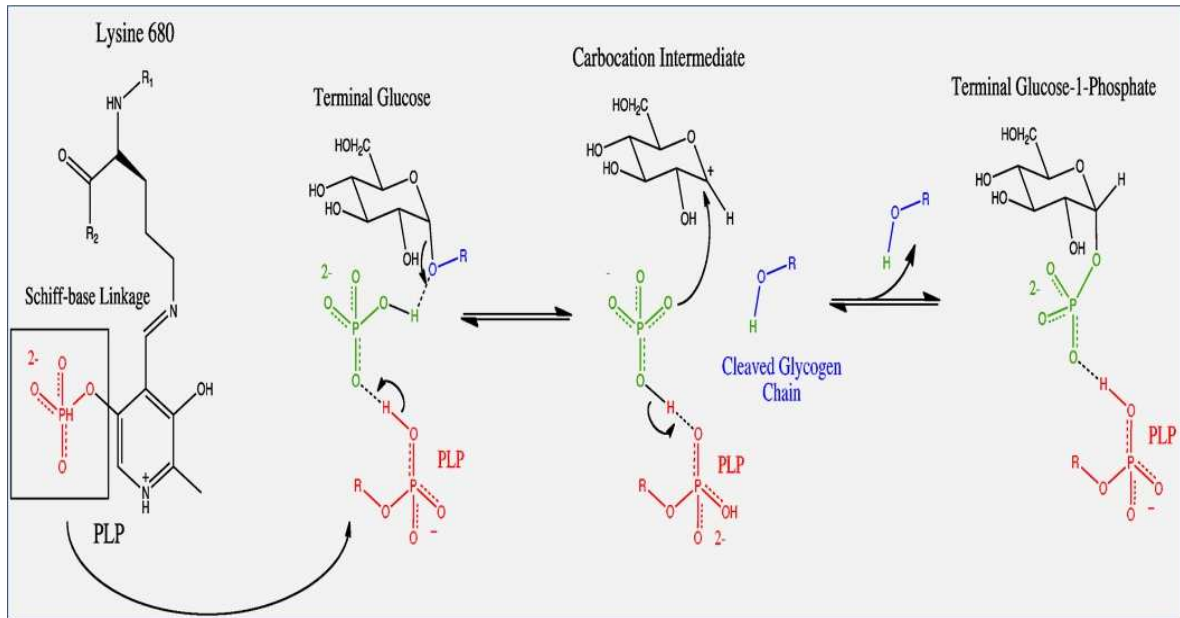


Figure 5 Catabolism of glycogen by glycogen phosphorylase.

Glycogen phosphorylase makes Schiff base by interacting with pyridoxal phosphate derived from vitamin B6. This Schiff base interacts with α -1-4 glycosidic linkage on linear chain of glycogen catalyzing glucose-1-phosphate residue.

The catalytic site is a site in glycogen phosphorylase believed to be buried in the hydrophobic pocket of the enzyme. Pyridoxal phosphate (PLP) derived from vitamin B6 acts as a co-factor in this reaction and makes a Schiff base by covalently binding to lysine residue at 680. This Schiff base interacts with α -1-4 glycosidic linkage on the linear chain of glycogen catalyzing glucose-1-phosphate residue (Dombrádi, 1981; Johnson, 1992).

GP binds with glycogen via storage site. This binding induces positive heterotropic action on the active and nucleotide sites (Dombrádi, 1981).

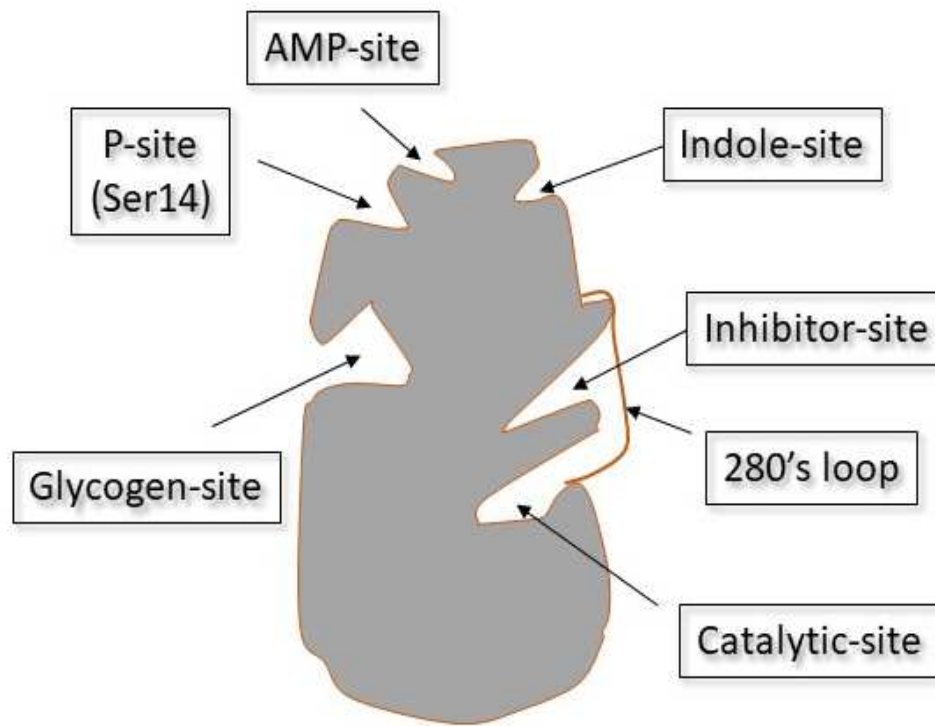


Figure 6: A schematic representation of a monomer subunit of GP

1.7 Hormonal regulation of Glycogen phosphorylase (GP)

Hormones like adrenaline, noradrenaline, and glucagon activate GP via phosphorylation of S14, whereas insulin deactivates GP via promoting its dephosphorylation.

Phosphorylase kinase (PhK) is upstream kinase for GP made of four distinct subunits α , β , γ , and δ . γ unit is a catalytic and its activity is controlled by regulatory units α , β , and δ .

Adrenaline, noradrenaline, and glucagon activate adenylyl cyclase and increases cAMP level in the cell. cAMP activates protein kinase A (PKA), which further phosphorylates α and β subunits of PhK. This relieves inhibitory activity over γ unit of PhK and activates GP by its phosphorylation. δ unit of PhK is identical to calmodulin and binds to Ca^{+2}

ions. An increase in intracellular calcium will relieve the inhibitory activity of δ unit over γ unit of PhK and activate GP by its phosphorylation (Brushia, 1999; T. E. Jensen & Richter, 2012; Nadeau et al., 2018; Vénien-Bryan et al., 2002).

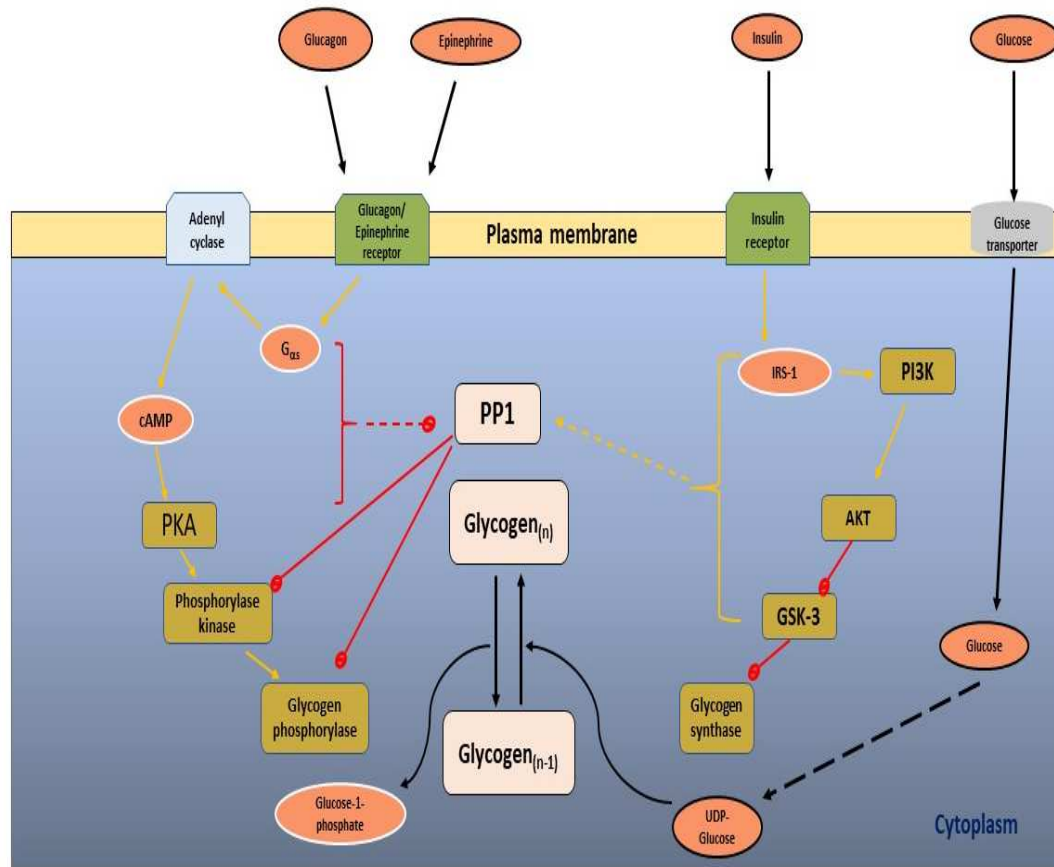


Figure 7: Regulation of hepatic glycogen metabolism

Under fasting conditions, glucagon and epinephrine induces cAMP-dependent signaling cascades, leading to the activation of GP and glycogenolysis while inhibiting glycogenesis. Conversely, feeding enhances insulin-mediated signaling in the liver, leading to the activation of both PP1 and Akt, thus promoting glycogen synthesis to increase glucose uptake in the liver.

Insulin inhibits glycogen phosphorylase activity by promoting GP dephosphorylation.

Insulin binding to insulin receptor activates PI3-kinase/PKC/PKB pathway. This leads to

increase in phosphorylation of P1 site of G-subunit on PP1 (Ragolia & Begum, 1998; Zois & Harris, 2016). PP1, in association with its regulatory subunit, protein targeting glycogen (PTG/PPP1R3), causes dephosphorylation of proteins involved in glycogen metabolism like GP, PhK, and GS. This results in the activation of GS and deactivation of GP. Insulin also causes activation of GS vis deactivation of proteins like glycogen synthase kinase-3 (GSK-3). Activation of GP, GS, and metabolism of glycogen synthesis is reciprocal processes. Allosteric activators of GS deactivate GP and vice versa. Activation of PKA increases phosphorylation of P2 site of G -subunit of PP1 and reduces its activity. This leads to the deactivation of GS and activation of GP (Ragolia & Begum, 1998; Zois & Harris, 2016).

1.8 Glycogen in liver and GP as antidiabetic therapy

The liver is one of the primary storage sites for glycogen. Human skeletal muscles store about 500 gm of glycogen which accounts for 80 % of the body's glycogen stores. Liver stores about 100 gm of glycogen in 1.5 kg of tissue. Net glycogen synthesis in the liver can increase up to five-fold at portal insulin concentration of 192 pM or hyperglycemia (10.5 mM) (J. Jensen et al., 2011). Hepatic glycogen synthesis and turnover is negligible under basal peripheral insulinemia (54 pM). Basal peripheral glucagon (~55 pg/ml) can promote glycogen breakdown by the mechanism mentioned above (J. Jensen et al., 2011; Zois et al., 2014).

Many drugs which can inhibit GP are being developed to treat type 2 diabetes. These agents are being developed to inhibit glucagon-induced glycogenolysis and glucose release into the blood to treat type 2 diabetes (Treadway et al., 2001). These inhibitors

bind to different sites on GP such as active site, AMP site, purine nucleotide site, indole carboxamide site, glucose-based inhibitors, etc. of glycogen phosphorylase enzyme.

Table 1: Inhibitors of glycogen phosphorylase

Glycogen phosphorylase inhibitors	Pharmacological modulators of glycogen metabolism	GAA/1,4-α-glucosidase inhibitors
Active site inhibitors e.g., DAB	Sodium tungstate (increases glycogen synthesis)	Acarbose Miglitol Voglibose
AMP site inhibitors BAY1807, BAYR3401	Metformin (depletes glycogen)	
Indole carboxamide site inhibitors e.g., CP-91149 Ingliforib (CP-368296) CP-316819 CP-320626	Lithium (stimulates or inhibits glycogen synthesis)	
Purine nucleoside site inhibitors e.g., Olefin derivative	Valproate (decreases glycogen content)	
Glucose-based inhibitors	Dichloroacetate	

1,3,4-oxadiazole	(increases glycogen accumulation)	
------------------	-----------------------------------	--

Different modulators of Glycogen Phosphorylase (Donnier-Maréchal & Vidal, 2016; Gaboriaud-Kolar & Skaltsounis, 2013; Zois & Harris, 2016)

Many inhibitors among these have reached different stages of clinical trials. Inglicorib showed reduced peak glucose level compared to placebo after 0.5 mg of glucagon infusion in a phase 1 trial (Rotella et al., 2013). However, it didn't show any beneficial effect in the phase 2 trial alone or in combination with sulfonylureas. Similarly, investigational agents like AEV56588, GSK1362885, and PSN-357 underwent phase 1 and phase 2 trials as antidiabetic agents, but there isn't any information since then on their progress (Rotella et al., 2013).

CP-316819 is another inhibitor of GP. After 60 min of perfusion, CP-316819 showed more than 30% skeletal muscle fatigue compared to control one in the rat hindlimb perfused model (Baker et al., 2006). In another experiment, GPi921, an inhibitor of GP, was administered at 53 mg/kg/day for 28 days in ZFD rats. Peak plasma concentration of GPi921 reached 25 times high than the IC₅₀ value of the drug. Treatment caused increase in liver glycogen content and weight after ten days of treatment which kept on increasing for 28 days. At the end of 28 days, GPi921 treated mice also showed mild to moderate lipid accumulation, vacuolation, increased inflammation, fibrosis, necrosis, ALT, and AST level. Some of these features are also observed in the patients suffering from glycogen storage disease, indicating these adverse effects are more likely to occur due to prolonged GP inhibition rather than side effects of the drug (Floettmann et al., 2010).

Liver, muscle, and skeletal muscle isoforms of GP demonstrate more than 80% homology in their structures. Currently, there aren't any inhibitors available that can selectively target liver isoform sparing others (Baker et al., 2006). Thus, not reaching the therapeutic endpoint may be the reason for discontinuing GP inhibitors as an antidiabetic agent.

1.9 Glycogen phosphorylase as an alternative approach to treat liver cancer

Liver cancer is one of the deadly diseases with a poor prognosis in patients. Based on advancement of the disease, Barcelona Clinic Liver Cancer (BCLC) staging system classifies hepatocellular carcinoma (HCC) into five categories stage 0 (very early stage), stage A (early stage), stage B (intermediary stage), stage C (advance stage), stage D (end-stage) which serves as a guideline for therapy (Hartke et al., 2017). Treatment for HCC includes ablative electrochemical therapies (e.g., ethanol injection or radiofrequency ablation), surgical options (resection or liver transplantation), catheter-based embolic therapies (e.g., radioembolization and chemoembolization), stereotactic body radiotherapy (SBRT), systemic therapy of multikinase drug-like sorafenib, atezolizumab, and bevacizumab (Hartke et al., 2017).

The type of treatment given to patients depends on underlying cause and advancement of disease. Patients whose tumor hasn't progressed beyond liver are considered for curative treatment like liver surgery or transplantation (Malek et al., 2014). Patients with disease categorized in BCLC class 0, A, and B can benefit from locoregional therapies (Lurje et al., 2019). Therapies like chemical ablation are well tolerated even in patients with cirrhosis with the highest efficacy in HCC < 2 cm (Daher et al., 2018). However, chemical ablation is replaced with techniques like radiofrequency and microwave-based

ablation due to its higher rate of recurrence rates and inferior survival (Lencioni & Crocetti, 2012). Tumor localized to liver exceeding 3 nodules, 3 cm can be given trans-arterial chemoembolization (TACE). It is usually administered via femoral artery catheterization to cannulate the hepatic arterial branches. Chemotherapeutic agents like doxorubicin or cisplatin are then delivered to the highly vascularized liver tumor. Following that feeding vessel is blocked with embolization agent, commonly lipiodol, which causes ischemic necrosis of the tumor (Ko et al., 2020; Lurje et al., 2019). Dual blood supply from portal vein and the hepatic artery helps in preserving the rest of the liver parenchyma (Ko et al., 2020). Systemic therapy with multi kinase inhibitors like sorafenib, regorafenib, Atezolizumab plus bevacizumab, Lenvatinib are given to patients suffering from advanced stage HCC (Lurje et al., 2019). Ablative and surgical therapies are intended for curative purposes. Although other treatments have a durable response, they are not considered curative (Hartke et al., 2017). Thus, there is a dire need for an alternative approach to treat liver cancer.

Expression of many metabolic proteins is changed in liver cancer is through altered expression of proteins like hypoxia-inducible factor 1-alpha (HIF-1 α), sterol regulatory element-binding protein 1 (SREBP1), proliferator-activated receptor gamma (PPAR γ), Wnt signaling transducer β -catenin (CTNNB1), Nrf2, FoxO1 (Tenen et al., 2021). Thus, targeting metabolism can prove as a good strategy to treat liver cancer. Liver glycogen plays a vital role in glucose homeostasis in individuals. As discussed earlier, glucose utilization via glycogen catabolism has shown to sustain proliferation and prevent premature senescence in many cancer cells (Favaro et al., 2012). Glycogen catabolism also plays a vital role in the tumor microenvironment, where cancer-associated fibroblasts

(CAFs) have been shown to mobilize glycogen in tumor cells to support proliferation and metastasis in cancer cells in ovarian cancer (Curtis et al., 2019).

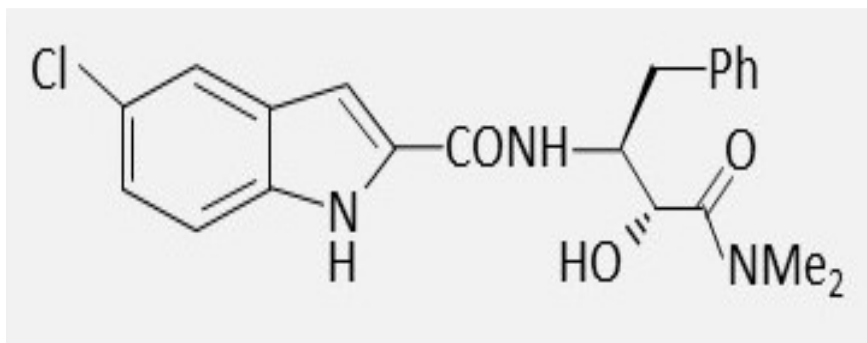


Figure 8: chemical structure of CP-91149

CP-91149 is an indole carboxamide site (allosteric) inhibitor of GP. It inhibits the action of GP by inhibiting dimerization of monomeric GP units. This further promotes T state of GP and subjects it to dephosphorylation (Lerín et al., 2004). It was initially designed as an antidiabetic agent and have shown to reduce glucose level in diabetic male C57BL/6J-Lep^(ob/ob) mice (Martin et al., 1998). Inhibition of GP action via depleting its expression or using inhibitors like CP-91149 has also shown to inhibit the growth of many cell lines (Favaro et al., 2012; Ma et al., 2012). The precise role of glycogen catabolism and the underlying cell death mechanism behind GP inhibition has never been studied in detail in liver cancer. In this study, we aimed to investigate the role of glycogen metabolisms in liver cancer.

1.10 Hypothesis

Inhibition of glycogen phosphorylase by CP-91149 will limit the availability of glucose through glycogen for metabolic reprogramming in hepatocellular carcinoma. GP inhibition will cause a metabolic imbalance in cells which will result in mitochondrial

dysfunction, alterations in expression and activity of metabolic proteins, and apoptotic cell death.

1.11 Aims

- I. To study viability and proliferation of hepatocellular carcinoma cells following treatment with CP-91149.
- II. To study the molecular mechanism of cell death in HepG2 cells following CP-91149 treatment.
- III. To study the synergistic effect of CP-91149 on chemotherapeutic drugs and experimental metabolic inhibitors.
- IV. To study metabolic and mitochondrial changes in HepG2 cells after CP-91149 treatment.
- V. To determine the expression of proteins involved in glycogen metabolism and energy homeostasis in HepG2 cells after treatment with CP-91149.
- VI. To analyze effect on growth of HepG2 3-D spheroids after treatment with CP-91149.

Materials and Methods

2.1 Reagents

Chemicals were purchased from the following sources: CP-91149, regorafenib, 2-deoxy-D-glucose, NS3694, 2-deoxy-D-glucose and etoposide (ApexBio, Houston, USA); carbonyl cyanide 3-chlorophenylhydrazone (CCCP) (Tocris Bioscience, Minneapolis, USA); 3-bromopyruvate, Antimycin A and chloroquine (Alfa Aesar, Tewksbury, USA); Metformin, Oligomycin and Carbonyl cyanide-4 (trifluoromethoxy) phenylhydrazone (FCCP) (Cayman Chemical, Ann Arbor, USA); MIDIVI-1, Mitochondrial Fusion Promoter M1, Glucose (HK) Assay Kit (GAHK20), Insulin (I9278) and Amyloglucosidase (A7420) (Sigma-Aldrich, St. Louis, USA); 6-aminonicotinamide (Acros-Organics, New Jersey, USA); Sorafenib (Fisher Scientific, Hampton, USA); Mitochondria/cytosol fractionation kit (Biovision, Milpitas, USA); PYGL plasmid was from Origene (RC210683, Rockville, USA); Accutase solution, Propidium iodide (PI), Hoechst 33342 (HO), MitoTracker Red CMXRos, FxCycle PI/RNase staining solution, CM-H₂DCFDA, and CyQuant Direct Cell Proliferation Assay kit (ThermoFisher Scientific, Waltham, USA); FITC-Annexin V apoptosis detection kit (BD Biosciences, Franklin Lakes, USA). All antibodies were from Cell Signaling Technology (Danvers, USA) except for the LC3B, GYS-2, PYGL and α -tubulin antibodies, which were from Proteintech Group (Rosemont, USA).

2.2 Cell culture and transfection

Human hepatocellular carcinoma (HepG2 and Hep3B) and rat hepatocellular carcinoma (H4IIE) cells were grown in Dulbecco's Modified Eagle's Medium (DMEM) normal glucose (5.5 mM) and supplemented with 10% v/v FBS. All drug treatments were carried

out 16 hr after subculturing cells to about 70% confluency. Duration of treatment for individual experiment was as mentioned in each assay. Cells were transfected, where indicated, with indicated plasmids using the TransIT-LT1 transfection reagent (Mirus Bio, Madison, USA) and serum-free medium as per the manufacturer's protocol. Cells were treated with inhibitors after 24 hr of transfection.

2.3 Cell viability determination

Cell viability was determined using MTT dye (3-(4,5-dimethylthiazol-2-yl)-2,5-diphenyltetrazolium bromide) and neutral red dye (3-amino-7-dimethylamino-2-methylphenazine hydrochloride). Cells were incubated with drugs at indicated concentrations and time points. For the MTT assay, at the end of the drug treatments, cells were treated with 0.05% (w/v) MTT dye for 3 hr at 37°C. The formazan crystals were dissolved in DMSO and absorbance was measured at 570 nm using the SpectraMax M5e plate reader (Molecular Devices, Sunnyvale, USA). The neutral red assay was performed as described by Repetto et al. with minor modifications (Repetto et al., 2008). Briefly, at the end of the drug treatments, cells were incubated with 40 µg/ml neutral red dye for 3 hr at 37 °C. Cells were then destained using a solution (50% ethanol, 49% deionized water, and 1% glacial acetic acid). Absorbance was measured at 540 nm using SpectraMax M5e plate reader.

2.4 Cell proliferation assay

Cell proliferation was determined using the CyQuant Direct Proliferation Assay kit as per the manufacturer's protocol. Briefly, at the end of drug treatments, medium was carefully aspirated from each well without disturbing the cells. 50 µl of 2X detection reagent was

added to each well containing 50 μ l medium containing cells for 1 hr at 37 °C.

Fluorescence was measured using the Spark 10M plate reader.

2.5 FITC-Annexin V/PI assay

For apoptosis detection, HepG2 cells were dual-stained using the FITC-Annexin V apoptosis detection kit. Briefly, at the end of the drug treatments, cells were washed with PBS and detached using Accutase solution (Corning, Carlsbad, USA). Collected cells were further washed twice with cold PBS, resuspended in cold 1X binding buffer, and dual stained with FITC-Annexin V and PI in the dark at 25 °C for 15 min. Flow cytometry was immediately performed on cells using the BD Accuri C6 flow cytometer (BD Biosciences) and analyzed using FlowJo v.10 software.

2.6 HO-PI staining

At the end of CP-91149 treatment, HepG2 cells were incubated with PI (25 μ g/mL) for 10 min in the dark. Next, cells were washed with PBS and incubated with HO dye (11.25 μ g/mL). Images were taken immediately using the EVOS FL Auto Imaging System (ThermoFisher Scientific, Waltham, USA) and quantified using ImageJ 1.8.0 software.

2.7 Subcellular fractionation

Mitochondrial and cytoplasmic fractions were isolated using the Mitochondria/Cytosol fractionation kit according to the manufacturer's protocol. HepG2 cells were collected at the end of the treatments and washed with ice-cold PBS, then centrifuged at 600g for 5 min at 4 °C, followed by resuspension of pellet in 1X cytosol extraction buffer mix. An ice-cold dounce tissue grinder was used for cellular homogenization. The homogenates were centrifuged at 700g for 10 min at 4 °C, and the supernatants were collected and centrifuged at 10,000g for 30 min at 4 °C. The supernatant was considered the cytosolic

fraction while the pellet was resuspended using the mitochondrial extraction buffer mix and was considered the mitochondrial fraction.

2.8 Western blotting

Cells were lysed by scraping in modified RIPA buffer (50 mM Tris pH 8.0, 150 mM NaCl, 1% v/v NP40, 0.5% w/v deoxycholate, 0.1% w/v SDS, 10% v/v glycerol, 10 mM NaF, 0.4 mM EDTA) with protease inhibitors. The lysates were cleared by centrifugation at 10,000g for 10 min. Next, Laemmli sample buffer containing SDS and β -mercaptoethanol was added and samples were denatured by heat. Subsequently, samples were separated on polyacrylamide gels and transferred to PVDF membrane and processed for Western blotting with chemiluminescence detection. Images were obtained using ChemiDoc MP or Azure C500 imaging system (Bio-Rad) or Azure C500 imaging system and analyzed using ImageJ 1.8.0 software.

2.9 Mitochondrial membrane potential (MMP) assay

MMP was assessed using MitoTracker Red CMXRos according to the manufacturer's protocol. Briefly, at the end of CP-91149 treatment, HepG2 cells were washed twice with PBS and incubated with MitoTracker Red CMXRos dye (100 nM) prepared in serum-free medium for 30 min at 37 °C. Cells were washed twice with PBS and fixed in 3.7% v/v formaldehyde in PBS for 15 mins. Cells were detached using Accutase solution and analyzed using the BD Accuri C6 flow cytometer and FCS Express 6 software.

2.10 Measurement of the total reactive oxygen species (ROS) levels

Cellular oxidative stress was evaluated using the chloromethyl derivative of 2',7'-dichlorodihydrofluorescein diacetate (CM-H₂DCFDA). Briefly, at the end of the drug treatments, HepG2 cells were washed with PBS and detached using Accutase solution.

Collected cells were washed twice with PBS, resuspended in serum-free medium, and stained with CM-H₂DCFDA (20 μM) for 30 min. at 37 °C in the dark. Flow cytometry was performed on cells using the Amnis FlowSight Imaging flow cytometer (MilliporeSigma, Burlington, USA) and analyzed using the Amnis IDEAS software to gate live and single positively stained cells.

2.11 Cell cycle analysis

Cell cycle analysis was performed using the FxCycle PI/RNase Staining Solution. Briefly, at the end of the drug treatments, cells were washed twice with PBS and detached using Accutase solution. Cells were fixed using 70% ethanol at –20 °C overnight. Ethanol was removed from samples by centrifugation at 850 g and then cells were incubated with PI/RNase for 30 min. Subsequently, cells were analyzed using the BD Accuri C6 flow cytometer and FCS Express 6 software.

2.12 Immunofluorescence microscopy

HepG2 cells were cultured on poly-D-lysine-coated glass coverslips in 24-well cell culture plates. Cells were then treated with indicated drugs on the following day. Next, cells were washed with PBS and fixed using formaldehyde (3.7% v/v in PBS). Cells were permeabilized using cold Triton X-100 (0.25% v/v in PBS), for 5 minutes, washed, and incubated in FBS solution (10% v/v in PBS) for 1 hr. Next, samples were incubated with LC3B antibody overnight followed by washes and incubation with Alexa Fluor 594-conjugated secondary antibody. Coverslips were mounted on slides using DAPI Fluoromount-G (SouthernBiotech), and images were taken using the EVOS FL Auto Imaging System (ThermoFisher Scientific).

2.13 Formation & treatment of 3D multicellular tumor spheroids

Formation of 3D multicellular tumor spheroids of HepG2 cells was achieved by seeding cells at a density of 2000 cells/well in an ultra-low attachment 96-well plate (Corning Life Sciences, MA, USA). Once the spheroids had formed, they were treated with different concentrations of CP-91149. Media was replaced with a fresh medium containing an appropriate concentration of CP-91149 every 48 h for 12 days. During the incubation, spheroids were observed for their growth in terms of their diameter and surface area using EVOS FL Auto 2 cell imaging system (ThermoFisher scientific, Waltham, USA). At the 12th days cells live/dead cells in spheroid were visualized via live/dead cell discrimination method using LIVE/DEAD® Viability/Cytotoxicity kit (ThermoFisher scientific, Waltham, USA), and images were taken using EVOS FL Auto 2 cell imaging system.

2.14 Glucose entry

At the end of treatment, HepG2 cells were washed five times with PBS and incubated for 45 minutes with DMEM containing 5.5 mM glucose, radioactive 2-deoxy-D-glucose [1,2-³H(N)- 29.9 mCi/mmol] (Moravek Biochemicals Inc, Brea, USA) and supplemented with 10% v/v FBS. Cells were then washed five times with PBS and incubated for 1 hour with 1 % Triton X-100. 400 micro litter of lysates were transferred to a scintillation vial containing 10 ml of Ultima Gold (PerkinElmer, Waltham, USA). Radioactivity was counted using Tri-Carb liquid scintillation counter (PerkinElmer, Waltham, USA) for 10 minutes. The remaining quantity of sample was used to quantify protein content by BCA assay. Samples were normalized for counts per milligram of protein.

2.15 Glycogen determination

At the end of treatment, HepG2 cells were washed three times with PBS and scrapped in 0.2 N Sodium acetate (pH 4.8). Two aliquots of 100 micro liters of fraction were taken. One fraction was treated with 1 unit/ml amyloglucosidase, and the other was treated with water for two hours. The reaction was neutralized by bringing pH from 7.5 to 9 using sodium hydroxide. Mixtures were centrifuged at 700 g for 5 mins, and the supernatant was taken. The amount of glucose in samples was determined using Glucose (HK) Assay Kit (GAHK20, Sigma-Aldrich, St. Louis, USA) following manufactures protocol. Background was subtracted using aliquoted treated with water, and the amount of glycogen in cells was determined using the standard curve. The remaining quantity of sample was used to quantify protein content by BCA assay.

2.17 Glycolysis Stress assay

At the end of treatment, DMEM media was replaced with assay medium (XF base medium supplemented with 2 mM glutamine), and cells were incubated in a non-CO₂ incubator at 37°C for 1 h before the assay. XF Analyzer was calibrated prior to assay and glycolytic stress was determined using test assay protocol as suggested by Agilent Seahorse technologies (Billerica, MA, USA). ECAR was measured under basal conditions followed by the sequential addition of glucose, oligomycin and 2-DG to achieve final well concentration of 5 mM glucose, 1 μM oligomycin and 50 mM 2-DG. At end of measurement, media was removed, and cells were incubated with 1 % Triton X-100 for 1 hour. Protein content was determined by BCA assay.

2.18 Mito stress assay

At the end of treatment, DMEM media was replaced with assay medium (XF base medium supplemented with 5.5 mM glucose, 2 mM glutamine and 1 mM sodium pyruvate), and cells were incubated in a non-CO₂ incubator at 37°C for 1 h before the assay. XF Analyzer was calibrated prior to assay and mito stress was determined using test assay protocol as suggested by Agilent Seahorse technologies (Billerica, MA, USA). OCR was measured under basal conditions followed by the sequential addition of oligomycin, FCCP, as well as rotenone & antimycin A to achieve final well concentration of 1 μM oligomycin, 0.5 μM FCCP, rotenone & antimycin A. At end of measurement, media was removed, and cells were incubated with 1 % Triton X-100 for 1 hour. Protein content was determined by BCA assay.

2.19 Cell metabolomics

At the end of treatment, cells were washed scraped in 150 mM ammonium acetate on ice. Cells were centrifuged at 2000 g for 2 mins and immediately frozen in liquid nitrogen. Cell pellets were extracted with of 80% methanol (containing 2.5μM U13C succinate, and 5μM U13C citrate as internal standards). The supernatants transferred in the gas chromatography (GC) sampling vial were dried under nitrogen flow, and a two-step derivatization with methoximation and silylation. The derivatized metabolites were analyzed with GC time-of-flight mass spectrometry (GC-TOFMS premier; Waters Corporation, Milford, MA, USA). The data was analyzed with Genedata Expressionist (Genedata, Basel, Switzerland) software. The output data was normalized to internal standards, sum of all the metabolites within each sample and protein content.

2.20 Scanning electron microscopy (SEM) sample preparation

HepG2 cells were cultured on poly-D-lysine-coated glass coverslips. At the end of treatment HepG2 cells were fixed in 3 % glutaraldehyde made in 0.1 M sorenson's phosphate buffer pH 7.4 for 60 min at room temperature (RT). Cells were washed three times with .1 M sorenson's phosphate buffer and immersed in 1% OsO₄ (aq.) solution for 30 minutes. Cells were then dehydrated in 30%, 60%, 90% and 100% acetone for 10 minutes. Cover slips were dried using Critical Point Dryer (CPD) using CO₂ at 38 °C at 1200 psi. Specimens were subsequently sputter coated and analyzed using JEOL JSM – 6010LA SEM (JEOL, Ltd., Tokyo, Japan).

2.21 Transmission electron microscopy (TEM) sample preparation

At the end of treatment, cells were fixed in 3 % glutaraldehyde made in 0.1 M sorenson's phosphate buffer pH 7.4 for 60 min at 4 °C. Cells were then scraped and pelleted at 453 g for 5 min. Pelleted cells were subsequently washed three times in 0.1 M sorenson's phosphate buffer pH 7.4 and immersed in 1% OsO₄ (aq.) solution for 60 min, then dehydrated in 30%, 60%, 90% and 100% acetone for 10 minutes. The dehydrated cell pellets were then soaked in 33%, 50%, 67% and 100% resin (Araldite) 10 minutes and placed into molds at 60 °C for week. When solidified, ultrathin sections of the resin embedded samples were produced, stained with uranyl acetate and lead citrate and subsequently analyzed using a JEOL 1200EX TEM (JEOL, Ltd., Tokyo, Japan).

2.22 Statistical analysis

Values are mean ± SEM of at least three independent experiments. Differences between groups are analyzed by one-way analysis of variances with either Dunnett's or Tukey

post hoc test. The significance has been considered at * $p \leq 0.05$ and ** $p \leq 0.01$. Data for Western blotting, imaging, and flow cytometry are representative of at least three independent determinations.

Results

3.1.1 Determination of viability and proliferation of hepatocellular carcinoma cells following treatment with CP-91149

We used an MTT cell viability assay in human (HepG2 and Hep3B)- and rat (H4IIE) hepatocellular carcinoma cells to examine the effects of the glycogen phosphorylase (GP) allosteric inhibitor CP-91149. MTT assay involves the reduction of a yellow water-soluble 3-(4,5-dimethylthiazol-2-yl)-2,5-diphenyltetrazolium bromide (MTT dye) to purple-colored formazan crystals. This conversion is based upon NAD(P)H-dependent cellular oxidoreductase enzymes and thus MTT assay reflects the number of viable cells (Berridge et al., 2005).

Treatment with CP-91149 decreased the viability of HepG2, Hep3B, and H4IIE cells in a concentration-dependent manner (0, 25, 50, 75, or 100 μ M), respectively (**Fig. 9-11**).

Etoposide, an anticancer agent, was used as a positive control in the experiment. In addition, we performed a neutral red dye uptake assay, which measures the capacity of viable cells to incorporate and bind to neutral red dye in HepG2 and H4IIE (Barot et al., 2019; Repetto et al., 2008). A concentration-dependent decrease in HepG2 and H4IIE cells' viability by CP-91149 treatment was confirmed (**Fig. 12**).

In addition, we measured the effect of CP-91149 treatment on HepG2 cell proliferation using CyQuant assay. The assay involves CyQUANT GR dye, which produces a large amount of fluorescence upon binding to cellular nucleic acids (Jones et al., 2001). HepG2 cells showed a significant reduction in cell proliferation after incubation with CP-91149 for 48 h (**Fig. 13**).

3.1.2 Determination of cell cycle analysis and reactive oxygen species in HepG2 cells

One of the critical needs for the metabolic reprogramming of cancer cells is the constant supply of nucleotides for rapid proliferation. Thus, we determined whether inhibition of glycogen catabolism interferes with cell division in HepG2 cells. A propidium iodide-based flow cytometric determination of cell cycle analysis indicated that cells treated with lower concentrations of CP-91149 were arrested in the G₀/G₁ phase, and cells treated with 100 μM CP-91149 were arrested in the S phase (**Fig. 14**). Therefore, our data indicates that CP-91149 induces concentration-dependent cell cycle alterations in HepG2 cells.

We measured reactive oxygen species (ROS) levels as a marker to study oxidative stress. The ROS-reactive fluorescent probe, 2',7'-dichlorodihydrofluorescein diacetate (H₂DCFDA), was used to determine ROS level in the cell. The number of HepG2 cells with higher ROS levels increased upon CP-91149 treatment, as evident by the rightward shift of the curve (**Fig. 15**) and quantification of fluorescence intensity (**Fig. 16**).

3.1.3 Determination of the molecular mechanism of cell death following CP-91149 incubation in HepG2 cells

Based on the morphological observations of HCC cells upon CP-91149 treatment, we hypothesized apoptosis as the primary cell death mechanism and probed HCC cells with various markers of apoptosis. We performed annexin V-FITC/propidium iodide (PI) staining and flow cytometric analysis of HCC cells. During the early phase of apoptosis, phosphatidylserine is translocated from the cytosolic side to the plasma membrane's cell surface. This translocation exposes phosphatidylserine to the extracellular environment with the plasma membrane left intact. Annexin V protein has a high affinity and

specificity for PS and can be used as a marker of early apoptosis. Annexin V can be used with reagents that determine the integrity of the cell membrane, such as propidium iodide, to rule out "leaky" necrotic cells (Vermes et al., 1995). The number of HepG2 cells in the early apoptotic phase (lower right quadrant) increased significantly upon CP-91149 treatment (**Fig. 17 and 18**).

We wanted to decipher the signaling pathway of apoptosis upon glycogen perturbations in HepG2 cells. Mitochondrial dysfunction and mitochondrial outer membrane permeabilization (MOMP), a process that leads to the leakage of mitochondrial intermembrane space proteins, often precedes the intrinsic pathway of apoptosis (Green & Kroemer, 2004). First, we measured the mitochondrial membrane potential (MMP) using MitoTracker Red CMXRos dye, the accumulation of which in the mitochondria is dependent upon MMP. We utilized carbonyl cyanide m-chlorophenyl hydrazine (CCCP), a protonophore uncoupler of oxidative phosphorylation, as a positive control known to dissipate MMP. Flow cytometric analysis revealed that MMP decreased significantly upon CP-91149 treatment in HepG2 cells (**Fig. 19**).

Under the influence of many apoptotic stimuli, BAX moves from cytosol to mitochondria and forms oligomeric pores on the mitochondrial outer membrane (M. Zhang et al., 2017). This results in mitochondrial outer membrane permeabilization many and cytochrome release from mitochondria to cytosol. When the concentration of cytochrome C in the cytosol reaches cytotoxic levels, it activates caspase-9 and caspase-3 and eventually kills the cells by apoptosis (Garrido et al., 2006). We performed subcellular fractionation of HepG2 cells and probed for the apoptotic markers in the mitochondrial and the cytosolic fractions using COX-IV and α -tubulin expression to assess the purity of

the fractions, respectively. Upon CP-91149 treatment, the expression of Bax decreased in the cytosolic fraction and increased in the mitochondrial fraction (**Fig. 20 and 21**), whereas the expression of cytochrome c increased in the cytosolic fraction and decreased in the mitochondrial fraction (**Fig. 20 and 22**). The changes in cytochrome c localization increased the expression level of cleaved caspase-9 (**Fig. 23 and 25**), cleaved caspase-3 (**Fig. 23 and 24**), and a modest increase in cleaved caspase-8 (**Fig. 2 and 26**), indicating intrinsic apoptosis as an underlying mechanism involved in CP-91149 induced HepG2 cell death.

3.1.4 Determination of the synergistic effect of CP-91149 with sorafenib and regorafenib

Sorafenib and regorafenib are first-line and second-line drug treatments for advanced-stage hepatocellular carcinoma (Ikeda et al., 2018). The combinations of CP-91149 with various inhibitors for their synergy profiles were determined by the Chou-Talalay method combination index numbers. A number less than 1 indicates synergy, 1 indicates no effect, and a number greater than 1 indicates antagonism (Chou, 2010). CP-91149 combinations were synergistic with the multikinase inhibitors sorafenib (**Fig. 27 and 29**) and regorafenib (**Fig. 28 and 29**). The combinations of CP-91149 with 2-DG, and 3-BP were not synergistic, indicating that they possibly target the same or similar signaling pathway(s). The combination of CP-91149 with 6-AN was synergistic only at higher concentrations of CP-91149 employed (Barot et al., 2019).

3.2.1 Determination of the effect of CP-91149 on glycogen levels and expression of glycogen-metabolic proteins

We wanted to measure the impact of glycogen phosphorylase inhibition by CP-91149 on the levels of glycogen in HepG2 cells. The quantity of glycogen in HepG2 was

determined by converting glycogen to glucose using the amyloglucosidase enzyme. The amount of glucose is measured by converting glucose to glucose-6-phosphate (G6P) and then oxidizing to 6-phospho-gluconate in the presence of NAD. HepG2 cells were transfected with *protein targeting to glycogen* (PTG) as a positive control in reaction as it is known to increase glycogen level in cells by increasing protein phosphatase 1 activity against glycogen-metabolizing (Greenberg et al., 2003). Incubation of HepG2 cells with 75 μ M of CP-91149 for 24 hours resulted in increased glycogen content in cells (**Fig. 30**). We also measured the expression and post-translation modification of proteins involved in the glycogen metabolism. Phosphorylation of glycogen synthase on various sites like serine 8, 11, 627, 641, 645, 649, 653, 657, 683 causes decreases in its activity (J. Jensen & Lai, 2009; Roach, 1990). CP-91149 incubation with HepG2 cells for 24 hours showed decrease glycogen synthase phosphorylation which residue? (**Fig. 31 and 32**) and glycogen phosphorylase expression (**Fig. 31 and 33**) in a concentration-dependent manner (50, 75, or 100 μ M).

3.2.2 Determination of the effect of CP-91149 on proteins involved in energy homeostasis and glucose uptake

AMP-activated protein kinase (AMPK) is a heterotrimeric protein complex responsible for monitoring cellular energy status by sensing the concentrations of AMP (Hardie et al., 2012). Activation of AMPK restores energy balance in cell by activating catabolic pathways and inhibiting anabolic pathways (Herzig & Shaw, 2018). HepG2 cells incubation with different concentrations of CP-91149 (50, 75, or 100 μ M) decreased expression and increased phosphorylation of AMPK protein (**Fig. 34 and 35**). Pyruvate dehydrogenase (PDH) is an essential protein that acts as a gatekeeper for carbon flux

between glycolysis and tricarboxylic acid (TCA) cycle of a cell. Phosphorylation of PDH causes a decrease in its activity and reduction of carbon flux towards the TCA cycle (Haan et al., 2016). Incubation of HepG2 cells with different concentrations of CP-91149 (50, 75, or 100 μ M) for 24 hours increased the expression of PDH with no significant change in its phosphorylation (**Fig. 34 and 36**). We also determined the impact of CP-91149 mediated glycogen phosphorylase inhibition on glucose uptake in HepG2 cells by radiometric assays. Incubation of CP-91149 (75 μ M) with HepG2 cells for 4 hours, 16 hours, and 24 hours did not change the uptake of glucose (**Fig. 37-39**). Antidiabetic drug metformin (5 mM) was used as a positive control.

3.2.3 Determination of the effect of CP-91149 on glycolysis in HepG2 cells

The effect of CP-91149 on glycolysis was measured by glycolysis stress test using Seahorse XF analyzer. The machine measures net production and extrusion of protons into the extracellular medium during the conversion of glucose to pyruvate and subsequently to lactate. The acidification rate of media is reported as extracellular acidification rate (ECAR).

The assay involves measurement of ECAR by HepG2 cells incubated in the glycolysis stress test medium without glucose or pyruvate. The machine injects saturating concentration of glucose to glycolysis stress media. At this point HepG2 cells utilize glucose and catabolize it through the glycolytic pathway to pyruvate, producing ATP, NADH, and protons. The extrusion of protons into the surrounding medium causes a rapid decrease in pH. Seahorse XF analyzer reports this glucose-induced response as the rate of glycolysis under basal conditions.

Seahorse XF analyzer injects oligomycin, an ATP synthase inhibitor, as a second injection. Oligomycin blocks mitochondrial ATP production. At this point, HepG2 cells are dependent on glycolysis for energy production. This further decrease pH of glycolysis stress media and reveals the cellular maximum glycolytic capacity.

Seahorse XF analyzer finally injects hexokinase inhibitor 2-deoxy-glucose (2-DG). 2-DG inhibits glycolysis by inhibiting hexokinase. Seahorse XF analyzer measures an increase in pH and confirms the ECAR produced in the experiment is due to glycolysis. The difference between glycolytic capacity and glycolysis rate is termed as a glycolytic reserve. ECAR, prior to glucose injection, is termed as non-glycolytic acidification. This is caused by processes in the cell other than glycolysis.

HepG2 cells were incubated with CP-91149 (25 or 50 μ M) for 16 hours. Cell culture media was replaced with manufacturer-recommended media containing the appropriate concentration of CP-91149, and ECAR was measured as per manufacturer's protocol. CP-91149 incubation did not impact glycolysis and non-glycolytic acidification of HepG2 cells significantly in line with no increase in glucose uptake (**Fig. 40 and 41**) (**Fig. 40 and 42**). Inhibition of glycogen phosphorylase has shown to reduce expression of glycolytic proteins like glyceraldehyde-3-phosphate dehydrogenase, phosphoglycerate mutase 1, alpha-enolase briefly (Ma et al., 2012). CP-91149 incubation reduced glycolytic capacity (**Fig. 40 and 43**) and glycolytic reserve (**Fig. 40 and 44**) of HepG2 cells at 50 μ M concentration.

3.2.4 Determination of the effect of CP-91149 on oxygen consumption rate (OCR) and expression of proteins involved in mitochondrial dynamics in HepG2 cells

The effect of CP-91149 on mitochondria was determined by measuring the oxygen consumption rate (OCR) of HepG2 cells using Seahorse XF analyzer. The seahorse machine uses the built-in injection ports on XF sensor cartridges to add modulators of respiration like oligomycin, FCCP, rotenone, and antimycin into the cell well during the assay to reveal the key parameters of mitochondrial function.

HepG2 cells were incubated with CP-91149 (25 or 50 μM) for 16 hours. Cell culture media was replaced with manufacturer-recommended media containing the appropriate concentration of CP-91149, and OCR was measured as per manufacturer's protocol. The machine first measures basal respiration, which is an indication of the energetic demand of the cell under baseline conditions. CP-91149 treatment showed a reduction in basal oxygen consumption of HepG2 cells in a dose-dependent manner (**Fig. 45 and 46**).

The seahorse machine then injects oligomycin, an ATP synthase inhibitor. This causes a reduction in OCR linked to ATP generation by mitochondria. Reduction in OCR upon oligomycin injection represents basal oxygen consumption linked to ATP production and H^+ (Proton) leak. CP-91149 treatment showed a reduction in ATP production by HepG2 cells in a dose-dependent manner (**Fig. 45 and 47**). CP-91149 treatment showed a reduction in proton leak at 25 μM concentration but had no impact at 50 μM concentration in HepG2 cells (**Fig. 45 and 48**). Oxygen consumption that persists after inhibition of all mitochondrial complexes is due to a subset of cellular enzymes consuming oxygen for processes other than mitochondrial energy generation. CP-91149

treatment reduced non-mitochondrial oxygen consumption in HepG2 cells (**Fig. 45 and 49**).

We have observed mitochondrial dysfunction by CP-91149 treatment in HepG2 cells. Therefore, we wanted to assess the effect of CP-91149 incubation on mitochondrial dynamics in HepG2 cells. We used MFN-1 as mitochondrial fusion marker and DRP-1 as mitochondrial fission marker (Yu et al., 2020). We used MDIVI-1, a known DRP-1 inhibitor, and mitochondrial fusion promoter, M1, as a positive control (Bordt et al., 2017; Ding et al., 2020). Incubation of HepG2 cells with CP-91149 for 24 hours reduced expression of DRP-1 in a dose-dependent manner (**Fig. 50 and 51**) and expression of MFN-1 only at 100 μ M concentration (**Fig. 50 and 52**).

Next, we performed morphological analysis of HepG2 cells following CP-91149 treatment by transmission electron microscopy (TEM) and scanning electron microscopy (SEM) to reveal ultrastructural changes by this treatment. During the execution phase of apoptosis, marked changes in cell morphology like membrane blebbing are seen. It is believed that contractile force generated by actin-myosin cytoskeleton drives the formation of membrane blebs and apoptotic bodies (Coleman et al., 2001). Incubation of HepG2 cells with 50 μ M of CP-91149 showed blebbing (**Fig. 53**), indicating cells undergoing apoptosis.

3.2.5 Metabolomic analysis of HepG2 cells following CP-91149 treatment

We wanted to determine the impact of glycogen phosphorylase inhibition and observed induction of apoptosis on various metabolic pathways. 50 μ M treatment of CP-91149 for 16 hours caused alteration in many metabolic pathways in HepG2 cells (**Fig. 54**). Among this pentose phosphate pathway (PPP) was affected the most. Concentrations of many

intermediates were changed significantly (**Fig. 55-60**). D-glucose-6-phosphate acts as the connecting point of many metabolic pathways. CP-91149 treatment showed a significant reduction in levels of glucose-6-phosphate after 16 hours of treatment (**Fig. 61**). Apart from these, levels of nucleotides like ADP and AMP were high in CP-91149 treated groups compared to control (appendix-2)

3.2.6 Effect of CP-91149 on the growth of 3-D spheroids of HepG2 cells

3D spheroids of HepG2 cells were grown by seeding cells at a density of 2000 cells/well in an ultra-low attachment, round bottom 96-well plate. The growth of HepG2 3D spheroids was determined by calculating surface area. Cells were grown over a period of 12 days and media was replaced with a fresh medium containing an appropriate concentration of CP-91149 every 48 h. CP-91149 treatment caused a reduction in the growth of HepG2 spheroids in a dose-dependent manner (**Fig. 62 and 63**). On the 12th day a live/dead assay was performed in spheroids by visualizing cells stained by ethidium homodimer-1 and calcein-AM fluorescent dyes. Calcein AM is a cell-permeant dye that gives green fluorescence after getting hydrolyzed by intracellular esterase of live cells. Ethidium homodimer-1 is a positively charged membrane-impermeable dye that gives red fluorescence after binding to DNA of dead cells. CP-91149 treatment showed less green fluorescence intensity compared to control. This indicates fewer numbers of viable cells in CP-91149 treated spheroids compared to control (**Fig. 64**).

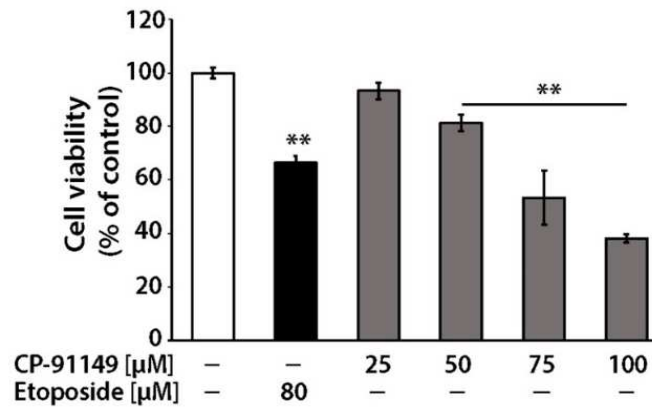


Figure 9: CP-91149 treatment reduces viability of HepG2 cells.

HepG2 Cell viability was determined by MTT assay following 24 hours incubation with CP-91149 (0, 25, 50, 75, or 100 μM). Anticancer drug etoposide (80 μM) was used as a positive control. Data represent mean percent of control ± SEM. Results were analyzed by one-way ANOVA followed by Dunnett’s multiple comparison post-hoc test.

Representative graph of n = 3, **p < 0.01

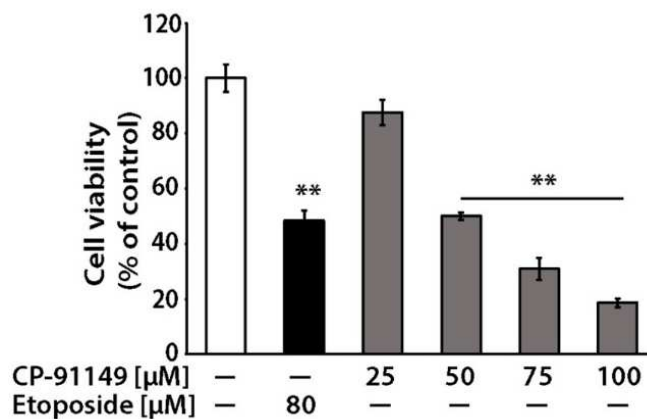


Figure 10 : CP-91149 treatment reduces viability of Hep3B cells.

Hep3B Cell viability was determined by MTT assay following 24 hours incubation with CP-91149 (0, 25, 50, 75, or 100 μM). Anticancer drug etoposide (80 μM) was used as a positive control. Data represent mean percent of control ± SEM. Results were analyzed by one-way ANOVA followed by Dunnett's multiple comparison post-hoc test.

Representative graph of n = 3, **p < 0.01

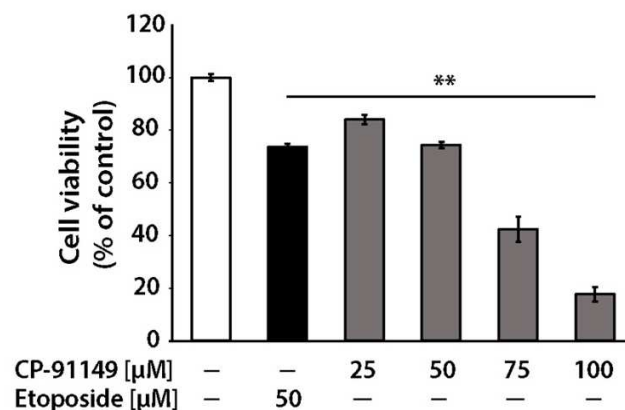


Figure 11: CP-91149 treatment reduces viability of H4IIE cells.

H4IIE Cell viability was determined by MTT assay following 24 hours incubation with CP-91149 (0, 25, 50, 75, or 100 μM). Anticancer drug etoposide (50 μM) was used as a positive control. Data represent mean percent of control ± SEM. Results were analyzed by one-way ANOVA followed by Dunnett's multiple comparison post-hoc test.

Representative graph of n = 3, **p < 0.01

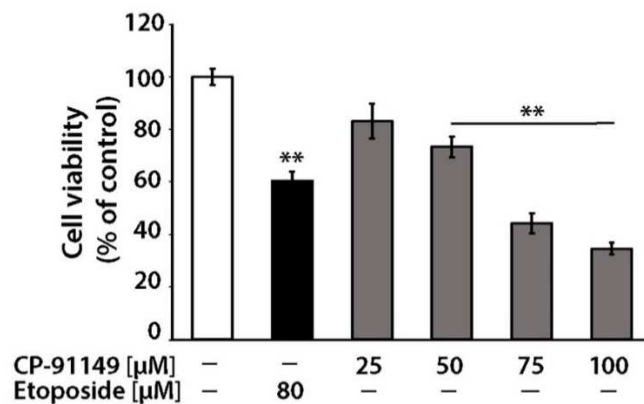


Figure 12: CP-91149 treatment reduces viability of HepG2 cells.

HepG2 Cell viability was determined by neutral red dye uptake assay following 24 hours incubation with CP-91149 (0, 25, 50, 75, or 100 μM). Anticancer drug etoposide (80 μM) was used as a positive control. Data represent mean percent of control ± SEM. Results were analyzed by one-way ANOVA followed by Dunnett's multiple comparison post-hoc test. Representative graph of n = 3, **p < 0.01

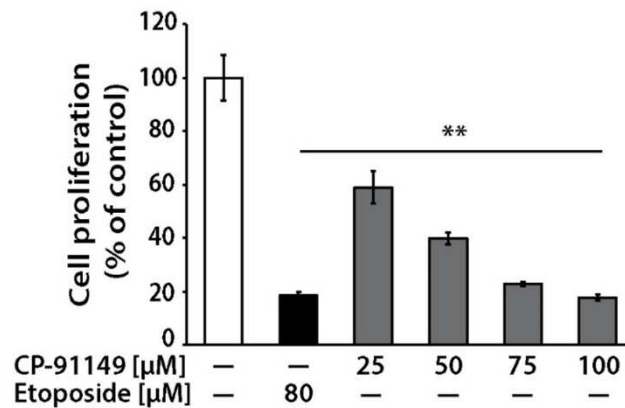


Figure 13: CP-91149 treatment reduces proliferation of HepG2 cells.

HepG2 Cell proliferation was determined by CyQuant assay following 48 hours incubation with CP-91149 (0, 25, 50, 75, or 100 μM). Anticancer drug etoposide (80 μM) was used as a positive control. Data represent mean percent of control ± SEM. Results were analyzed by one-way ANOVA followed by Dunnett's multiple comparison post-hoc test. Representative graph of n = 3, **p < 0.01

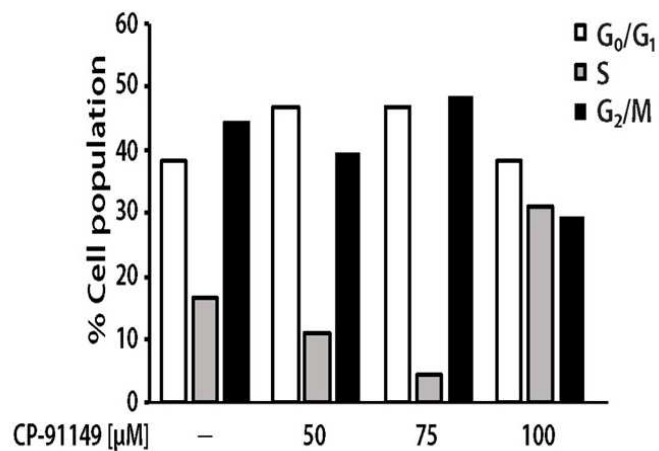


Figure 14: CP-91149 treatment causes cell cycle disturbance in HepG2 cells.

Cell cycle analysis was determined by propidium iodide form-based flow cytometric assay following 24 hours incubation of CP-91149 (0, 50, 75, or 100 μM). Data represent mean percent of total cells. The experiment was repeated to confirm the results.

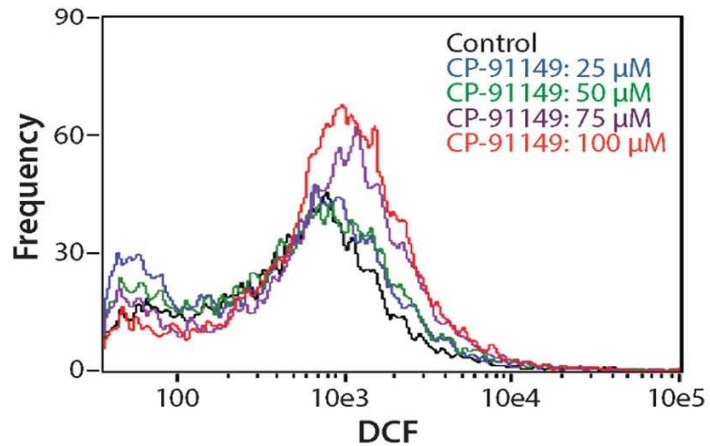


Figure 15: CP-91149 treatment increases reactive oxygen species level in HepG2 cells.

Levels of reactive oxygen species in HepG2 cells was determined by measuring the oxidation of CM-H₂DCFDA using a flow cytometer. Cells were incubated with different concentrations of CP-91149 (0, 25, 50, 75, or 100 μM) for 24 hours. Representative graph of n = 3. (Experiment conducted by Ehab M. Abo Ali)

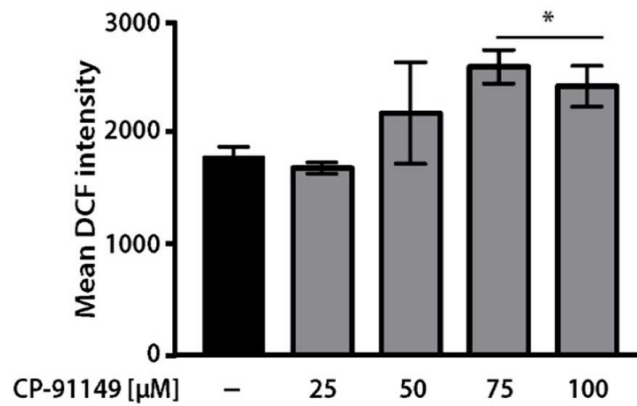


Figure 16: CP-91149 treatment increases reactive oxygen species level in HepG2 cells.

Levels of reactive oxygen species in HepG2 cells was quantified by measuring the oxidation of CM-H₂DCFDA using a flow cytometer. Cells were incubated with different concentrations of CP-91149 (0, 25, 50, 75, or 100 μM) for 24 hours. Results were analyzed by one-way ANOVA followed by Dunnett's multiple comparison post-hoc test. Representative graph of n = 3, *p < 0.05 (Experiment conducted by Ehab M. Abo Ali)

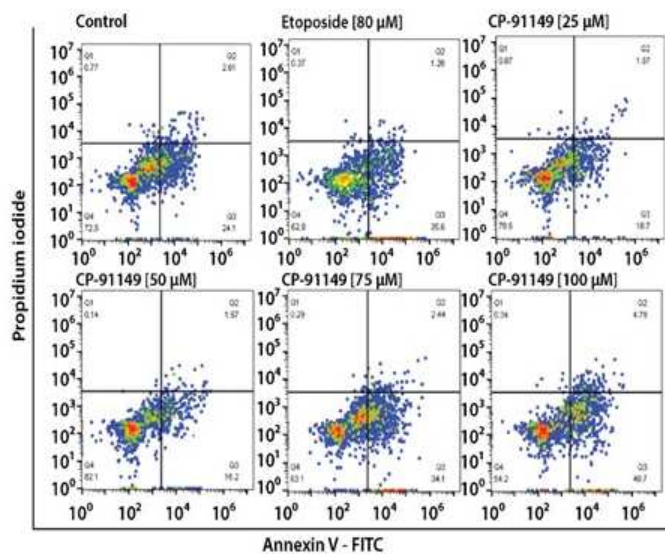


Figure 17: CP-91149 causes cell death in HepG2 cell via apoptosis.

Stage of apoptosis of HepG2 cells following 24 hours incubation with CP-91149 was categorized based on the dye uptake as follows: viable cells (negative for annexin-V and PI), early apoptotic cells (positive for annexin-V only), late apoptotic cells (positive for both annexin-V and PI), and necrotic cells (positive for PI only) using a flow cytometer. Cells were incubated with different concentrations of CP-91149 (0, 25, 50, 75, or 100 μM) for 24 hours. Anticancer drug etoposide (80 μM) was used as a positive control. Representative image of n = 4 (Experiment conducted by Ehab M. Abo Ali)

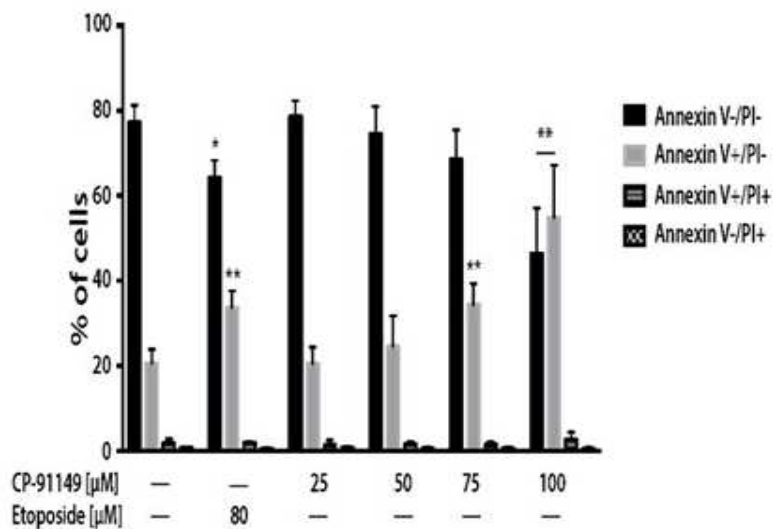


Figure 18: CP-91149 causes cell death in HepG2 cell via apoptosis.

Quantification of state apoptosis of HepG2 cells following 24 hours incubation with CP-91149 was done based on the dye uptake as follows: viable cells (negative for annexin-V and PI), early apoptotic cells (positive for annexin-V only), late apoptotic cells (positive for both annexin-V and PI), and necrotic cells (positive for PI only) using a flow cytometer. Cells were incubated with different concentrations of CP-91149 (0, 25, 50, 75, or 100 μM) for 24 hours. Anticancer drug etoposide (80 μM) was used as a positive control. Results were analyzed by one-way ANOVA followed by Dunnett’s multiple comparison post-hoc test. Representative graph of n = 4, *p < 0.05, **p < 0.01.

(Experiment conducted by Ehab M. Abo Ali)

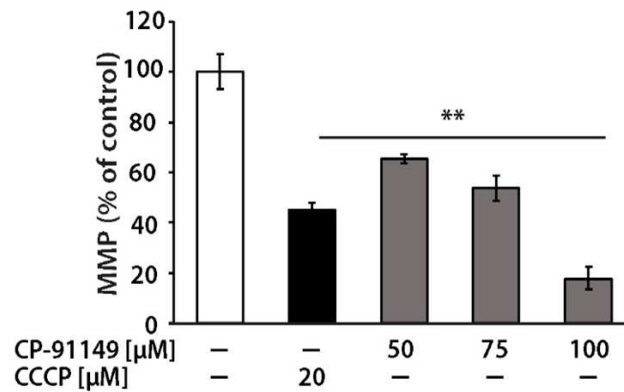


Figure 19: CP-91149 treatment reduces mitochondrial membrane (MMP) potential in HepG2 cells.

MMP of HepG2 cells was determined using MitoTracker Red CMXRos dye. Cells were incubated with different concentrations of CP-91149 (0, 25, 50, 75, or 100 µM) for 24 hours. CCCP, an uncoupler of oxidative phosphorylation (20 µM), was used as a positive control. Results were analyzed by one-way ANOVA followed by Dunnett's multiple comparison post-hoc test. Representative graph of n = 3, **p < 0.01.

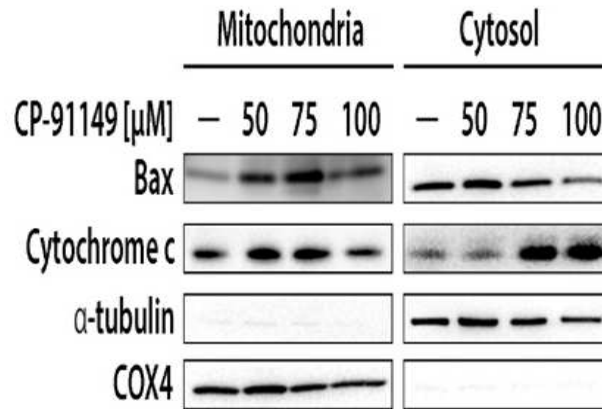


Figure 20: CP-91149 treatment promotes intrinsic apoptosis by changing mitochondrial and cytosolic localization of cytochrome c and BAX in HepG2 cells.

Expression of indicated proteins in the mitochondrial and cytosolic fractions obtained from HepG2 cell lysates was determined using western blot analysis. Cells were incubated with different concentrations of CP-91149 (0, 50, 75, or 100 μ M) for 24 hours. COX-4 and tubulin were used to show the relative purity of fractions. Representative image of n = 3.

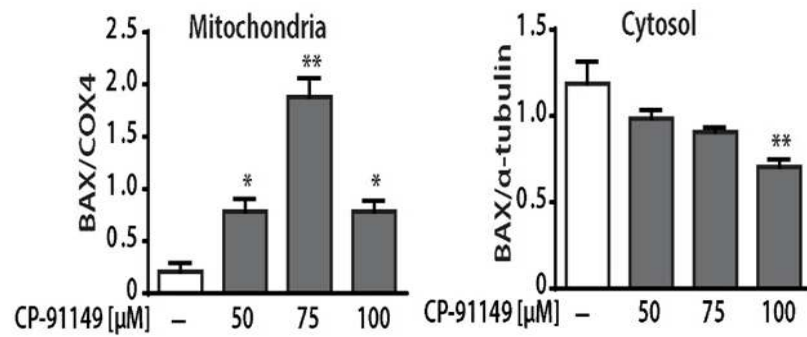


Figure 21: CP-91149 treatment promotes BAX localization from cytosol to mitochondria in HepG2 cells.

Expression of BAX protein in the mitochondrial and cytosolic fractions obtained from HepG2 cell lysates was quantified using ImageJ software from western blot images. Cells were incubated with different concentrations of CP-91149 (0, 50, 75, or 100 μM) for 24 hours. Results were analyzed by one-way ANOVA followed by Dunnett's multiple comparison post-hoc test. n = 3, *p < 0.05, **p < 0.01.

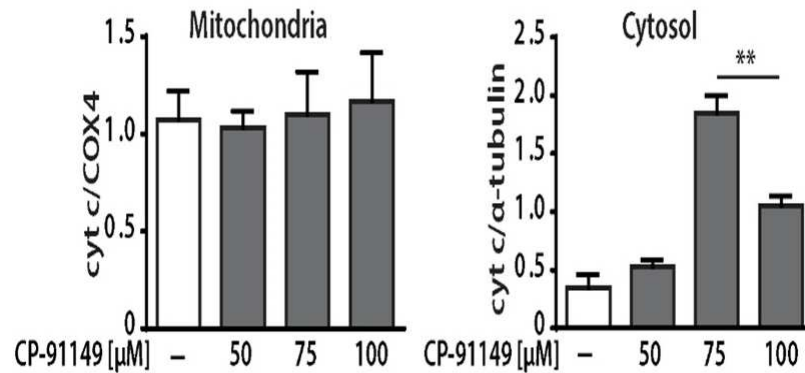


Figure 22: CP-91149 treatment induces cytochrome c release from mitochondria to cytosol in HepG2 cells.

Expression of cytochrome c protein in the mitochondrial and cytosolic fractions of HepG2 cells from western blot images lysates was quantified using NIH ImageJ software. Cells were incubated with different concentrations of CP-91149 (0, 50, 75, or 100 μM) for 24 hours. Results were analyzed by one-way ANOVA followed by Dunnett's multiple comparison post-hoc test. n = 3, *p < 0.05, **p < 0.01.

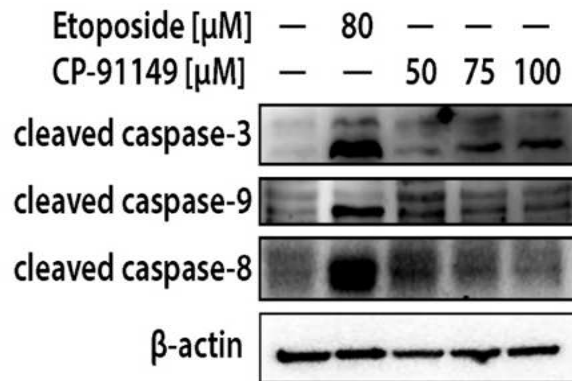


Figure 23: CP-91149 treatment activates intrinsic apoptotic cascade in HepG2 cells.

Expression of indicated proteins obtained from HepG2 cell lysates was determined using western blot analysis. Cells were incubated with different concentrations of CP-91149 (0, 50, 75, or 100 μM) for 24 hours. Anticancer drug etoposide (80 μM) was used as a positive control. Representative image of $n = 3$.

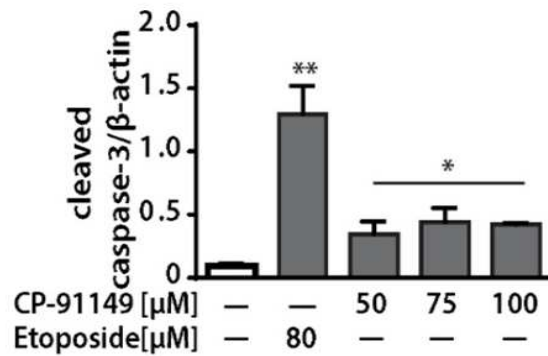


Figure 24: CP-91149 treatment induces apoptosis by increasing cleaved caspase 3 expression in HepG2 cells.

Quantification of cleaved caspase-3 protein expression was determined from western blot images obtained from HepG2 cell lysates. Cells were incubated with different concentrations of CP-91149 (0, 50, 75, or 100 μM) for 24 hours. Anticancer drug etoposide (80 μM) was used as a positive control. Results were analyzed by one-way ANOVA followed by Dunnett's multiple comparison post-hoc test. n = 3, *p < 0.05, **p < 0.01.

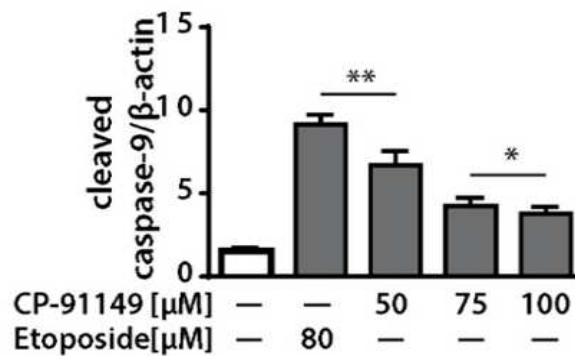


Figure 25: CP-91149 treatment activates intrinsic apoptosis by increasing cleaved caspase 9 expression in HepG2 cells.

Quantification of cleaved caspase-9 protein expression was determined from western blot images obtained from HepG2 cell lysates. Cells were incubated with different concentrations of CP-91149 (0, 50, 75, or 100 μM) for 24 hours. Anticancer drug etoposide (80 μM) was used as a positive control. Results were analyzed by one-way ANOVA followed by Dunnett's multiple comparison post-hoc test. n = 3, *p < 0.05, **p < 0.01.

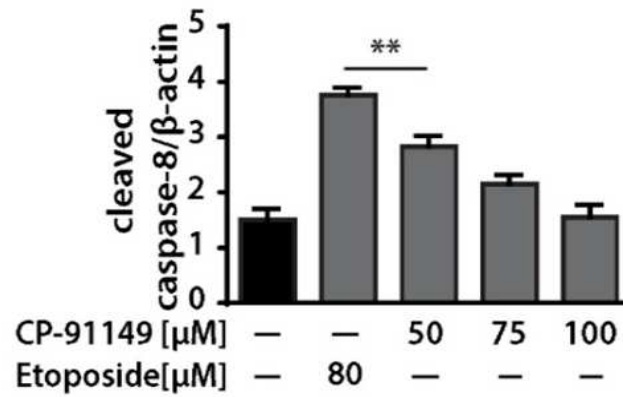


Figure 26: CP-91149 treatment has not much impact on cleaved caspase 8 activation in HepG2 cells.

Quantification of the cleaved caspase-8 protein expression was determined from western blot images obtained from HepG2 cell lysates. Cells were incubated with different concentrations of CP-91149 (0, 50, 75, or 100 μ M) for 24 hours. Anticancer drug etoposide (80 μ M) was used as a positive control. Results were analyzed by one-way ANOVA followed by Dunnett's multiple comparison post-hoc test. $n = 3$, $**p < 0.01$

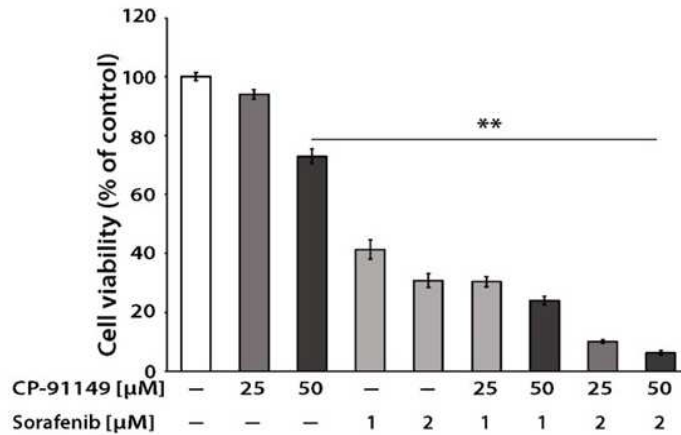


Figure 27: CP-91149 treatment potentiates action of multi-kinase inhibitor sorafenib in HepG2 cells.

The synergistic effect of CP-91149 on sorafenib was determined by measuring the viability of HepG2 cells following 24 hours incubation of CP-91149 (0, 25, or 50 µM) and Sorafenib (0, 1, or 2 µM) via MTT assay. Data represent mean percent of control ± SEM. Results were analyzed by one-way ANOVA followed by Dunnett's multiple comparison post-hoc test. Representative graph of n = 3, **p < 0.01

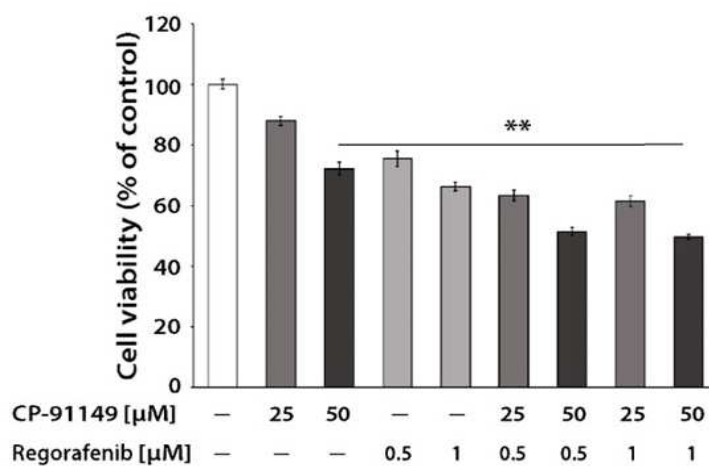


Figure 28: CP-91149 treatment potentiates action of multi-kinase inhibitor regorafenib in HepG2 cells.

The synergistic effect of CP-91149 on regorafenib was determined by measuring the viability of HepG2 cells following 24 hours incubation of CP-91149 (0, 25, or 50 μM) and Regorafenib (0, 0.5, or 1 μM) via MTT assay. Data represent mean percent of control \pm SEM. Results were analyzed by one-way ANOVA followed by Dunnett's multiple comparison post-hoc test. Representative graph of $n = 3$, $**p < 0.01$

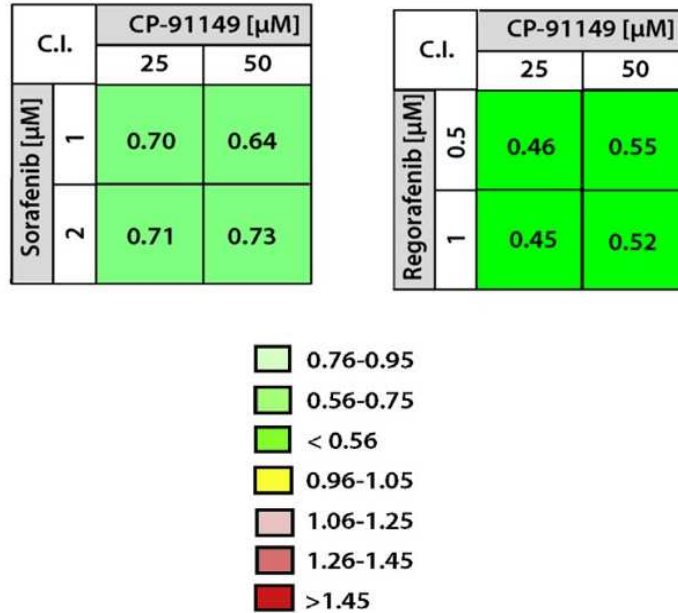


Figure 29: CP-91149 treatment potentiates action of multi-kinase inhibitors sorafenib and regorafenib in HepG2 cells.

Combination index values of sorafenib and regorafenib with CP-91149 were calculated by the Chou-Talalay method using CompuSyn software. A number lesser than 1 indicates synergy (green), 1 indicates no effect (yellow), and a number greater than 1 indicates antagonism (red).

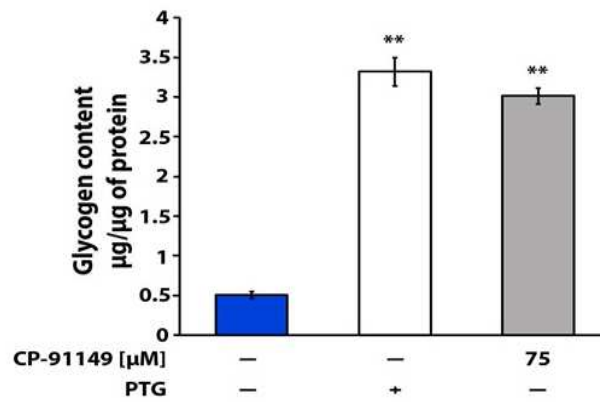


Figure 30: CP-91149 treatment increases glycogen level in HepG2 cells.

Glycogen content in HepG2 cells was determined using Glucose (HK) Assay Kit. Cells were treated with CP-91149 (75 µM) or were transfected with PTG (protein targeting glycogen) plasmid as a positive control. Results were analyzed by one-way ANOVA followed by Dunnett's multiple comparison post-hoc test. Representative graph of n = 3, **p < 0.01

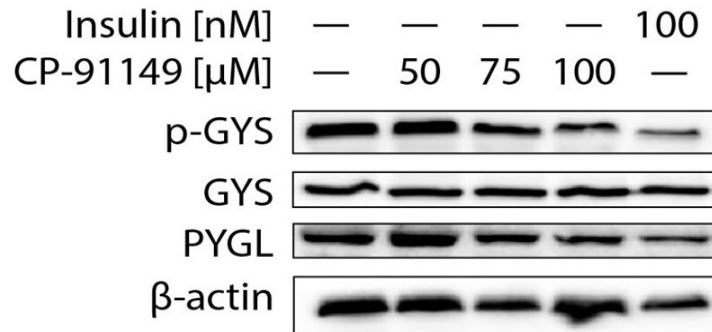


Figure 31: CP-91149 treatment activates glycogen anabolic pathway in HepG2 cells.

Expression of indicated proteins obtained from HepG2 cell lysates was determined using western blot analysis. Cells were incubated with different concentrations of CP-91149 (0, 50, 75, or 100 μM) for 24 hours. Insulin (100 nM) was used as a positive control.

Representative image of n = 3.

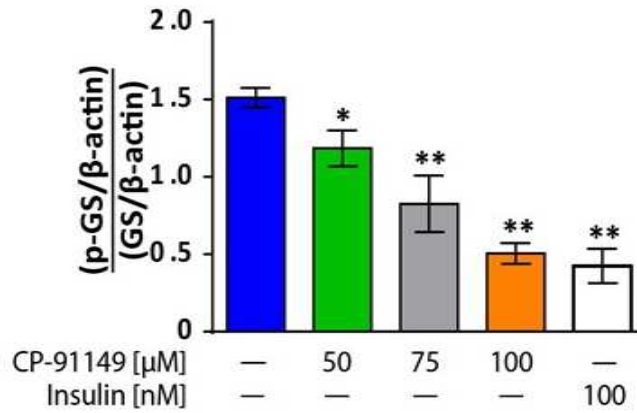


Figure 32: CP-91149 treatment activates glycogen synthase by decreasing its phosphorylation in HepG2 cells.

Quantification of glycogen synthase protein's phosphorylation was determined from western blot images obtained from HepG2 cell lysates. Cells were incubated with different concentrations of CP-91149 (0, 50, 75, or 100 μM) for 24 hours. Insulin (100 nM) was used as a positive control. Results were analyzed by one-way ANOVA followed by Dunnett's multiple comparison post-hoc test. n = 3, *p < 0.05, **p < 0.01.

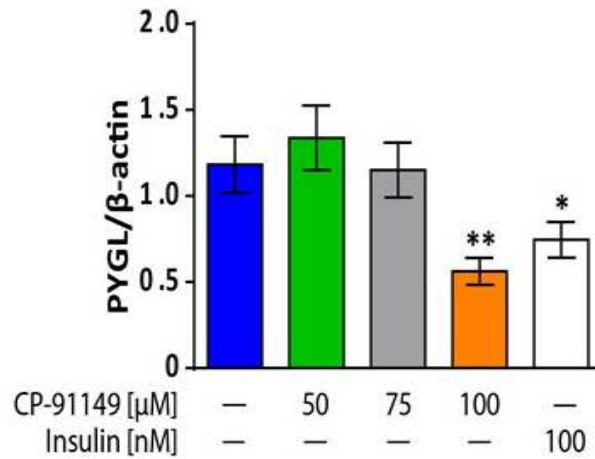


Figure 33: High dose of CP-91149 treatment reduces glycogen phosphorylase expression in HepG2 cells.

Quantification of expression of glycogen phosphorylase from western blot images obtained from HepG2 cell lysates. Cells were incubated with different concentrations of CP-91149 (0, 50, 75, or 100 μM) for 24 hours. Insulin (100 nM) was used as a positive control. Results were analyzed by one-way ANOVA followed by Dunnett's multiple comparison post-hoc test. n = 3, *p < 0.05, **p < 0.01.

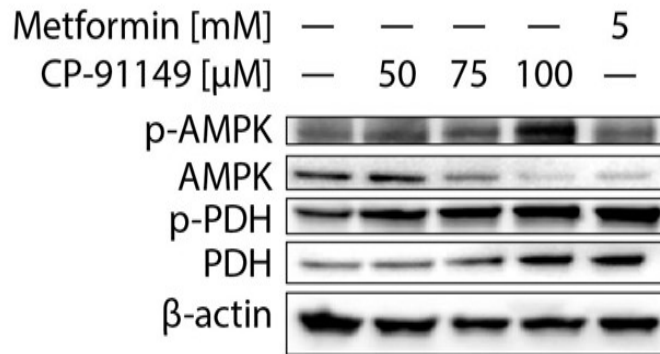


Figure 34: CP-91149 treatment activates AMP-activated protein kinase (AMPK) by increasing its phosphorylation in HepG2 cells.

Expression of indicated proteins from HepG2 cell lysates was determined using western blot analysis. Cells were incubated with different concentrations of CP-91149 (0, 50, 75, or 100 μM) for 24 hours. Antidiabetic drug metformin (5 mM) was used as a positive control. Representative images of n = 3.

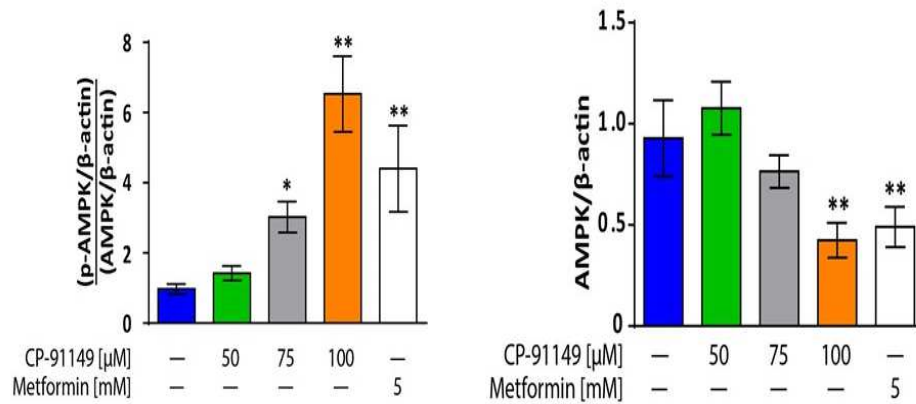


Figure 35: CP-91149 treatment activates AMPK by increasing its phosphorylation in HepG2 cells.

Quantification of expression and phosphorylation of AMPK protein from western blot images. HepG2 cells were incubated with different concentrations of CP-91149 (0, 50, 75, or 100 μM) for 24 hours. Antidiabetic drug metformin (5mM) was used as a positive control. Results were analyzed by one-way ANOVA followed by Dunnett's multiple comparison post-hoc test. n = 3, *p < 0.05, **p < 0.01.

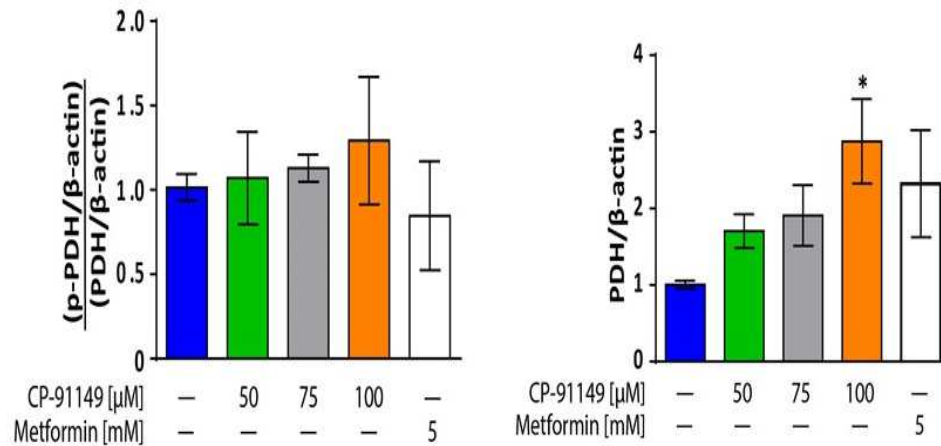


Figure 36: CP-91149 treatment increases expression of pyruvate dehydrogenase (PDH) but has no impact on its phosphorylation level in HepG2 cells.

Quantification of phosphorylation and expression of PDH protein from western blot images obtained from HepG2 cell lysates. Cells were incubated with different concentrations of CP-91149 (0, 50, 75, or 100 μM) for 24 hours. Antidiabetic drug metformin (5mM) was used as a positive control. Results were analyzed by one-way ANOVA followed by Dunnett's multiple comparison post-hoc test. n = 3, *p < 0.05.

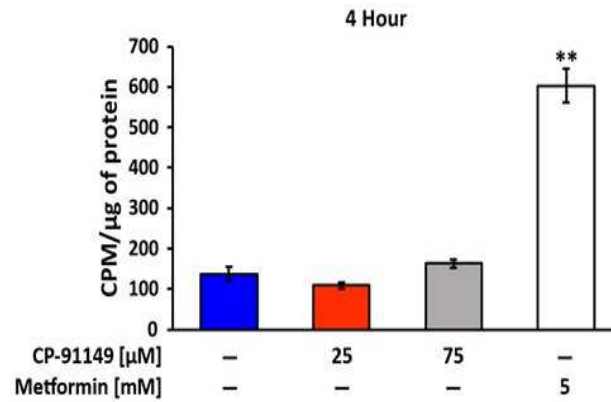


Figure 37: CP-91149 treatment has no impact on glucose uptake of HepG2.

Glucose uptake by HepG2 cells following 4 hours of incubation with CP-91149 (75 μM) was determined using radiolabeled glucose analog (2-deoxy-D-glucose). Antidiabetic drug metformin (5 mM, 24 hours incubation) was used as a positive control. Results were analyzed by one-way ANOVA followed by Dunnett's multiple comparison post-hoc test. n = 3, *p < 0.05.

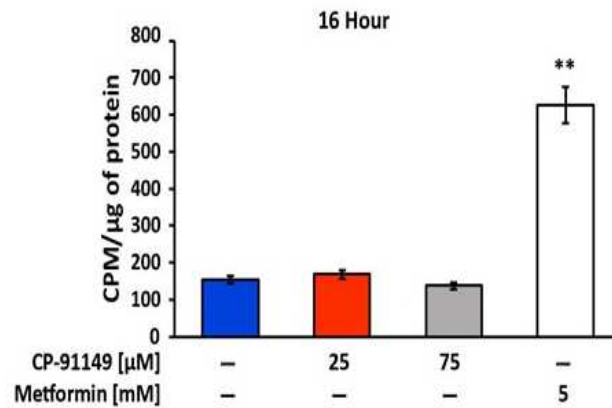


Figure 38: CP-91149 treatment has no impact on glucose uptake of HepG2.

Glucose uptake by HepG2 cells following 16 hours of incubation with CP-91149 (75 μM) was determined using radiolabeled glucose analog (2-deoxy-D-glucose). Antidiabetic drug metformin (5 mM, 24 hours incubation) was used as a positive control. Results were analyzed by one-way ANOVA followed by Dunnett's multiple comparison post-hoc test. $n = 3$, $*p < 0.05$.

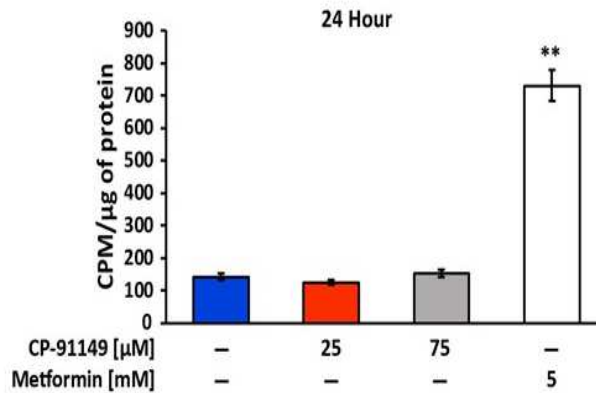


Figure 39: CP-91149 treatment has no impact on glucose uptake of HepG2.

Glucose uptake by HepG2 cells following 24 hours of incubation with CP-91149 (75 μM) was determined using radiolabeled glucose analog (2-deoxy-D-glucose). Antidiabetic drug metformin (5 mM, 24 hours incubation) was used as a positive control. Results were analyzed by one-way ANOVA followed by Dunnett's multiple comparison post-hoc test. $n = 3$, $*p < 0.05$.

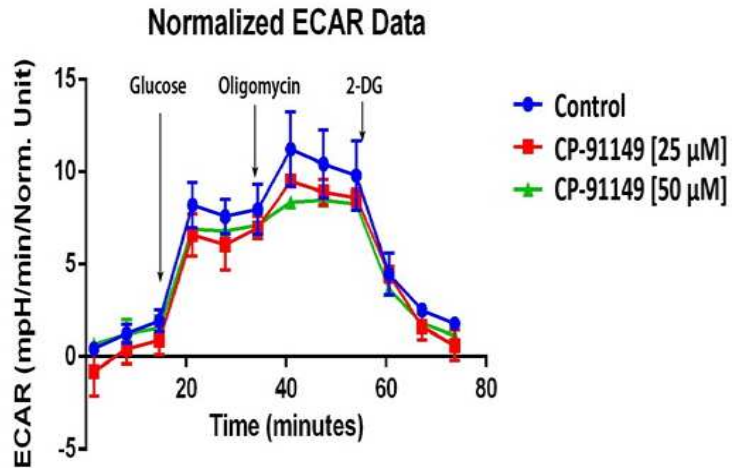


Figure 40: CP-91149 treatment has no impact on glycolysis but reduces glycolytic capacity of HepG2 cells.

Extracellular acidification rate (ECAR) of HepG2 cells was determined by Seahorse XF Analyzer following 16 hours of incubation with CP-91149 (25, or 50 μ M) was measured using Seahorse XF Analyzer. n = 3.

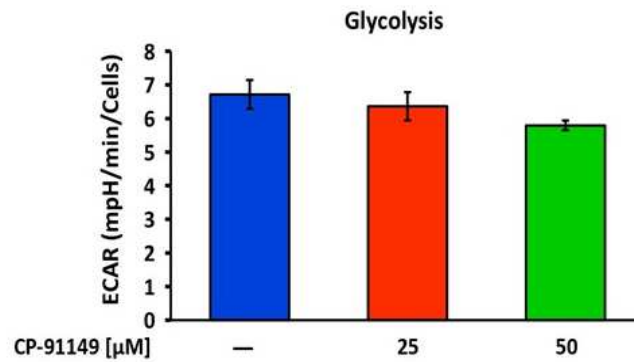


Figure 41: CP-91149 treatment has no impact on glycolysis of HepG2 cells.

Glycolysis of HepG2 cells was determined by Seahorse XF Analyzer following 16 hours of incubation with CP-91149 (25, or 50 μM). Results were analyzed by one-way ANOVA followed by Dunnett's multiple comparison post-hoc test. n = 3.

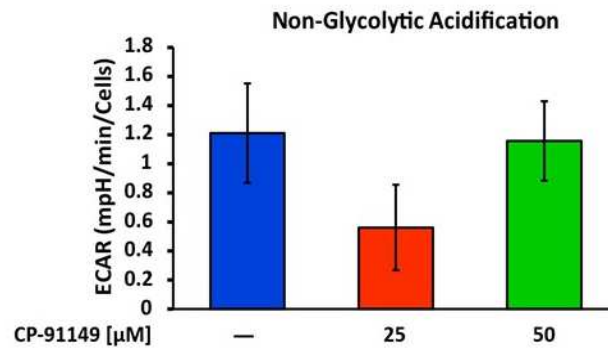


Figure 42: CP-91149 treatment has no impact on non-glycolytic acidification of HepG2 cells.

Non-glycolytic acidification of HepG2 cells was determined by Seahorse XF Analyzer following 16 hours of incubation with CP-91149 (25, or 50 μ M). Results were analyzed by one-way ANOVA followed by Dunnett's multiple comparison post-hoc test. n = 3.

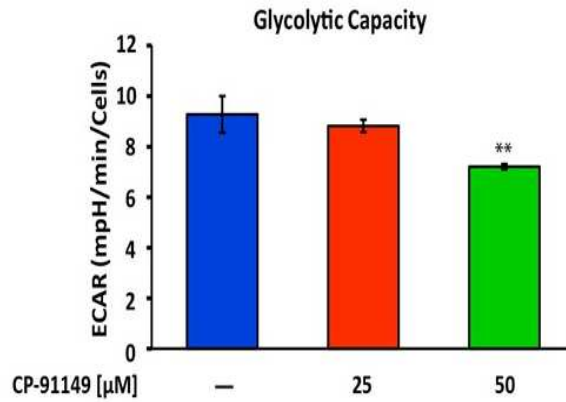


Figure 43: CP-91149 treatment reduces glycolytic capacity of HepG2 cells.

Glycolytic capacity of HepG2 cells was determined by Seahorse XF Analyzer following 16 hours of incubation with CP-91149 (25, or 50 μM). Results were analyzed by one-way ANOVA followed by Dunnett's multiple comparison post-hoc test. $n = 3$, $**p < 0.01$.

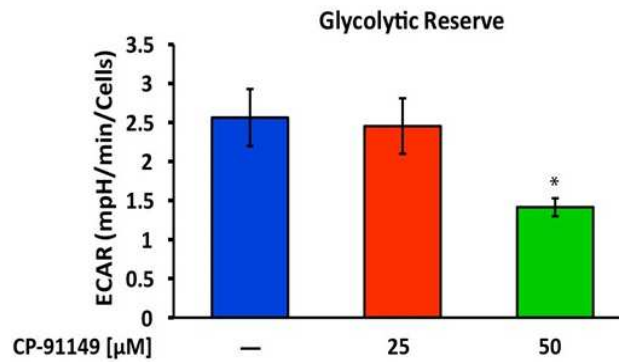


Figure 44: CP-91149 treatment reduces glycolytic reserve of HepG2 cells.

Glycolytic reserve of HepG2 cells was determined by Seahorse XF Analyzer following 16 hours of incubation with CP-91149 (25, or 50 μM). Results were analyzed by one-way ANOVA followed by Dunnett's multiple comparison post-hoc test. n = 3, *p < 0.05.

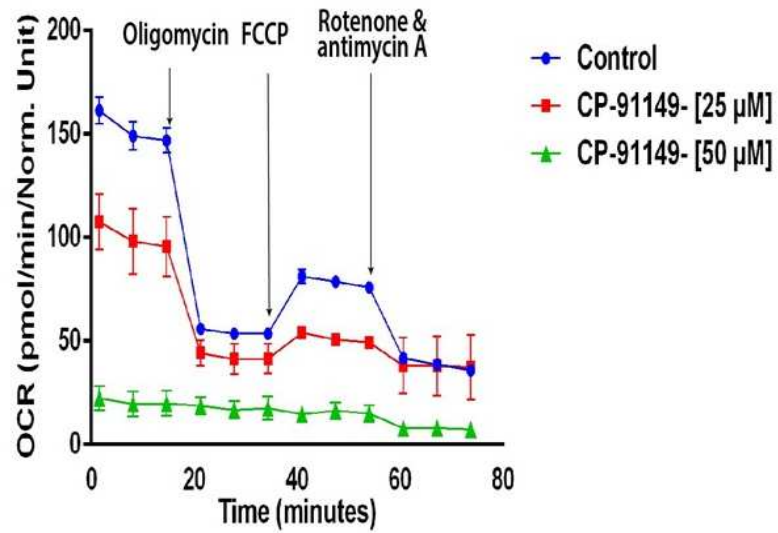


Figure 45: CP-91149 treatment reduces oxygen consumption rate (OCR) and mitochondria linked ATP production of HepG2 cells.

Determination of OCR of HepG2 cells following 16 hours of incubation with CP-91149 (25, or 50 μM) using Seahorse XF Analyzer. n = 3.

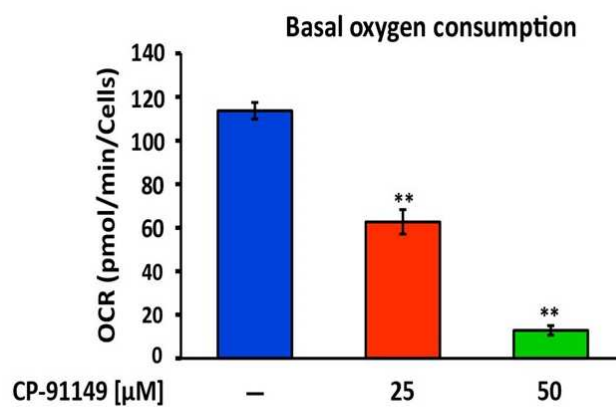


Figure 46: CP-91149 treatment reduces basal oxygen consumption of HepG2 cells.

Basal oxygen consumption of HepG2 cells was determined by Seahorse XF Analyzer following 16 hours of incubation with CP-91149 (25, or 50 μM). Results were analyzed by one-way ANOVA followed by Dunnett's multiple comparison post-hoc test. n = 3, **p < 0.01.

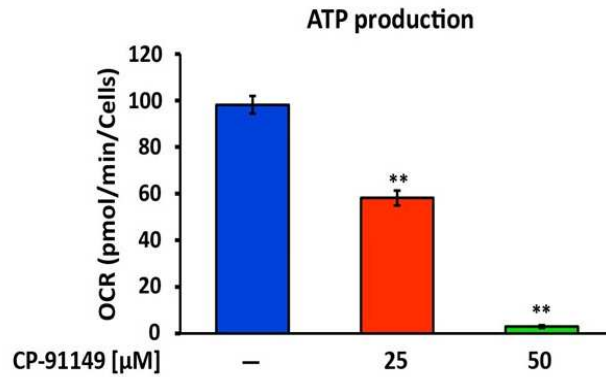


Figure 47: CP-91149 treatment reduces glycolytic capacity of HepG2 cells.

ATP production in HepG2 cells was determined by Seahorse XF Analyzer following 16 hours of incubation with CP-91149 (25, or 50 μM). Results were analyzed by one-way ANOVA followed by Dunnett's multiple comparison post-hoc test. n = 3, **p < 0.01.

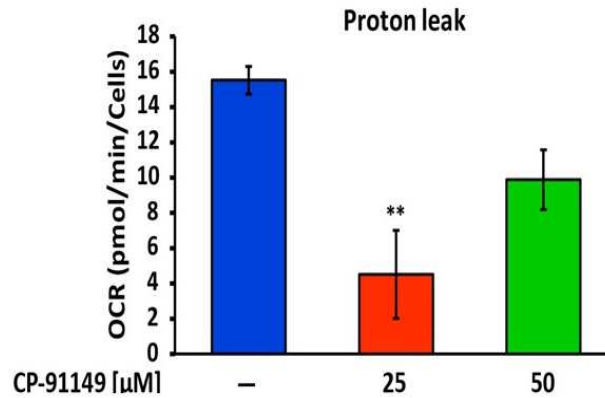


Figure 48: Determination of proton leak in HepG2 cells following 16 hours of incubation with CP-91149 using Seahorse XF Analyzer.

Proton leak in HepG2 cells was determined by Seahorse XF Analyzer following 16 hours of incubation with CP-91149 (25, or 50 μM). Results were analyzed by one-way ANOVA followed by Dunnett's multiple comparison post-hoc test. n = 3, **p < 0.01.

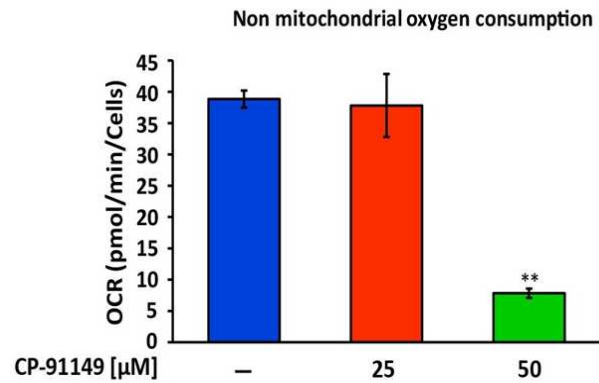


Figure 49: Determination of non-mitochondrial oxygen consumption in HepG2 cells following 16 hours of incubation with CP-91149 using Seahorse XF Analyzer.

Non-mitochondrial oxygen consumption in HepG2 cells was determined by Seahorse XF Analyzer following 16 hours of incubation with CP-91149 (25, or 50 μ M). Results were analyzed by one-way ANOVA followed by Dunnett's multiple comparison post-hoc test. n = 3, **p < 0.01.

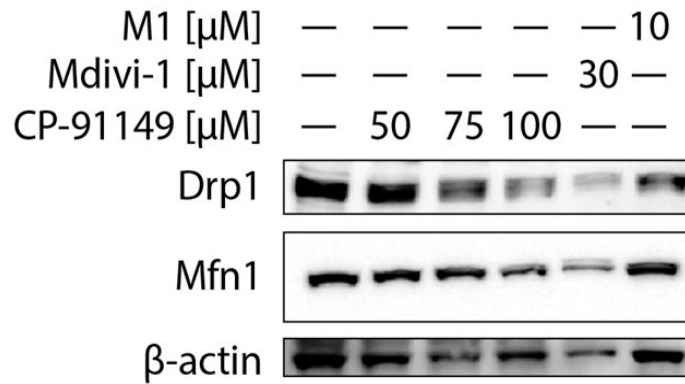


Figure 50: CP-91149 treatment decreased Drp-1 expression in HepG2 cells.

Expression of indicated proteins obtained from HepG2 cell lysates was determined using western blotting. Cells were incubated with different concentrations of CP-91149 (0, 50, 75, or 100 μ M) for 24 hours. M1 (10 μ M) and Mdivi-1 (30 μ M) were used as positive control. Representative image of n = 3.

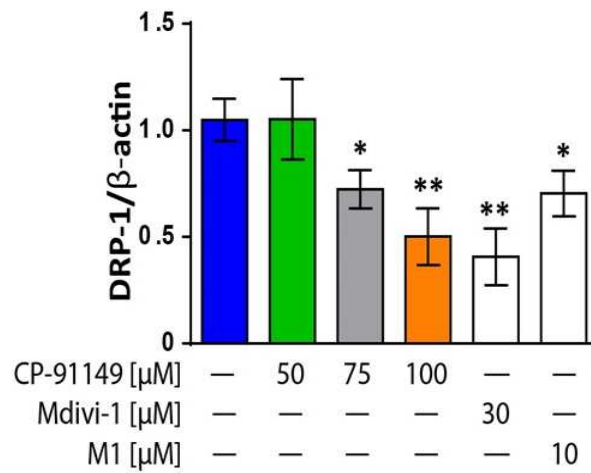


Figure 51: CP-91149 treatment decreased Drp1 expression in HepG2 cells.

Quantification of expression of Drp1 protein was determined from western blot images obtained from HepG2 cell lysates. Cells were incubated with different concentrations of CP-91149 (0, 50, 75, or 100 μ M) for 24 hours. M1 (10 μ M) and Mdivi-1 (30 μ M) were used as positive control. Results were analyzed by one-way ANOVA followed by Dunnett's multiple comparison post-hoc test. $n = 3$, * $p < 0.05$, ** $p < 0.01$.

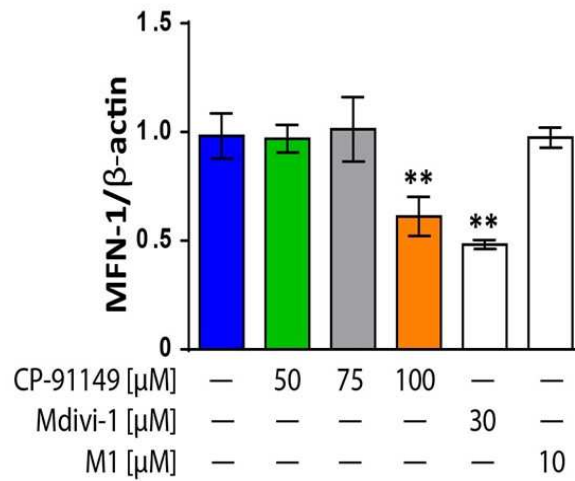


Figure 52: CP-91149 treatment has no impact on Mfn1 expression in HepG2 cells.

Quantification of expression of Mfn1 protein was determined from western blot images obtained from HepG2 cell lysates. Cells were incubated with different concentrations of CP-91149 (0, 50, 75, or 100 μ M) for 24 hours. M1 (10 μ M) and Mdivi-1 (30 μ M) were used as a positive control. Results were analyzed by one-way ANOVA followed by Dunnett's multiple comparison post-hoc test. $n = 3$, ** $p < 0.01$.

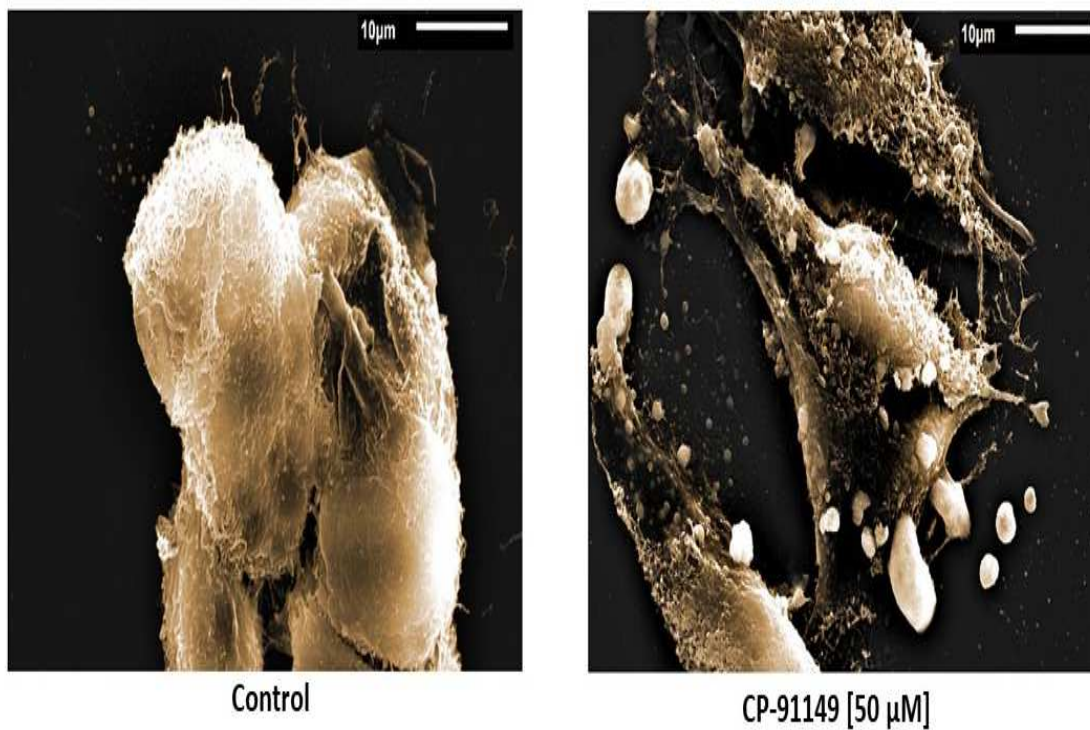


Figure 53: Transmission electron micrograph of HepG2 cells.

Representative micrographs of HepG2 cells after treatment with CP-91149 (50 μ M) for 24 hours.

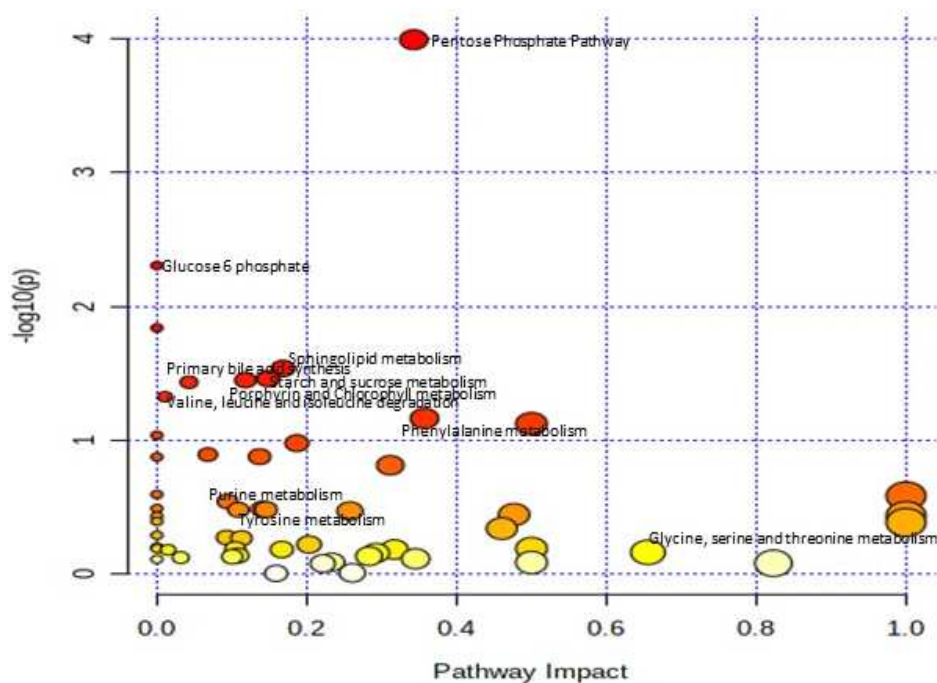


Figure 54: CP-91149 treatment alters level of metabolites of various metabolic pathways.

Inhibition of glycogen phosphorylase in HepG2 cells was induced for 16 hours using CP-91149 (50 μ M) in HepG2 cells. Levels of metabolites were determined by GC time-of-flight mass spectrometry. Metabolic pathways analysis was done using MetaboAnalyst 5.0. Samples were analyzed at Stable Isotope and Metabolomics Core Facility of the Diabetes Research and Training Center (DRTC) of the Albert Einstein College of Medicine. (Supported by NIH/NCI grant P60DK020541. Results were analyzed by Hari Priya), n = 4.

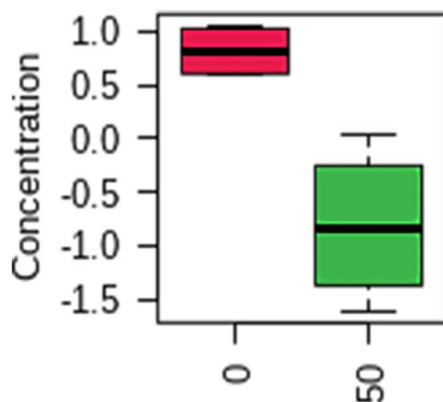


Figure 55: CP-91149 treatment reduces 6-phospho-D-gluconate levels in HepG2 cells.

Levels of 6-phospho-D-gluconate in HepG2 cells following 16 hours of CP-91149 (50 μ M) treatment was determined by metabolomics analysis. Comparison among various metabolic pathways was done using MetaboAnalyst 5.0. Samples were analyzed at Stable Isotope and Metabolomics Core Facility of the Diabetes Research and Training Center (DRTC) of the Albert Einstein College of Medicine. (Supported by NIH/NCI grant P60DK020541. Results analyzed by Hari Priya), n = 4. p value: 0.001657775

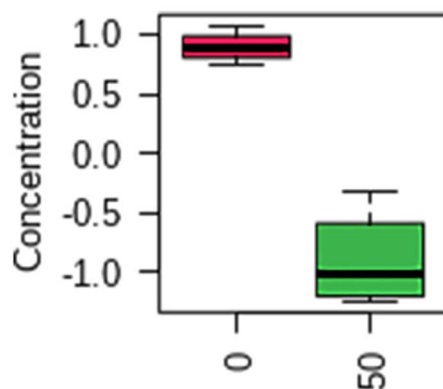


Figure 56: CP-91149 treatment reduces D-gluconic acid levels in HepG2 cells.

Levels of D-gluconic acid in HepG2 cells following 16 hours of CP-91149 (50 μM) treatment was determined by metabolomic analysis. Comparison among various metabolic pathways was done using MetaboAnalyst 5.0. Samples were analyzed at Stable Isotope and Metabolomics Core Facility of the Diabetes Research and Training Center (DRTC) of the Albert Einstein College of Medicine. (Supported by NIH/NCI grant P60DK020541. Results analyzed by Hari Priya), n = 4. P value: 8.89874e-05

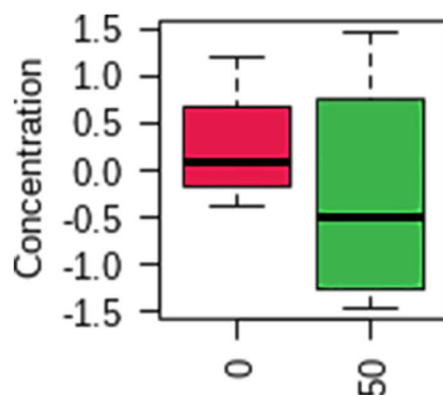


Figure 57: CP-91149 treatment reduces D-Glycerate levels in HepG2 cells.

Levels of D-Glycerate in HepG2 cells following 16 hours of CP-91149 (50 μM) treatment was determined by metabolomics analysis. Comparison among various metabolic pathways was done using MetaboAnalyst 5.0. Samples were analyzed at Stable Isotope and Metabolomics Core Facility of the Diabetes Research and Training Center (DRTC) of the Albert Einstein College of Medicine. (Supported by NIH/NCI grant P60DK020541. Results analyzed by Hari Priya), n = 4. P value: 0.7776507

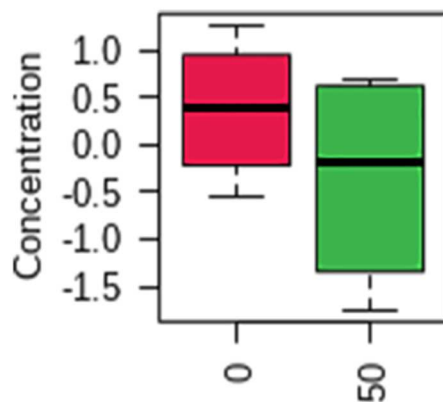


Figure 58: CP-91149 treatment reduces Sedoheptulose 7-phosphate levels in HepG2 cell.

Levels of Sedoheptulose 7-phosphate in HepG2 cells following 16 hours of CP-91149 (50 μ M) treatment was determined by metabolomics analysis. Comparison among various metabolic pathways was done using MetaboAnalyst 5.0. Samples were analyzed at Stable Isotope and Metabolomics Core Facility of the Diabetes Research and Training Center (DRTC) of the Albert Einstein College of Medicine. (Supported by NIH/NCI grant P60DK020541. Results analyzed by Hari Priya), n = 4. P value: 0.3762321

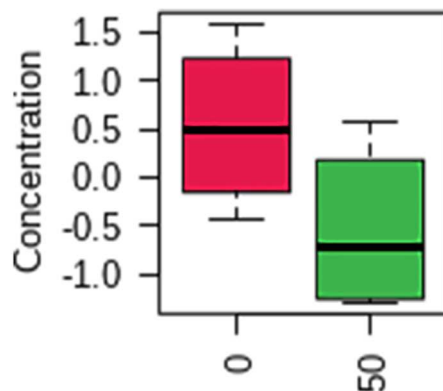


Figure 59: CP-91149 treatment reduces D-Erythrose 4-phosphate levels in HepG2 cells.

Levels of D-Erythrose 4-phosphate in HepG2 cells following 16 hours of CP-91149 (50 μM) treatment was determined by metabolomics analysis. Comparison among various metabolic pathways was done using MetaboAnalyst 5.0. Samples were analyzed at Stable Isotope and Metabolomics Core Facility of the Diabetes Research and Training Center (DRTC) of the Albert Einstein College of Medicine. (Supported by NIH/NCI grant P60DK020541. Results analyzed by Hari Priya), n = 4. P value: 0.1493566

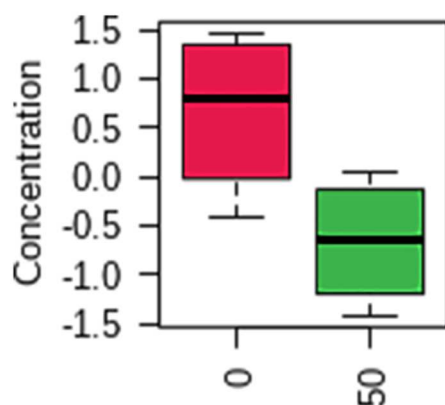


Figure 60: CP-91149 treatment reduces D-Fructose 1,6-bisphosphate levels in HepG2 cells.

Levels of D-Fructose 1,6-bisphosphate in HepG2 cells following 16 hours of CP-91149 (50 μ M) treatment was determined by metabolomics analysis. Comparison among various metabolic pathways was done using MetaboAnalyst 5.0. Samples were analyzed at Stable Isotope and Metabolomics Core Facility of the Diabetes Research and Training Center (DRTC) of the Albert Einstein College of Medicine. (Supported by NIH/NCI grant P60DK020541. Results analyzed by HariPriya), n = 4. P value: 0.05083391

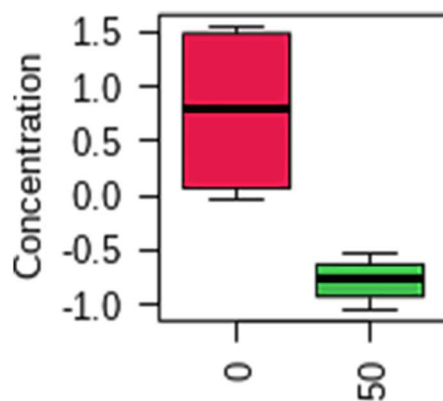


Figure 61: CP-91149 treatment reduces D-Glucose-6-phosphate levels in HepG2 cells.

Levels of D-Glucose-6-phosphate in HepG2 cells following 16 hours of CP-91149 (50 μ M) treatment was determined by metabolomic analysis. Comparison among various metabolic pathways was done using MetaboAnalyst 5.0. Samples were analyzed at Stable Isotope and Metabolomics Core Facility of the Diabetes Research and Training Center (DRTC) of the Albert Einstein College of Medicine. It is supported by NIH/NCI grant P60DK020541 (Results analyzed by HariPriya), n = 4. p value: 0.01069321

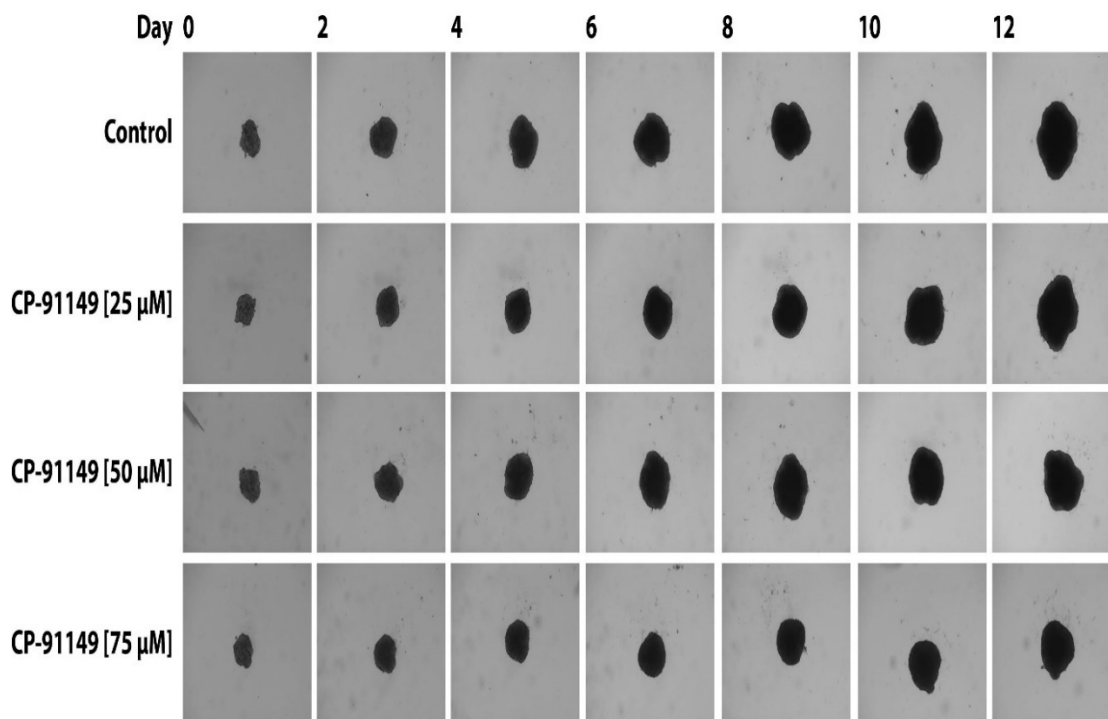


Figure 62: CP-91149 treatment reduces growth of 3D spheroid of HepG2 cells.

Representative images of 3d spheroid of HepG2 cells following incubation with CP-91149 (0, 25, 50, or 75 μ M) taken over 12 days. Images were taken on days 0, 2, 4, 6, 8, 10, and 12 of treatment. n = 3. Magnification 40X.

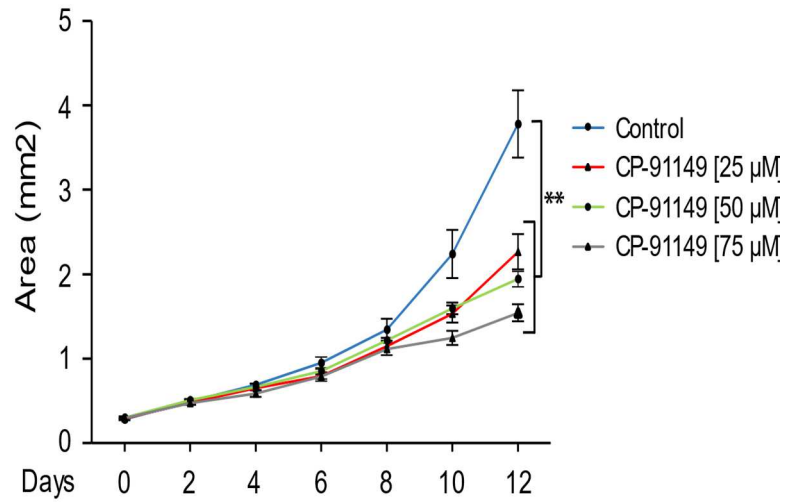


Figure 63: CP-91149 treatment reduces growth of 3D spheroid of HepG2 cells.

The growth curves of 3D spheroids of HepG2 cells were plotted using images of 3D spheroid taken on day 0, 2, 4, 6, 8, 10, and 12 of treatment with CP-91149 (0, 25, 50, or 75 μM). Results were analyzed by one-way ANOVA followed by Dunnett's multiple comparison post-hoc test. $n = 3$, $**p < 0.01$.

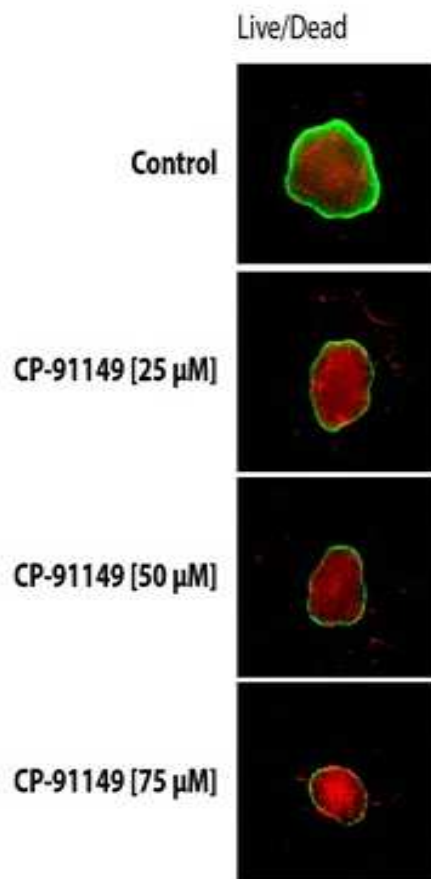


Figure 64: CP-91149 treatment reduces number of live cells in 3D spheroid of HepG2 cells.

Representative merged fluorescent images of live (for calcein-AM) or necrotic (for ethidium homodimer-1) cells. Images were taken following 12 days incubation with CP-91149 (0, 25, 50, or 75 μ M). n = 3. Magnification 40X.

Discussion

4.1 Molecular mechanism of CP-91149 induced cell death in HepG2 cells and impact on chemotherapeutic agents

Cancer cells reprogram their glucose metabolism to fulfill increased cellular demand for proliferation and the altered biological processes such as metastasis (Hanahan & Weinberg, 2011). The reprogrammed glucose metabolism provides intermediates for nucleic acid biosynthesis, bolsters antioxidant defense, and augments amino acid biosynthesis (Ward & Thompson, 2012). Considerable efforts have been devoted to halting this reprogramming with the use of pharmacological inhibitors of metabolic enzymes such as 3-bromopyruvate (3-BP), 2-deoxy-d-glucose (2-DG), FX11, etc. (Gill et al., 2016). Malignant tissues are known to store higher amounts of glycogen than their tissue of origin (Rousset et al., 1981). However, not much is known about the role of glycogen in cancer biology, limiting the ability to utilize glycogen metabolism as a chemotherapy target (Zois & Harris, 2016). In this study, we demonstrated that treatment with CP-91149, an allosteric inhibitor of glycogen phosphorylase (GP), induced the intrinsic pathway of apoptosis-mediated cell death in HepG2 cells. Mitochondrial dysfunction and increased oxidative stress were observed in this cell death. Interestingly, CP-91149 potentiated the effects of anticancer drugs such as multikinase, anti-angiogenic inhibitors sorafenib and regorafenib, and potential drugs like 6-aminonicotinamide which targets the pentose phosphate pathway. These combined findings suggest CP-91149 as a potential drug for the treatment of hepatocellular carcinoma (HCC).

Cancer treatment approaches such as chemotherapy, radiation, and immunotherapy all aim to induce the death of cancer cells. Cell death by apoptosis is one of the critical

barriers to carcinogenesis as well as one of the key processes employed by chemotherapy drugs (Adams & Cory, 2007; Fulda & Debatin, 2006). Many cancer chemotherapy agents operate through the intrinsic/mitochondria-mediated pathway of apoptosis that is regulated by the BH3-domain family of pro and anti-apoptotic proteins (Adams & Cory, 2007). Activation of the intrinsic apoptosis pathway causes the release of cytochrome c from mitochondria, which binds to procaspase-9 and Apaf-1 and forms an apoptosome. Clustering of procaspase-9 in this fashion leads to the activation of caspase-9. Our study showed the presence of multiple markers of mitochondrial dysfunction and the intrinsic apoptosis in HepG2 cells induced by CP-91149 (Fig. 4). Thus, we showed that the intrinsic pathway of apoptosis was the primary cell death mechanism induced by CP-91149 treatment in HepG2 cells. Some cancers are known to evade the apoptotic pathway, and such resistance makes these cancers aggressive (Igney & Krammer, 2002). Because inhibition of glycogen metabolism induced apoptosis in HCC cells, this strategy could be studied in other apoptosis-resistant cancer cells (Curtis et al., 2019). Thus, these findings indicate that there are marked differences in targeting glycolysis and glycogen metabolism. More studies are needed to delineate the differences between glycogen inhibitors and glycolytic inhibitors in the context of cancer biology.

Most studies of CP-91149 have focused on its role in the management of diabetes, where it was shown to be a specific inhibitor for GP causing glycogen accumulation (Treadway et al., 2001). However, only a handful of studies have investigated the inhibition of glycogen metabolism in cancer. In a key study, Favaro et al. showed that hypoxia in glioblastoma cell cultures or ischemia in tumor xenografts led to increased gene and protein expression of glycogen metabolic enzymes such as GP (Favaro et al., 2012). This

study indicated that the silencing of GP in glioblastoma cells leads to oxidative stress and causes senescence through p53 activation (Favaro et al., 2012). Glycogen-metabolic proteins such as GP and glycogen synthase are key players in the hypoxic response of cancers and regulate cell survival and metastasis (Brahimi-Horn et al., 2011; Favaro et al., 2012; Winter et al., 2007). CP-320626, an indole carboxamide allosteric inhibitor of GP, induced defects in the pentose phosphate pathway, de novo fatty acid synthesis, and changes in cellular proteome in pancreatic cancer cells (Lee et al., 2004; Ma et al., 2012). Similarly, CP-91149 treatment increased glycogenosis and potentiated hormone therapy in prostate cancer (Schnier et al., 2003). Another study suggested the potential of blocking the glycogen debranching enzyme, involved in glycogen catabolism, for bladder cancer (Ritterson Lew et al., 2015). A recent study has also highlighted the key role of fibroblasts to alter tumor glycogen and thereby promoting proliferation and metastasis (Curtis et al., 2019). Collectively, these studies underline the importance of targeting glycogen metabolism for anticancer therapy.

Drug resistance is one of the major limiting factors to achieve cure for patients suffering from cancer. Combination therapy with drugs having non-overlapping mechanisms of action is used to overcome drug resistance. However, combination of surgery, radiotherapy and polychemotherapy are clearly not enough to cure many types of tumors and successes achieved with polychemotherapy had largely plateaued. Hence, there is a dire need of new drugs inhibiting tumor growth by different mechanisms (Vasan et al., 2019). Drug repurposing is a strategy that has inherent advantages over developing an entire new drug for given indication in the drug development process as the drug has already acceptable safety profile and hence the chance of failure reduces. This also

decreases time and investment to develop a new drug to develop a new drug as many of the pre-clinical, clinical, and formulation related problems are already addressed (Pushpakom et al., 2019). Clinical trials of various metabolic modulators like metformin and chloroquine as cancer therapeutic are already under way. These drugs show synergy with current chemotherapeutic agents (Chae et al., 2016; Verbaanderd et al., 2017). CP-91149 is an indole carboxamide site (allosteric) inhibitor of GP which acts by binding to dimerization site of GP. It inhibits dimerization of monomeric GP units. This promotes T state of GP, subjects it to dephosphorylation and inactivation of GP (Lerín et al., 2004). It was initially designed as an antidiabetic agent and have shown to reduce glucose level in diabetic male C57BL/6J-Lep^(ob/ob) mice. CP-91149 showed IC₅₀ value of 0.13 μ M in isolated human liver GP enzyme (Martin et al., 1998). However, many factors like drug influx, efflux, off-target activity, etc. can affect its overall activity and can account for higher dose to achieve inhibitory activity.

CP-91149 can affect overall cell metabolism and tumor cell growth by GP inhibition. Sorafenib (first-line) and regorafenib (second-line) are the only drugs indicated with survival benefits in advanced-stage hepatocellular carcinoma (Ikeda et al., 2018). Sorafenib and regorafenib are multikinase inhibitors that block the signaling by RAF, VEGFR, and PDGFR, thereby affecting proliferation signaling, angiogenesis, and apoptosis (Bajetta et al., 2009). By inhibiting GP, CP-91149 acts on a different target than that of sorafenib and regorafenib. Our results showed synergy between CP-91149 and sorafenib or regorafenib, which could be due to targeting prominent cancer biological alterations such as proliferation signaling, angiogenesis, and metabolic reprogramming.

4.2 Effect of CP-91149 induced inhibition of glycogen catabolism on overall metabolism of HepG2 cells

CP-91149 was developed to treat non-insulin-dependent diabetes mellitus (Martin et al., 1998). Its oral administration at 25–50 mg/kg to diabetic ob/ob mice has been shown to inhibit glucagon-stimulated glycogenolysis (Martin et al., 1998). GP and GS are critical proteins involved in the catabolism and anabolism of glycogen, respectively.

Phosphorylation and allosteric modulators can regulate their activity reciprocally (Roach et al., 2012; Zois & Harris, 2016). Our results in HepG2 cells showed CP-91149 treatment caused a reduction in GP expression and also induced activation of GS by decreasing its phosphorylation. Similarly, CP-91149 treatment in primary human muscle cells caused a decrease in dephosphorylation of GP and GS, resulting in a net increase in glycogen synthesis (Lerín et al., 2004, p. 91149). A similar finding was observed in rat hepatocytes, and primary human hepatocytes upon CP-91149 treatment (Martin et al., 1998). These data can explain our results about an increase in basal glycogen level in HepG2 cells.

AMP-activated protein kinase (AMPK) is a heterotrimeric protein complex and its activity is known to reflect cellular energetic status (Hardie et al., 2012). An increase in cellular AMP or ADP level causes its activation by allosteric modulation (Hardie et al., 2012). Activated AMPK is known to restore cellular energy balance and help in cell survival by switching on energy-generating pathways by upregulating glucose uptake, glycolysis, fatty acid oxidation, autophagy, etc. (Hardie et al., 2012). Our results show CP-91149 treatment results in activation of AMPK by increasing its phosphorylation. Consistent with the effect of AMPK activation, we saw a mild activation of autophagy,

and change in the metabolism of many amino acid pathways (**Fig. 54**) (Barot et al., 2019). However, AMPK activation didn't show any change in glucose uptake, and overall glycolysis wasn't affected. The inability of cells to increase glucose uptake and glycolysis could be a reason behind CP-91149 induced cell death, and exact molecular mechanism underlying this process needs further investigation.

Mitochondria are highly dynamic organelles which continuously move along the cytoskeleton and undergo fusion and fission (Yu et al., 2020). Change in mitochondrial morphodynamics helps the cell to fight various stress conditions like nutrient starvation, pathogen attack, disease state, etc. (Zemirli et al., 2018). Proteins like Mfn1 and Mfn2 play a significant role in mitochondrial fusion, whereas Drp1 is a key protein for mitochondrial fission (Yu et al., 2020; Zemirli et al., 2018). Downregulation of Drp1 showed decreased proliferation, mitochondrial activity, and higher rate of cytochrome c release to cytosol in human colorectal cell lines (Inoue-Yamauchi & Oda, 2012). Similarly, loss of Drp1 activity caused mitochondrial dysfunction and increased reactive oxygen species levels in porcine oocyte which resulted in their failed maturation (H. Zhang et al., 2020). CP-91149 treatment in HepG2 cells showed similar results where it caused a reduction in Drp1 expression, reduction in mitochondrial oxygen consumption, membrane potential, and cytochrome c mediated apoptosis.

Various growth signals like the PI3K/Akt/mTOR pathway can stabilize HIF-1 α even during normoxia. HIF stabilization is known to alter the expression of many metabolic proteins and affect glucose metabolism in cells (DeBerardinis et al., 2008). HIF stabilization increases glucose uptake and causes accumulation of glycogen synthesis by increasing expression of proteins like glycogen synthase (Pescador et al., 2010, p. 1).

Indeed, many tumors show a higher amount of glycogen than their tissue of origin (Rousset et al., 1981). Colorectal cancer shows cell cycle-specific accumulation of glycogen levels with the highest level during the G₁ phase of the cell cycle and subsequent reduction with S phase progression (Takahashi et al., 1999). Inhibition of glycogen catabolism caused cell cycle arrest in many types of cancers (Barot et al., 2019; Favaro et al., 2012; Schnier et al., 2003, p. 149). This inhibition is associated with inhibition in expression of cell progression proteins Cyclin E-Cdk2 and increase in expression of cell cycle inhibitor proteins p21 and p27 in MIA PaCa-2 pancreatic cancer cells and HSF55 normal skin fibroblasts cells (Coqueret, 2003; Hwang & Clurman, 2005; Ma et al., 2012; Schnier et al., 2003). Cells can divert glucose-1-phosphate derived from glycogen catabolism to the pentose phosphate pathway (PPP). This can help to synthesize nucleotides required to sustain proliferation and NADPH to fight ROS. Our study and others showed a reduction in PPP activity and an increase in ROS level upon glycogen phosphorylase inhibition (Favaro et al., 2012). Indeed, this inhibition potentiated the action of 6-aminonicotinamide (6-AN), indicating the significance of glycogen catabolism to support PPP (Barot et al., 2019).

4.3 Conclusion

CP-91149 binds to the indole carboxamide site of glycogen phosphorylase and inhibits its activity. This inhibition resulted in an increase in glycogen levels in HepG2 cells.

Proteins like AMPK showed an increase in their phosphorylation, but glucose entry or glycolysis was not affected. There was a significant decrease in mitochondrial oxygen consumption and membrane potential. Cytochrome c got released from mitochondria to cytosol and activated the intrinsic pathway of cell death. Glucose derived from glycogen

can support nucleotide synthesis which is needed for the progression of cell cycle. Inhibition of glycogen catabolism resulted in the downregulation of the pentose phosphate pathway (PPP) and cell cycle arrest. Chemotherapeutic drugs sorafenib and regorafenib are first-line and second-line therapy for advanced-stage hepatocellular carcinoma. The combination of CP-91149 with these drugs resulted in the synergism of these drugs and PPP inhibitor 6-aminonicotinamide. A study investigated inhibitory activity of CP-91149 on at least 50 pharmacological targets other than GP but didn't find any inhibitory activity (Martin et al., 1998). However, molecular mechanisms other than GP inhibition can't be eliminated entirely for its action.

4.4 Future directions

Glycogen is compartmentalized in the cell as nuclear and cytosolic pools. Proteins involved in glycogen metabolism also shows translocation between nucleus and cytosol. As a future study, it will be interesting to know if a specific pool of glycogen has a role in cell growth and cell cycle progression.

Table 2: Appendix- A Summary of pathway analysis

Pathway Name	Match Status	p
Pentose phosphate pathway	5/22	1.0273E-4
Glucose-6-phosphate	1/2	0.0049721
Inositol phosphate metabolism	2/30	0.01451
Sphingolipid metabolism	3/21	0.029115
Starch and sucrose metabolism	2/18	0.034694
Porphyrin and chlorophyllmetabolism	4/30	0.035601
Primary bile acid biosynthesis	5/46	0.036878
Valine, leucine and isoleucine degradation	2/40	0.047324
Phenylalanine metabolism	2/10	0.068651
Phenylalanine, tyrosine and tryptophan biosynthesis	1/4	0.07515
Phosphonate and phosphinate metabolism	1/6	0.091707
Glycerophospholipid metabolism	6/36	0.105
Pantothenate and CoA biosynthesis	7/19	0.12774
Glycerolipid metabolism	2/16	0.13233
Valine, leucine and isoleucine biosynthesis	3/8	0.1331
Cysteine and methionine metabolism	9/33	0.15355
Biotin metabolism	1/10	0.2533
Linoleic acid metabolism	1/5	0.25989

Purine metabolism	11/65	0.28548
N-Glycan biosynthesis	1/41	0.32246

Table 3: Appendix- B Table for data of individual metabolite analyzed by metabolomics analysis

NO	Metabolite name	Average [control]	SEM [control]	Average [CP-91149- 50 μ M]	SEM [CP-91149- 50 μ M]
1	p-Hydroxyphenyllactic acid	0.173735	0.056428	0.317189	0.085898
2	Butyryl-carnitine	0.746176	0.266387	1.84669	0.527012
3	Lactic acid	21.84265	4.598201	29.42791	7.109781
4	Phenylalanine	1.158769	0.462278	2.739965	0.764212
5	2'-Deoxyadenosine	0.09413	0.034652	0.099318	0.032729
6	Stearic acid	0.020287	0.006094	0.022365	0.002856
7	Thymidine 5'-monophosphate	4.67345	1.680165	7.196233	2.482136
8	Phylloquinone (K1)	0.239183	0.115301	0.9962	0.338288
9	Trehalose 6-phosphate	0.777445	0.136865	1.088005	0.091465
10	N-Acetyl-serine	0.234305	0.095093	0.430896	0.150838
11	Valeryl-carnitine/ Isovaleryl-carnitine (Carnitine_C5)	0.021454	0.007568	0.03784	0.011835
12	Taurine	50.38234	13.69676	102.3408	28.86239
13	Propionyl Carnitine	0.064365	0.026242	0.122815	0.04043
14	3-Phosphoglyceric acid	1.108773	0.160652	1.02411	0.139037

15	Oxalacetic acid/methylsuccinic acid	0.070677	0.035501	0.117311	0.042768
16	Malic acid	7.52245	2.746719	15.32742	5.298047
17	Protoporphyrin IX	0.00495	0.000869	0.021015	0.001336
18	Suberic acid	0.889131	0.28012	1.463695	0.429014
19	4-Hydroxy-3-methoxyphenylglycol/ 3,4-Dihydroxymandelic acid	0.057538	0.003843	0.08386	0.011441
20	trans-Cinnamic acid	4.969728	0.593942	7.023855	1.147873
21	tauroolithocholate	0.16962	0.017346	0.174922	0.013374
22	cAMP	0.051181	0.017086	0.055495	0.015601
23	Nicotinic acid	8.695732	2.82032	11.82443	2.592958
24	Acetyl-l-aspartic acid	192.7669	53.09167	334.5161	60.82517
25	2-Hydroxyglutaric acid	2.422963	0.846735	4.219343	1.269045
26	glycoursodeoxycholate	0.300066	0.07861	0.324168	0.041389
27	Citric acid	141.2896	38.84956	223.7949	57.56138
28	Gluconic acid	1.699045	0.542753	1.81174	0.378187
29	Uridine	7.813249	3.062966	8.847065	2.850824
30	3-Hydroxy-3-methylglutaric acid	0.334469	0.124469	1.275909	0.447242
31	Uridine 5'-diphosphoglucose	22.68859	10.0569	34.2877	9.773942
32	Fructose 1,6-bisphosphate	3.226336	0.803467	4.050122	0.658284
33	Pantothenic acid	43.97867	12.2015	106.8874	18.3912
34	Pimelic acid	0.24481	0.016557	0.366086	0.043292
35	Glutaric acid	0.072101	0.021564	0.134766	0.027611

36	guanosine	0.306697	0.125757	0.482793	0.173115
37	Petroselinic acid	0.054648	0.007479	0.077116	0.00801
38	glycocholate	0.02445	0.007364	0.030457	0.004568
39	Cholesteryl acetate	0.50682	0.109308	0.914201	0.068866
40	Hexose-phosphate	5.394683	2.113384	4.608782	1.208602
41	glycochenodeoxycholate	0.297955	0.075567	0.310209	0.046522
42	Aspartic acid	3.460741	1.063691	4.190856	1.178053
43	Pentose-phosphate	2.049134	0.509751	4.150615	0.743864
44	Glucosamine 6-phosphate	0.610314	0.196848	0.93332	0.238475
45	CDP-ethanolamine	0.464648	0.08372	0.591819	0.125805
46	Erythrose 4-phosphate	2.113316	0.486304	2.603864	0.326263
47	Nonadecanoic acid	0.337957	0.005047	0.488396	0.078667
48	3,4-Dihydroxymandelic acid	0.019628	0.001463	0.027596	0.004097
49	Dihydroorotic acid	0.362469	0.072251	0.623829	0.049496
50	Aminoadipic acid	6.602192	1.884062	9.900708	2.003374
51	Glycerol 3-phosphate	4.151248	1.098976	6.176778	1.532169
52	Uridine 5'-monophosphate	181.3607	59.01145	332.6165	88.30031
53	Uridine 5'-diphosphogalactose	36.09199	16.2905	53.62515	15.11982
54	Succinic acid/ 3-Hydroxy-2-methylbutanoic acid	13.51589	5.05305	18.88991	4.516379
55	Indoxyl sulfate	0.049524	0.009355	0.042951	0.020666
56	Fumaric acid	1.080861	0.258978	2.020548	0.452713
57	5'-Deoxy-5'-(methylthio)adenosine	0.512148	0.177279	0.980162	0.250077

58	2-Hydroxybutyric acid	0.037745	0.007668	0.063721	0.010674
59	Pyruvic acid/butyric acid	1.758536	0.690392	2.908309	1.133265
60	β -Nicotinamide adenine dinucleotide	0.916392	0.271074	1.658597	0.515896
61	Glutamic acid	108.1545	23.82418	181.7493	35.87077
62	7-Dehydrocholesterol	6.656387	0.371165	9.09992	2.002554
63	6-Phosphogluconic acid	5.370149	2.036017	3.026229	1.320318
64	cAMP	0.118089	0.035789	0.092811	0.012404
65	Maleic acid	0.875553	0.206131	1.517936	0.354688
66	α -Tocopherol	0.023987	0.002415	0.035706	0.01037
67	glycodeoxycholate	0.313266	0.080798	0.318131	0.048176
68	taurohyodeoxycholate	1.882738	0.551184	2.074795	0.347836
69	Adenosine triphosphate	1.935759	0.848363	2.422987	0.483405
70	Riboflavin	0.021085	0.004801	0.029878	0.006484
71	Cysteinesulfinic acid	0.38113	0.119207	0.43517	0.068707
72	Nicotinic acid adenine dinucleotide	3.215704	1.091379	8.061468	2.997338
73	Uridine 5'-diphospho-N-acetylgalactosamine	53.06403	22.51481	88.27436	23.60222
74	Hydroxyisocaproic acid	0.193043	0.05428	0.263622	0.044354
75	3-Hydroxyanthranilic acid	0.199637	0.025669	0.425194	0.07512
76	O-Succinyl-homoserine	0.049804	0.024388	0.148828	0.095043
77	Ethylmalonic acid	0.287652	0.028303	0.423524	0.035073
78	Hexanoyl-L-carnitine (Carnitine_C6)	0.012132	0.00372	0.023408	0.004859
79	taurodeoxycholate	2.052783	0.599287	2.127274	0.387892

80	Tetradecanedioic acid	0.649963	0.191872	1.163737	0.113107
81	glycolithocholate	0.032365	0.002659	0.041571	0.002849
82	Pentadecanoic acid	0.053747	0.023483	0.068736	0.03538
83	glycohyodeoxycholate	0.241286	0.062123	0.256463	0.039731
84	Erythro-Dihydro-sphingosine	0.006279	0.00056	0.012085	0.001675
85	Flavin adenine dinucleotide	0.889996	0.283706	1.533684	0.37984
86	Cytidine 5'-diphosphocholine	1.308244	0.641266	1.0907	0.319893
87	5-Aminolevulinic acid	0.116034	0.030579	0.141607	0.035816
88	Caprylic acid	0.007629	0.002623	0.023724	0.011963
89	Phosphonoacetic acid	0.668833	0.159807	1.124861	0.207151
90	Guanosine 5'-diphospho-D-mannose	0.348247	0.187393	0.563398	0.127736
91	Carnitine (Carnitine_C0)	0.786014	0.345352	1.001789	0.203344
92	Tryptophan	0.312583	0.085477	0.564241	0.138476
93	Myristoyl-carnitine (Carnitine_C14)	3.791241	0.572359	11.50328	2.007749
94	Uridine 5'-diphospho-N-acetylglucosamine	27.0937	11.55395	46.1061	12.0719
95	2-Hydroxy-4-(methylthio)butyric acid	0.001852	0.000492	0.003325	0.000732
96	Valine	1.826229	0.757939	2.049417	0.416428
97	Riboflavin 5'-monophosphate	0.074087	0.016275	0.112594	0.022181
98	Lithocholic acid	0.113033	0.037338	0.235486	0.059615
99	O-Phosphorylethanolamine	0.831902	0.237995	0.743143	0.143703

100	Cystathionine	0.282614	0.100579	0.429307	0.117828
101	Hippuric acid	0.001968	0.000452	0.004885	0.001178
102	taurochenodeoxycholate	7.570161	2.304029	8.098337	1.670896
103	2'-Deoxyuridine 5'-monophosphate	0.258229	0.084379	0.380735	0.097048
104	5'-Deoxyadenosine	0.006407	0.002417	0.009951	0.003374
105	Azelaic acid	0.33251	0.115803	1.198306	0.404631
106	Creatine	32.02071	13.62207	41.38159	10.84149
107	Adenosine-5'-diphosphoglucose	13.65609	4.26977	28.92279	10.09837
108	cytosine	0.573888	0.241213	0.83721	0.167768
109	Proline	13.0002	5.598675	16.53774	4.192014
110	Lysine	1.441149	0.641981	1.085861	0.12864
111	Guanidine	10.43008	4.349571	10.46571	1.866974
112	Adenosine 3',5'-diphosphate	13.00397	5.899507	18.08648	4.07041
113	N-Acetyl-D-Glucosamine 6-Phosphate	1.045418	0.317159	1.376208	0.281157
114	tauro α -muricholate	0.098961	0.030192	0.109661	0.021919
115	Glucuronic acid	0.048128	0.002774	0.067152	0.005018
116	creatinine	0.547828	0.224922	0.766813	0.182416
117	1-Methyladensine	0.003685	0.00132	0.003189	0.000904
118	3,3',5-Triiodo-thyronine	0.018556	0.003246	0.009585	0.001108
119	L-Cysteic acid	0.297964	0.127723	0.296214	0.026336
120	hexol_Dulcitol/Sorbitol	0.121099	0.015972	0.138536	0.023363
121	dimethylglycine	0.370792	0.181491	0.317995	0.109916

122	Kynurenic acid	0.049418	0.012363	0.105877	0.015022
123	Betaine	1.28747	0.618306	1.651224	0.515712
124	3-Dehydroshikimic acid	1.113492	0.181983	1.230588	0.144505
125	Adenosine 5'-monophosphate	79.9141	37.57059	146.0823	48.4401
126	Pipecolinic acid	6.177323	2.17441	7.554523	0.476338
127	cis-4,7,10,13,16,19-Docosaenoic acid	2.267631	0.553221	2.728844	0.306874
128	3-Hydroxybenzaldehyde	0.019612	0.002974	0.027948	0.006229
129	Ribitol	0.037157	0.014106	0.062801	0.011085
130	Xanthurenic acid	0.092607	0.025734	0.118067	0.043072
131	2'-Deoxycytidine 5'-diphosphate	4.835661	1.63725	5.659736	1.095009
132	Oleic acid	0.000579	7.27E-05	0.000777	0.000128
133	3,4-Dihydroxyphenyl glycol	0.072633	0.014948	0.179878	0.077327
134	lithocholate	0.133647	0.046449	0.323349	0.101288
135	N-Acetylglycine	0.056228	0.008199	0.087171	0.031346
136	Citramalate	0.229483	0.050173	0.325561	0.05169
137	3-Ureidopropionic acid	0.601742	0.254376	0.75987	0.217055
138	γ -Linolenic acid	0.084687	0.022828	0.121431	0.009716
139	3-Indolepropionic acid	0.256821	0.028137	0.351169	0.059598
140	Thyroxine	0.08544	0.018429	0.102658	0.008044
141	Quinoline	0.012845	0.003049	0.025439	0.006248
142	Asparagine	1.23821	0.570206	1.287507	0.387216

143	3-(2-Hydroxyphenyl)propionic acid	0.017642	0.006224	0.029818	0.012889
144	2-Aminoethylphosphonic acid	0.033542	0.007948	0.046207	0.009101
145	Dihydroxyfumaric acid	0.204356	0.045597	0.285778	0.050008
146	Guanidinosuccinic acid	1.410954	0.649449	2.010677	0.652999
147	Alpha-ketoisovaleric acid	0.039404	0.009418	0.031502	0.011111
148	Saccharic acid	0.032224	0.008075	0.059745	0.013616
149	Norvaline	0.920684	0.384885	1.01067	0.26054
150	Palmitic acid	2.398582	0.410782	2.826075	0.569365
151	β -Nicotinamide mononucleotide	0.651004	0.232291	0.71058	0.114547
152	Homoserine	0.57979	0.239828	0.709579	0.105569
153	N-Methyl-glutamic acid	0.455861	0.207601	0.56071	0.108939
154	Neopterin	0.028586	0.013948	0.06895	0.024538
155	D-Psicose	0.004514	0.000404	0.006432	0.000584
156	Trimethylamine	0.162731	0.07797	0.186146	0.053956
157	trans-1,2-Cyclohexanediol	0.023702	0.003671	0.030315	0.004676
158	S-(5'-Adenosyl)-homocysteine	0.043598	0.016976	0.034119	0.002211
159	Lauroyl-carnitine (Carnitine_C12)	0.008521	0.002629	0.012103	0.004256
160	Octanoyl-carnitine (Carnitine_C8)	0.001624	0.000249	0.003545	0.000434
161	N1-Acetylspermine	0.011961	0.005524	0.022137	0.006125
162	Allantoin	1.363953	0.41588	2.143003	0.657249

163	3-Phenyllactic acid	0.015366	0.005165	0.028561	0.006643
164	Tricosanoic acid	0.062394	0.022501	0.136864	0.020334
165	Decanoyl-carnitine (Carnitine_C10)	0.000758	0.000262	0.000792	0.000221
166	Mannose	0.491548	0.271463	0.455298	0.190023
167	Deoxycorticosterone acetate	0.000336	0.000127	0.000563	0.000274
168	Choline	3.904525	1.915902	3.165571	1.067189
169	Stachyose	6.545989	3.39131	10.91427	2.847572
170	4-aminobutyrate	0.021527	0.012687	0.020613	0.008901
171	1,2-Didecanoyl-glycero-3- phosphocholine	0.04668	0.007777	0.083616	0.032178
172	meso-Tartaric acid	0.030067	0.008551	0.044175	0.013203
173	Citrulline	0.053981	0.025736	0.042987	0.019211
174	7,12-diketolithocholate	0.301922	0.055737	0.223641	0.037214
175	Inosine	0.033964	0.015603	0.054605	0.009838
176	Lanosterol	0.064908	0.007468	0.071636	0.003117
177	Alanine/Sarcosine	2.677784	1.23962	2.905609	0.56336
178	Histidine	0.168351	0.066222	0.232535	0.050534
179	trans-4-Hydroxy-proline	0.289906	0.123615	0.405987	0.119353
180	Glyceric acid	0.008852	0.001957	0.011717	0.002085
181	Homogentisic acid	0.004928	0.001433	0.010719	0.001115
182	glycine	0.025777	0.01366	0.023546	0.003987
183	Threonine/Homoserine	0.784459	0.359406	0.673998	0.086605
184	Seleno-methionine	0.00151	0.000602	0.002289	0.001195
185	Uracil	1.03904	0.270336	1.101465	0.200549

186	5-Methylcytosine	0.006239	0.002888	0.004874	0.002017
187	3-Indoleacetic acid	0.000667	0.00018	0.001579	0.000645
188	Trimethylamine N-oxide	0.226404	0.10197	0.221084	0.038747
189	Xanthosine	0.000888	0.000206	0.001838	0.00033
190	N-Acetyl-5-hydroxytryptamine	0.053146	0.026243	0.195792	0.046708
191	Adenylosuccinic acid	0.008325	0.00373	0.007994	0.000725
192	4-Aminobenzoic acid	0.005138	0.001597	0.00644	0.000693
193	Glutamine_Pos	1.742279	0.976666	1.127002	0.295083
194	acetyl phosphate	0.033464	0.011478	0.049428	0.005001
195	3-Aminoisobutanoic acid	0.017247	0.00439	0.030325	0.005893
196	L-Alpha-aminobutyric acid/ 2-Aminoisobutyric acid	0.135729	0.058836	0.091763	0.023076
197	Phosphocholine	4.68217	2.427531	4.747457	1.189858
198	Bis(2-ethylhexyl) phthalate	0.101777	0.010244	0.186642	0.01456
199	Serine	0.184532	0.068576	0.223485	0.017078
200	ursodeoxycholate	1.675067	0.300069	0.473651	0.118464
201	4-Trimethylammoniobutanoic acid	0.399429	0.194153	0.577907	0.110166
202	Adenosine 5'-diphosphoribose	0.073482	0.007098	0.132894	0.058499
203	O-Phospho-L-serine	0.02609	0.003198	0.082445	0.022872
204	Palmitoylcarnitine (Carnitine_C16)	3.666316	0.326088	6.759872	1.140437
205	2-Methylglutaric acid	1.396792	0.649297	3.163053	0.360496

206	3-Methylhistamine/ 1-Methylhistamine	0.006242	0.002396	0.013091	0.001494
207	Sedoheptulose-7-phosphate	0.003456	0.000746	0.004339	0.000268
208	N-Methyl-aspartic acid	0.145649	0.059216	0.231368	0.05189
209	Cytidine 5'-diphosphate	3.93789	1.966728	6.736944	1.789658
210	Linoleic acid	0.000409	6.44E-05	0.000377	0.000117
211	Hypotaurine	0.035801	0.016675	0.058821	0.013901
212	beta aminobutyric acid	0.025507	0.01355	0.028141	0.015787
213	Ergocalciferol	0.000981	0.000274	0.001238	0.000146
214	Phosphocreatine	0.005912	0.002706	0.010062	0.007645

References

- Adams, J. M., & Cory, S. (2007). The Bcl-2 apoptotic switch in cancer development and therapy. *Oncogene*, *26*(9), 1324–1337. <https://doi.org/10.1038/sj.onc.1210220>
- Bajetta, E., Procopio, G., Colombo, A., Guadalupi, V., Verzoni, E., Pietrantonio, F., Pusceddu, S., Manzoni, M., Gevorgyan, A., & Buzzoni, R. (2009). Sorafenib in Hepatocellular Carcinoma. *Clinical Medicine. Therapeutics*, *1*, CMT.S2314. <https://doi.org/10.4137/CMT.S2314>
- Baker, D. J., Greenhaff, P. L., MacInnes, A., & Timmons, J. A. (2006). The Experimental Type 2 Diabetes Therapy Glycogen Phosphorylase Inhibition Can Impair Aerobic Muscle Function During Prolonged Contraction. *Diabetes*, *55*(6), 1855–1861. <https://doi.org/10.2337/db05-1687>
- Barot, S., Abo-Ali, E. M., Zhou, D. L., Palaguachi, C., & Dukhande, V. V. (2019). Inhibition of glycogen catabolism induces intrinsic apoptosis and augments multikinase inhibitors in hepatocellular carcinoma cells. *Experimental Cell Research*, *381*(2), 288–300. <https://doi.org/10.1016/j.yexcr.2019.05.017>
- Berridge, M. V., Herst, P. M., & Tan, A. S. (2005). Tetrazolium dyes as tools in cell biology: New insights into their cellular reduction. In *Biotechnology Annual Review* (Vol. 11, pp. 127–152). Elsevier. [https://doi.org/10.1016/S1387-2656\(05\)11004-7](https://doi.org/10.1016/S1387-2656(05)11004-7)
- Bhagavan, N. V., & Ha, C.-E. (2011). Carbohydrate Metabolism II. In *Essentials of Medical Biochemistry* (pp. 151–168). Elsevier. <https://doi.org/10.1016/B978-0-12-095461-2.00014-X>
- Bobarykina, A. Y., Minchenko, D. O., Opentanova, I. L., Moenner, M., Caro, J., Esumi, H., & Minchenko, O. H. (2006). Hypoxic regulation of PFKFB-3 and PFKFB-4 gene expression in

gastric and pancreatic cancer cell lines and expression of PFKFB genes in gastric cancers. *Acta Biochimica Polonica*, 53(4), 789–799.

Bordt, E. A., Clerc, P., Roelofs, B. A., Saladino, A. J., Tretter, L., Adam-Vizi, V., Cherek, E., Khalil, A., Yadava, N., Ge, S. X., Francis, T. C., Kennedy, N. W., Picton, L. K., Kumar, T., Uppuluri, S., Miller, A. M., Itoh, K., Karbowski, M., Sesaki, H., ... Polster, B. M. (2017). The Putative Drp1 Inhibitor mdivi-1 Is a Reversible Mitochondrial Complex I Inhibitor that Modulates Reactive Oxygen Species. *Developmental Cell*, 40(6), 583-594.e6.
<https://doi.org/10.1016/j.devcel.2017.02.020>

Brahimi-Horn, M. C., Bellot, G., & Pouysségur, J. (2011). Hypoxia and energetic tumour metabolism. *Current Opinion in Genetics & Development*, 21(1), 67–72.
<https://doi.org/10.1016/j.gde.2010.10.006>

Brushia, R., J. (1999). Phosphorylase kinase: The complexity of its regulation is reflected in the complexity of its structure. *Frontiers in Bioscience*, 4(1–3), d618.
<https://doi.org/10.2741/Brushia>

Chae, Y. K., Arya, A., Malecek, M.-K., Shin, D. S., Carneiro, B., Chandra, S., Kaplan, J., Kalyan, A., Altman, J. K., Plataniias, L., & Giles, F. (2016). Repurposing metformin for cancer treatment: Current clinical studies. *Oncotarget*, 7(26), 40767–40780.
<https://doi.org/10.18632/oncotarget.8194>

Chakraborty, S., & Rahman, T. (2012). The difficulties in cancer treatment. *Ecancermedicalscience*, 6, ed16. <https://doi.org/10.3332/ecancer.2012.ed16>

Chen, Z., Zhang, H., Lu, W., & Huang, P. (2009). Role of mitochondria-associated hexokinase II in cancer cell death induced by 3-bromopyruvate. *Biochimica et Biophysica Acta (BBA) - Bioenergetics*, 1787(5), 553–560. <https://doi.org/10.1016/j.bbabi.2009.03.003>

- Chesney, J., Clark, J., Lanceta, L., Trent, J. O., & Telang, S. (2015). Targeting the sugar metabolism of tumors with a first-in-class 6-phosphofructo-2-kinase (PFKFB4) inhibitor. *Oncotarget*, 6(20), 18001–18011. <https://doi.org/10.18632/oncotarget.4534>
- Chou, T.-C. (2010). Drug combination studies and their synergy quantification using the Chou-Talalay method. *Cancer Research*, 70(2), 440–446. <https://doi.org/10.1158/0008-5472.CAN-09-1947>
- Coleman, M. L., Sahai, E. A., Yeo, M., Bosch, M., Dewar, A., & Olson, M. F. (2001). Membrane blebbing during apoptosis results from caspase-mediated activation of ROCK I. *Nature Cell Biology*, 3(4), 339–345. <https://doi.org/10.1038/35070009>
- Coqueret, O. (2003). New roles for p21 and p27 cell-cycle inhibitors: A function for each cell compartment? *Trends in Cell Biology*, 13(2), 65–70. [https://doi.org/10.1016/S0962-8924\(02\)00043-0](https://doi.org/10.1016/S0962-8924(02)00043-0)
- Curtis, M., Kenny, H. A., Ashcroft, B., Mukherjee, A., Johnson, A., Zhang, Y., Helou, Y., Batlle, R., Liu, X., Gutierrez, N., Gao, X., Yamada, S. D., Lastra, R., Montag, A., Ahsan, N., Locasale, J. W., Salomon, A. R., Nebreda, A. R., & Lengyel, E. (2019). Fibroblasts Mobilize Tumor Cell Glycogen to Promote Proliferation and Metastasis. *Cell Metabolism*, 29(1), 141-155.e9. <https://doi.org/10.1016/j.cmet.2018.08.007>
- Daher, S., Massarwa, M., Benson, A. A., & Khoury, T. (2018). Current and Future Treatment of Hepatocellular Carcinoma: An Updated Comprehensive Review. *Journal of Clinical and Translational Hepatology*, 6(1), 1–10. <https://doi.org/10.14218/JCTH.2017.00031>
- Davidescu, M., Macchioni, L., Scaramozzino, G., Cristina Marchetti, M., Migliorati, G., Vitale, R., Corcelli, A., Roberti, R., Castigli, E., & Corazzi, L. (2015). The energy blockers bromopyruvate and lonidamine lead GL15 glioblastoma cells to death by different p53-dependent routes. *Scientific Reports*, 5(1), 14343. <https://doi.org/10.1038/srep14343>

- de la Cruz-López, K. G., Castro-Muñoz, L. J., Reyes-Hernández, D. O., García-Carrancá, A., & Manzo-Merino, J. (2019). Lactate in the Regulation of Tumor Microenvironment and Therapeutic Approaches. *Frontiers in Oncology*, *9*, 1143.
<https://doi.org/10.3389/fonc.2019.01143>
- DeBerardinis, R. J., Lum, J. J., Hatzivassiliou, G., & Thompson, C. B. (2008). The Biology of Cancer: Metabolic Reprogramming Fuels Cell Growth and Proliferation. *Cell Metabolism*, *7*(1), 11–20. <https://doi.org/10.1016/j.cmet.2007.10.002>
- Ding, M., Liu, C., Shi, R., Yu, M., Zeng, K., Kang, J., Fu, F., & Mi, M. (2020). Mitochondrial fusion promoter restores mitochondrial dynamics balance and ameliorates diabetic cardiomyopathy in an optic atrophy 1-dependent way. *Acta Physiologica*, *229*(1).
<https://doi.org/10.1111/apha.13428>
- Dombrádi, V. (1981). Structural aspects of the catalytic and regulatory function of glycogen phosphorylase. *International Journal of Biochemistry*, *13*(2), 125–139.
[https://doi.org/10.1016/0020-711X\(81\)90147-6](https://doi.org/10.1016/0020-711X(81)90147-6)
- Donnier-Maréchal, M., & Vidal, S. (2016). Glycogen phosphorylase inhibitors: A patent review (2013 - 2015). *Expert Opinion on Therapeutic Patents*, *26*(2), 199–212.
<https://doi.org/10.1517/13543776.2016.1131268>
- Eales, K. L., Hollinshead, K. E. R., & Tennant, D. A. (2016). Hypoxia and metabolic adaptation of cancer cells. *Oncogenesis*, *5*(1), e190–e190. <https://doi.org/10.1038/oncsis.2015.50>
- Ertle, J., Dechêne, A., Sowa, J.-P., Penndorf, V., Herzer, K., Kaiser, G., Schlaak, J. F., Gerken, G., Syn, W.-K., & Canbay, A. (2011). Non-alcoholic fatty liver disease progresses to hepatocellular carcinoma in the absence of apparent cirrhosis: Absence of Cirrhosis in NASH-Derived HCC. *International Journal of Cancer*, *128*(10), 2436–2443.
<https://doi.org/10.1002/ijc.25797>

- Farhadi, P., Yarani, R., Dokaneheifard, S., & Mansouri, K. (2020). The emerging role of targeting cancer metabolism for cancer therapy. *Tumor Biology*, *42*(10), 101042832096528.
<https://doi.org/10.1177/1010428320965284>
- Favaro, E., Bensaad, K., Chong, M. G., Tennant, D. A., Ferguson, D. J., Snell, C., Steers, G., Turley, H., Li, J. L., Gunther, U. L., Buffa, F. M., McIntyre, A., & Harris, A. L. (2012). Glucose utilization via glycogen phosphorylase sustains proliferation and prevents premature senescence in cancer cells. *Cell Metab*, *16*(6), 751–764.
<https://doi.org/10.1016/j.cmet.2012.10.017>
- Feldwisch-Drentrup, H. (2016). Candidate cancer drug suspected after death of three patients at an alternative medicine clinic. *Science Insider*.
- Floettmann, E., Gregory, L., Teague, J., Myatt, J., Hammond, C., Poucher, S. M., & Jones, H. B. (2010). Prolonged Inhibition of Glycogen Phosphorylase in Livers of Zucker Diabetic Fatty Rats Models Human Glycogen Storage Diseases. *Toxicologic Pathology*, *38*(3), 393–401. <https://doi.org/10.1177/0192623310362707>
- Fulda, S., & Debatin, K. M. (2006). Extrinsic versus intrinsic apoptosis pathways in anticancer chemotherapy. *Oncogene*, *25*(34), 4798–4811. <https://doi.org/10.1038/sj.onc.1209608>
- Gaboriaud-Kolar, N., & Skaltsounis, A.-L. (2013). Glycogen phosphorylase inhibitors: A patent review (2008 – 2012). *Expert Opinion on Therapeutic Patents*, *23*(8), 1017–1032.
<https://doi.org/10.1517/13543776.2013.794790>
- Garrido, C., Galluzzi, L., Brunet, M., Puig, P. E., Didelot, C., & Kroemer, G. (2006). <https://doi.org/10.1093/jjco/hyx180>. *Cell Death and Differentiation*, *13*(9), 1423–1433.
<https://doi.org/10.1038/sj.cdd.4401950>

- Ge, T., Yang, J., Zhou, S., Wang, Y., Li, Y., & Tong, X. (2020). The Role of the Pentose Phosphate Pathway in Diabetes and Cancer. *Frontiers in Endocrinology*, *11*, 365.
<https://doi.org/10.3389/fendo.2020.00365>
- Gill, K. S., Fernandes, P., O'Donovan, T. R., McKenna, S. L., Doddakula, K. K., Power, D. G., Soden, D. M., & Forde, P. F. (2016). Glycolysis inhibition as a cancer treatment and its role in an anti-tumour immune response. *Biochimica et Biophysica Acta (BBA) - Reviews on Cancer*, *1866*(1), 87–105. <https://doi.org/10.1016/j.bbcan.2016.06.005>
- Green, D. R., & Kroemer, G. (2004). The pathophysiology of mitochondrial cell death. *Science (New York, N.Y.)*, *305*(5684), 626–629. <https://doi.org/10.1126/science.1099320>
- Greenberg, C. C., Meredith, K. N., Yan, L., & Brady, M. J. (2003). Protein Targeting to Glycogen Overexpression Results in the Specific Enhancement of Glycogen Storage in 3T3-L1 Adipocytes. *Journal of Biological Chemistry*, *278*(33), 30835–30842.
<https://doi.org/10.1074/jbc.M303846200>
- Haan, C., Walbrecq, G., Kozar, I., Behrmann, I., & Zimmer, A. D. (2016). Phosphorylation of the PDH complex precedes HIF-1-mediated effects and PDK1 upregulation during the first hours of hypoxic treatment in HCC cells. *Hypoxia*, *Volume 4*, 135–145.
<https://doi.org/10.2147/HP.S99044>
- Hagner, N., & Joerger, M. (2010). Cancer chemotherapy: Targeting folic acid synthesis. *Cancer Management and Research*, *2*, 293–301. <https://doi.org/10.2147/CMR.S10043>
- Hanahan, D., & Weinberg, R. A. (2011). Hallmarks of cancer: The next generation. *Cell*, *144*(5), 646–674. <https://doi.org/10.1016/j.cell.2011.02.013>
- Hanselmann, R. G., & Welter, C. (2016). Origin of Cancer: An Information, Energy, and Matter Disease. *Frontiers in Cell and Developmental Biology*, *4*, 121.
<https://doi.org/10.3389/fcell.2016.00121>

- Hardie, D. G., Ross, F. A., & Hawley, S. A. (2012). AMPK: A nutrient and energy sensor that maintains energy homeostasis. *Nature Reviews. Molecular Cell Biology*, *13*(4), 251–262.
<https://doi.org/10.1038/nrm3311>
- Hartke, J., Johnson, M., & Ghabril, M. (2017). The diagnosis and treatment of hepatocellular carcinoma. *Seminars in Diagnostic Pathology*, *34*(2), 153–159.
<https://doi.org/10.1053/j.semmp.2016.12.011>
- Herzig, S., & Shaw, R. J. (2018). AMPK: Guardian of metabolism and mitochondrial homeostasis. *Nature Reviews Molecular Cell Biology*, *19*(2), 121–135.
<https://doi.org/10.1038/nrm.2017.95>
- Hwang, H. C., & Clurman, B. E. (2005). Cyclin E in normal and neoplastic cell cycles. *Oncogene*, *24*(17), 2776–2786. <https://doi.org/10.1038/sj.onc.1208613>
- Igney, F. H., & Krammer, P. H. (2002). Death and anti-death: Tumour resistance to apoptosis. *Nature Reviews Cancer*, *2*(4), 277–288. <https://doi.org/10.1038/nrc776>
- Ikeda, M., Morizane, C., Ueno, M., Okusaka, T., Ishii, H., & Furuse, J. (2018). Chemotherapy for hepatocellular carcinoma: Current status and future perspectives. *Japanese Journal of Clinical Oncology*, *48*(2), 103–114. <https://doi.org/10.1093/jjco/hyx180>
- Inoue-Yamauchi, A., & Oda, H. (2012). Depletion of mitochondrial fission factor DRP1 causes increased apoptosis in human colon cancer cells. *Biochemical and Biophysical Research Communications*, *421*(1), 81–85. <https://doi.org/10.1016/j.bbrc.2012.03.118>
- Jensen, J., & Lai, Y.-C. (2009). Regulation of muscle glycogen synthase phosphorylation and kinetic properties by insulin, exercise, adrenaline and role in insulin resistance. *Archives of Physiology and Biochemistry*, *115*(1), 13–21.
<https://doi.org/10.1080/13813450902778171>

- Jensen, J., Rustad, P. I., Kolnes, A. J., & Lai, Y.-C. (2011). The Role of Skeletal Muscle Glycogen Breakdown for Regulation of Insulin Sensitivity by Exercise. *Frontiers in Physiology*, 2. <https://doi.org/10.3389/fphys.2011.00112>
- Jensen, T. E., & Richter, E. A. (2012). Regulation of glucose and glycogen metabolism during and after exercise: Regulation of glucose and glycogen metabolism in exercise. *The Journal of Physiology*, 590(5), 1069–1076. <https://doi.org/10.1113/jphysiol.2011.224972>
- Johnson, L. N. (1992). Glycogen phosphorylase: Control by phosphorylation and allosteric effectors. *The FASEB Journal*, 6(6), 2274–2282. <https://doi.org/10.1096/fasebj.6.6.1544539>
- Jones, L. J., Gray, M., Yue, S. T., Haugland, R. P., & Singer, V. L. (2001). Sensitive determination of cell number using the CyQUANT® cell proliferation assay. *Journal of Immunological Methods*, 254(1–2), 85–98. [https://doi.org/10.1016/S0022-1759\(01\)00404-5](https://doi.org/10.1016/S0022-1759(01)00404-5)
- Ko, K.-L., Mak, L.-Y., Cheung, K.-S., & Yuen, M.-F. (2020). Hepatocellular carcinoma: Recent advances and emerging medical therapies. *F1000Research*, 9, 620. <https://doi.org/10.12688/f1000research.24543.1>
- Lee, W.-N. P., Guo, P., Lim, S., Bassilian, S., Lee, S. T., Boren, J., Cascante, M., Go, V. L. W., & Boros, L. G. (2004). Metabolic sensitivity of pancreatic tumour cell apoptosis to glycogen phosphorylase inhibitor treatment. *British Journal of Cancer*, 91(12), 2094–2100. <https://doi.org/10.1038/sj.bjc.6602243>
- Lencioni, R., & Crocetti, L. (2012). Local-Regional Treatment of Hepatocellular Carcinoma. *Radiology*, 262(1), 43–58. <https://doi.org/10.1148/radiol.11110144>
- Lerín, C., Montell, E., Nolasco, T., García-Rocha, M., Guinovart, J. J., & Gómez-Foix, A. M. (2004). Regulation of glycogen metabolism in cultured human muscles by the glycogen

- phosphorylase inhibitor CP-91149. *Biochemical Journal*, 378(3), 1073–1077.
<https://doi.org/10.1042/bj20030971>
- Liberti, M. V., & Locasale, J. W. (2016). The Warburg Effect: How Does it Benefit Cancer Cells? *Trends in Biochemical Sciences*, 41(3), 211–218.
<https://doi.org/10.1016/j.tibs.2015.12.001>
- Liu, C.-Y., Chen, K.-F., & Chen, P.-J. (2015). Treatment of Liver Cancer. *Cold Spring Harbor Perspectives in Medicine*, 5(9), a021535. <https://doi.org/10.1101/cshperspect.a021535>
- Lurje, I., Czigany, Z., Bednarsch, J., Roderburg, C., Isfort, P., Neumann, U. P., & Lurje, G. (2019). Treatment Strategies for Hepatocellular Carcinoma – a Multidisciplinary Approach. *International Journal of Molecular Sciences*, 20(6), 1465.
<https://doi.org/10.3390/ijms20061465>
- Ma, D., Wang, J., Zhao, Y., Lee, W.-N. P., Xiao, J., Go, V. L. W., Wang, Q., Recker, R. R., & Xiao, G. G. (2012). Inhibition of Glycogen Phosphorylation Induces Changes in Cellular Proteome and Signaling Pathways in MIA Pancreatic Cancer Cells: *Pancreas*, 41(3), 397–408.
<https://doi.org/10.1097/MPA.0b013e318236f022>
- Malek, N. P., Schmidt, S., Huber, P., Manns, M. P., & Greten, T. F. (2014). The Diagnosis and Treatment of Hepatocellular Carcinoma. *Deutsches Aerzteblatt Online*.
<https://doi.org/10.3238/arztebl.2014.0101>
- Manners, D. J. (1991). Recent developments in our understanding of glycogen structure. *Carbohydrate Polymers*, 16(1), 37–82. [https://doi.org/10.1016/0144-8617\(91\)90071-J](https://doi.org/10.1016/0144-8617(91)90071-J)
- Markopoulos, C., Mantas, D., Philipidis, T., Kouskos, E., Antonopoulou, Z., Hatzinikolaou, M., & Gogas, H. (2008). Glycogen-rich clear cell carcinoma of the breast. *World Journal of Surgical Oncology*, 6(1), 44. <https://doi.org/10.1186/1477-7819-6-44>

- Martin, W. H., Hoover, D. J., Armento, S. J., Stock, I. A., McPherson, R. K., Danley, D. E., Stevenson, R. W., Barrett, E. J., & Treadway, J. L. (1998). Discovery of a human liver glycogen phosphorylase inhibitor that lowers blood glucose in vivo. *Proc Natl Acad Sci U S A*, *95*(4), 1776–1781.
- Menendez, J. A., & Lupu, R. (2007). Fatty acid synthase and the lipogenic phenotype in cancer pathogenesis. *Nature Reviews Cancer*, *7*(10), 763.
- Miller, K. D., Nogueira, L., Mariotto, A. B., Rowland, J. H., Yabroff, K. R., Alfano, C. M., Jemal, A., Kramer, J. L., & Siegel, R. L. (2019). Cancer treatment and survivorship statistics, 2019. *CA: A Cancer Journal for Clinicians*, *69*(5), 363–385. <https://doi.org/10.3322/caac.21565>
- Mookerjee, S. A., Gerencser, A. A., Nicholls, D. G., & Brand, M. D. (2017). Quantifying intracellular rates of glycolytic and oxidative ATP production and consumption using extracellular flux measurements. *The Journal of Biological Chemistry*, *292*(17), 7189–7207. <https://doi.org/10.1074/jbc.M116.774471>
- Murray, B., & Rosenbloom, C. (2018). Fundamentals of glycogen metabolism for coaches and athletes. *Nutrition Reviews*, *76*(4), 243–259. <https://doi.org/10.1093/nutrit/nuy001>
- Nadeau, O. W., Fontes, J. D., & Carlson, G. M. (2018). The regulation of glycogenolysis in the brain. *Journal of Biological Chemistry*, *293*(19), 7099–7107. <https://doi.org/10.1074/jbc.R117.803023>
- Pelletier, J., Bellot, G., Gounon, P., Lacas-Gervais, S., Pouyssegur, J., & Mazure, N. M. (2012). Glycogen Synthesis is Induced in Hypoxia by the Hypoxia-Inducible Factor and Promotes Cancer Cell Survival. *Front Oncol*, *2*, 18. <https://doi.org/10.3389/fonc.2012.00018>
- Pescador, N., Villar, D., Cifuentes, D., Garcia-Rocha, M., Ortiz-Barahona, A., Vazquez, S., Ordonez, A., Cuevas, Y., Saez-Morales, D., Garcia-Bermejo, M. L., Landazuri, M. O., Guinovart, J., & Peso, L. (2010). Hypoxia promotes glycogen accumulation through

- hypoxia inducible factor (HIF)-mediated induction of glycogen synthase 1. *PLoS One*, 5(3), e9644. <https://doi.org/10.1371/journal.pone.0009644>
- Prats, C., Graham, T. E., & Shearer, J. (2018). The dynamic life of the glycogen granule. *The Journal of Biological Chemistry*, 293(19), 7089–7098. <https://doi.org/10.1074/jbc.R117.802843>
- Pugh, C. W., & Ratcliffe, P. J. (2003). Regulation of angiogenesis by hypoxia: Role of the HIF system. *Nature Medicine*, 9(6), 677–684. <https://doi.org/10.1038/nm0603-677>
- Pushpakom, S., Iorio, F., Eyers, P. A., Escott, K. J., Hopper, S., Wells, A., Doig, A., Williams, T., Latimer, J., McNamee, C., Norris, A., Sanseau, P., Cavalla, D., & Pirmohamed, M. (2019). Drug repurposing: Progress, challenges and recommendations. *Nature Reviews Drug Discovery*, 18(1), 41–58. <https://doi.org/10.1038/nrd.2018.168>
- Ragolia, L., & Begum, N. (1998). Protein phosphatase-1 and insulin action. *Molecular and Cellular Biochemistry*, 182(1–2), 49–58.
- Rath, V. L., Ammirati, M., LeMotte, P. K., Fennell, K. F., Mansour, M. N., Danley, D. E., Hynes, T. R., Schulte, G. K., Wasilko, D. J., & Pandit, J. (2000). Activation of human liver glycogen phosphorylase by alteration of the secondary structure and packing of the catalytic core. *Molecular Cell*, 6(1), 139–148.
- Repetto, G., del Peso, A., & Zurita, J. L. (2008). Neutral red uptake assay for the estimation of cell viability/cytotoxicity. *Nature Protocols*, 3(7), 1125–1131. <https://doi.org/10.1038/nprot.2008.75>
- Ritterson Lew, C., Guin, S., & Theodorescu, D. (2015). Targeting glycogen metabolism in bladder cancer. *Nat Rev Urol*, 12(7), 383–391. <https://doi.org/10.1038/nrurol.2015.111>
- Roach, P. J. (1990). Control of glycogen synthase by hierarchical protein phosphorylation. *The FASEB Journal*, 4(12), 2961–2968. <https://doi.org/10.1096/fasebj.4.12.2168324>

- Roach, P. J., Depaoli-Roach, A. A., Hurley, T. D., & Tagliabracci, V. S. (2012). Glycogen and its metabolism: Some new developments and old themes. *Biochemical Journal*, *441*(3), 763–787. <https://doi.org/10.1042/BJ20111416>
- Rotella, D., Jones, R. M., & Thurston, D. E. (2013). *New Therapeutic Strategies for Type 2 Diabetes: Small Molecule Approaches*. Royal Society of Chemistry.
- Rousset, M., Chevalier, G., Rousset, J. P., Dussaulx, E., & Zweibaum, A. (1979). Presence and cell growth-related variations of glycogen in human colorectal adenocarcinoma cell lines in culture. *Cancer Research*, *39*(2 Pt 1), 531–534.
- Rousset, M., Zweibaum, A., & Fogh, J. (1981). Presence of glycogen and growth-related variations in 58 cultured human tumor cell lines of various tissue origins. *Cancer Research*, *41*(3), 1165–1170.
- Schnier, J. B., Nishi, K., Monks, A., Gorin, F. A., & Bradbury, E. M. (2003). Inhibition of glycogen phosphorylase (GP) by CP-91,149 induces growth inhibition correlating with brain GP expression. *Biochemical and Biophysical Research Communications*, *309*(1), 126–134. [https://doi.org/10.1016/S0006-291X\(03\)01542-0](https://doi.org/10.1016/S0006-291X(03)01542-0)
- Shearer, J., & Graham, T. E. (2004). Novel Aspects of Skeletal Muscle Glycogen and Its Regulation During Rest and Exercise: *Exercise and Sport Sciences Reviews*, *32*(3), 120–126. <https://doi.org/10.1097/00003677-200407000-00008>
- Siegel, R. L., Miller, K. D., Fuchs, H. E., & Jemal, A. (2021). Cancer Statistics, 2021. *CA: A Cancer Journal for Clinicians*, *71*(1), 7–33. <https://doi.org/10.3322/caac.21654>
- Siegel, R. L., Miller, K. D., & Jemal, A. (2020). Cancer statistics, 2020. *CA: A Cancer Journal for Clinicians*, *70*(1), 7–30. <https://doi.org/10.3322/caac.21590>
- Song, J., Lee, K., Park, S. W., Chung, H., Jung, D., Na, Y. R., Quan, H., Cho, C. S., Che, J.-H., Kim, J. H., Park, J.-H., & Seok, S. H. (2018). Lactic Acid Upregulates VEGF Expression in

- Macrophages and Facilitates Choroidal Neovascularization. *Investigative Ophthalmology & Visual Science*, 59(8), 3747. <https://doi.org/10.1167/iovs.18-23892>
- Takahashi, S., Satomi, A., Yano, K., Kawase, H., Tuji, Y., Murakami, S., Hirayama, R., & Tanimizu, T. (1999). Estimation of glycogen levels in human colorectal cancer tissue: Relationship with cell cycle and tumor outgrowth. *Journal of Gastroenterology*, 34(4), 474–480. <https://doi.org/10.1007/s005350050299>
- Tan, B. T., Park, C. Y., Ailles, L. E., & Weissman, I. L. (2006). The cancer stem cell hypothesis: A work in progress. *Laboratory Investigation*, 86(12), 1203–1207. <https://doi.org/10.1038/labinvest.3700488>
- Tang, W., Chen, Z., Zhang, W., Cheng, Y., Zhang, B., Wu, F., Wang, Q., Wang, S., Rong, D., Reiter, F. P., De Toni, E. N., & Wang, X. (2020). The mechanisms of sorafenib resistance in hepatocellular carcinoma: Theoretical basis and therapeutic aspects. *Signal Transduction and Targeted Therapy*, 5(1), 87. <https://doi.org/10.1038/s41392-020-0187-x>
- Tenen, D. G., Chai, L., & Tan, J. L. (2021). Metabolic alterations and vulnerabilities in hepatocellular carcinoma. *Gastroenterology Report*, 9(1), 1–13. <https://doi.org/10.1093/gastro/goaa066>
- Treadway, J. L., Mendys, P., & Hoover, D. J. (2001). Glycogen phosphorylase inhibitors for treatment of type 2 diabetes mellitus. *Expert Opinion on Investigational Drugs*, 10(3), 439–454. <https://doi.org/10.1517/13543784.10.3.439>
- Vander Heiden, M. G. (2011). Targeting cancer metabolism: A therapeutic window opens. *Nature Reviews Drug Discovery*, 10(9), 671–684. <https://doi.org/10.1038/nrd3504>

- Vander Heiden, M. G., Cantley, L. C., & Thompson, C. B. (2009). Understanding the Warburg effect: The metabolic requirements of cell proliferation. *Science (New York, N.Y.)*, 324(5930), 1029–1033. <https://doi.org/10.1126/science.1160809>
- Vasan, N., Baselga, J., & Hyman, D. M. (2019). A view on drug resistance in cancer. *Nature*, 575(7782), 299–309. <https://doi.org/10.1038/s41586-019-1730-1>
- Végran, F., Boidot, R., Michiels, C., Sonveaux, P., & Feron, O. (2011). Lactate Influx through the Endothelial Cell Monocarboxylate Transporter MCT1 Supports an NF- κ B/IL-8 Pathway that Drives Tumor Angiogenesis. *Cancer Research*, 71(7), 2550–2560. <https://doi.org/10.1158/0008-5472.CAN-10-2828>
- Vénien-Bryan, C., Lowe, E. M., Boisset, N., Traxler, K. W., Johnson, L. N., & Carlson, G. M. (2002). Three-Dimensional Structure of Phosphorylase Kinase at 22 Å Resolution and Its Complex with Glycogen Phosphorylase b. *Structure*, 10(1), 33–41. [https://doi.org/10.1016/S0969-2126\(01\)00691-8](https://doi.org/10.1016/S0969-2126(01)00691-8)
- Verbaanderd, C., Maes, H., Schaaf, M. B., Sukhatme, V. P., Pantziarka, P., Sukhatme, V., Agostinis, P., & Bouche, G. (2017). Repurposing Drugs in Oncology (ReDO)—Chloroquine and hydroxychloroquine as anti-cancer agents. *Ecancermedicalscience*, 11. <https://doi.org/10.3332/ecancer.2017.781>
- Vermes, I., Haanen, C., Steffens-Nakken, H., & Reutellingsperger, C. (1995). A novel assay for apoptosis Flow cytometric detection of phosphatidylserine expression on early apoptotic cells using fluorescein labelled Annexin V. *Journal of Immunological Methods*, 184(1), 39–51. [https://doi.org/10.1016/0022-1759\(95\)00072-1](https://doi.org/10.1016/0022-1759(95)00072-1)
- Warburg, O. (1956). On the Origin of Cancer Cells. *Science*, 123(3191), 309–314. <https://doi.org/10.1126/science.123.3191.309>

- Ward, P. S., & Thompson, C. B. (2012). Metabolic reprogramming: A cancer hallmark even warburg did not anticipate. *Cancer Cell*, *21*(3), 297–308.
<https://doi.org/10.1016/j.ccr.2012.02.014>
- Watt, M. J., Clark, A. K., Selth, L. A., Haynes, V. R., Lister, N., Rebello, R., Porter, L. H., Niranjana, B., Whitby, S. T., Lo, J., Huang, C., Schittenhelm, R. B., Anderson, K. E., Furic, L., Wijayarathne, P. R., Matzaris, M., Montgomery, M. K., Papargiris, M., Norden, S., ... Taylor, R. A. (2019). Suppressing fatty acid uptake has therapeutic effects in preclinical models of prostate cancer. *Science Translational Medicine*, *11*(478).
<https://doi.org/10.1126/scitranslmed.aau5758>
- Winter, S. C., Buffa, F. M., Silva, P., Miller, C., Valentine, H. R., Turley, H., Shah, K. A., Cox, G. J., Corbridge, R. J., Homer, J. J., Musgrove, B., Slevin, N., Sloan, P., Price, P., West, C. M. L., & Harris, A. L. (2007). Relation of a Hypoxia Metagene Derived from Head and Neck Cancer to Prognosis of Multiple Cancers. *Cancer Research*, *67*(7), 3441–3449.
<https://doi.org/10.1158/0008-5472.CAN-06-3322>
- Xu, X.-F., Xing, H., Han, J., Li, Z.-L., Lau, W.-Y., Zhou, Y.-H., Gu, W.-M., Wang, H., Chen, T.-H., Zeng, Y.-Y., Li, C., Wu, M.-C., Shen, F., & Yang, T. (2019). Risk Factors, Patterns, and Outcomes of Late Recurrence After Liver Resection for Hepatocellular Carcinoma: A Multicenter Study From China. *JAMA Surgery*, *154*(3), 209.
<https://doi.org/10.1001/jamasurg.2018.4334>
- Yang, F., Yan, S., He, Y., Wang, F., Song, S., Guo, Y., Zhou, Q., Wang, Y., Lin, Z., Yang, Y., Zhang, W., & Sun, S. (2008). Expression of hepatitis B virus proteins in transgenic mice alters lipid metabolism and induces oxidative stress in the liver. *Journal of Hepatology*, *48*(1), 12–19. <https://doi.org/10.1016/j.jhep.2007.06.021>

- Yu, R., Lendahl, U., Nistér, M., & Zhao, J. (2020). Regulation of Mammalian Mitochondrial Dynamics: Opportunities and Challenges. *Frontiers in Endocrinology*, *11*, 374.
<https://doi.org/10.3389/fendo.2020.00374>
- Zarrinpar, A. (2017). Metabolic Pathway Inhibition in Liver Cancer. *SLAS TECHNOLOGY: Translating Life Sciences Innovation*, *22*(3), 237–244.
<https://doi.org/10.1177/2472630317698683>
- Zemirli, N., Morel, E., & Molino, D. (2018). Mitochondrial Dynamics in Basal and Stressful Conditions. *International Journal of Molecular Sciences*, *19*(2), 564.
<https://doi.org/10.3390/ijms19020564>
- Zhai, L., Feng, L., Xia, L., Yin, H., & Xiang, S. (2016). Crystal structure of glycogen debranching enzyme and insights into its catalysis and disease-causing mutations. *Nature Communications*, *7*(1), 11229. <https://doi.org/10.1038/ncomms11229>
- Zhang, H., Pan, Z., Ju, J., Xing, C., Li, X., Shan, M., & Sun, S. (2020). DRP1 deficiency induces mitochondrial dysfunction and oxidative stress-mediated apoptosis during porcine oocyte maturation. *Journal of Animal Science and Biotechnology*, *11*(1), 77.
<https://doi.org/10.1186/s40104-020-00489-4>
- Zhang, M., Zheng, J., Nussinov, R., & Ma, B. (2017). Release of Cytochrome C from Bax Pores at the Mitochondrial Membrane. *Scientific Reports*, *7*(1), 2635.
<https://doi.org/10.1038/s41598-017-02825-7>
- Zhang, Z., Yao, L., Yang, J., Wang, Z., & Du, G. (2018). PI3K/Akt and HIF-1 signaling pathway in hypoxia-ischemia (Review). *Molecular Medicine Reports*.
<https://doi.org/10.3892/mmr.2018.9375>
- Zois, C. E., Favaro, E., & Harris, A. L. (2014). Glycogen metabolism in cancer. *Biochemical Pharmacology*, *92*(1), 3–11. <https://doi.org/10.1016/j.bcp.2014.09.001>

- Zois, C. E., & Harris, A. L. (2016). Glycogen metabolism has a key role in the cancer microenvironment and provides new targets for cancer therapy. *J Mol Med (Berl)*, *94*(2), 137–154. <https://doi.org/10.1007/s00109-015-1377-9>
- Zugazagoitia, J., Guedes, C., Ponce, S., Ferrer, I., Molina-Pinelo, S., & Paz-Ares, L. (2016). Current Challenges in Cancer Treatment. *Clinical Therapeutics*, *38*(7), 1551–1566. <https://doi.org/10.1016/j.clinthera.2016.03.026>

Vita

Name	<i>Shrikant Barot</i>
Baccalaureate Degree	<i>Bachelor of Pharmacy, Hemchandracharya North Gujarat University, Patan Major: Pharmacy</i>
Date Graduated	<i>May, 2011</i>
Other Degrees and Certificates	<i>Master of Pharmacy, Ganpat University, Mehsana, Major: Pharmacology</i>
Date Graduated	<i>May, 2013</i>